Effects of Vinblastine and Its Metabolites on Nausea and Alopecia Associated Receptors

by

© Caroline Manto Chagas

A thesis submitted to the School of Graduate Studies in partial fulfillment of the requirements for the degree of

Master of Science in Pharmacy

School of Pharmacy

Memorial University of Newfoundland

December 2018

St. John's, Newfoundland and Labrador, Canada

Abstract

The effects of vinblastine (VLB) and its thirty-five known metabolites were investigated on nausea and alopecia associated receptors by means of molecular docking simulations. The *in silico* pharmacokinetics (PK) properties and binding affinities of VLB and its metabolites with the vinca site of tubulin were also elucidated in the present study.

VLB and its metabolites have demonstrated binding affinities mainly for the muscarinic receptors M_1, M_4 and M_5 that display significant roles in the onset of nausea during chemotherapy. The metabolites of VLB interact with the binding site of acetylcholine and share similar binding interactions with residues involved with the endogenous substrate. Furthermore, VLB metabolites have also shown binding affinities for alopecia associated receptors such as vitamin D (VDR), androgen, smoothened and MDM2, which can trigger the death of hair follicle following cancer treatment.

The predicted PK properties of VLB and its metabolites have revealed that they are all substrates and inhibitors of CYP3A4 and P-glycoprotein, and inhibitors of CYP2D6. The majority of metabolites do not cross the blood-brain barrier, do not undergo glucuronidation and have no affinity for the human ether-à-go-go-related gene receptor. Finally, VLB metabolites docked into the vinca site of tubulin have revealed that metabolites 8, 10 and 11 have binding affinities for tubulin and interact with the same residues involved with VLB. Taking into account the PK properties, metabolite 10 (20-Hydroxy-VLB) has shown to be a potential active analog of VLB.

This research project has aimed to a better understanding of the VLB-induced off-targets events such as nausea and alopecia, and how the VLB metabolites can trigger these ADRs. These findings suggest that knowing which and how the metabolites of VLB are involved with off-targets receptors of nausea and alopecia, as well as their PK properties and effects on tubulin target, ADRs

during chemotherapy could be eliminated or lessened. This is possible if modifications on the chemical structure of VLB and advances in drug discovery and medicinal chemistry fields are taken into consideration in future studies. It would enhance target specificity as it could decrease formation of many metabolites and hence minimize the number of off-target interactions. That could result in providing a less unpleasant treatment for cancer patients and a higher quality of life during chemotherapy.

Acknowledgments

I would like to thank my supervisor Dr. Laleh Alisaraie for giving me the opportunity to be her student, to learn a lot from her and to grow as a professional and person. Thank you for all your support, patience and guidance during these 2 years. Thanks for all your advice in career wise choices and for being a fundamental key on my preparation for the future.

I would like to thank my mom, Stela, who has always been there for me. Despite the distances of where we live and the rush on our days, we have always been so close and inseparable, and I have never felt myself far from you. Thank you for all your love, support in both financial and psychological ways, encouragement and advice. I am so thankful for having you in my life and in all steps I take. In addition to that, I would like to thank my dad, Mauro, and my grandma, Elisa, for their support and love throughout my life. You three mean the world to me.

I would like to thank Arthur for being more than a boyfriend, my best friend. Thank you for all your caring, love, joy, patience and advice. You are the one who made me smile when I had no reasons to, and I am really glad to share my day-to-day with you.

I would like to thank all my family and friends from Brazil and Canada. Everyone contributed for my graduation in different aspects, but in really special ways.

I would like to thank my lab members for their support and fun moments.

Finally, I thank School of Pharmacy for providing a good environment for students and Memorial University of Newfoundland for partial stipend support.

Table of Contents

List of Tables

List of Figures

List of Abbreviations

ACh – Acetylcholine

ADMET – Absorption, Distribution, Metabolism, Excretion, Toxicity

ADRs – Adverse Drug Reactions

AR – Androgen Receptor

BBB – Blood-Brain Barrier

CIA – Chemotherapy-Induced Alopecia

CINV – Chemotherapy-Induced Nausea and Vomiting

CT – Catharantine (Portion of Vinblastine)

CYP450 – Cytochrome P450 Enzyme Complex

D_2R – Dopaminergic Receptor D_2

H_1R – Histaminic Receptor H_1

H_3R – Histaminic Receptor H_3

HBA – Hydrogen Bond Acceptor

HBD – Hydrogen Bond Donor

H-bond – Hydrogen Bond

HF – hair follicle

M_1R – Muscarinic Receptor M_1

M_4R – Muscarinic Receptor M_4

M_5R – Muscarinic Receptor M_5

MDM2 – Murine Double Minute 2 Homolog

MTs – Microtubules

MW – Molecular Weight

NB – Non Binding

PDB – Protein Data Bank

P-gp – Permeability-Glycoprotein

PK - pharmacokinetics

RO5 – Rule of Five

SMO – Smoothened Receptor

VD – Vindoline (Portion of Vinblastine)

VDR – Vitamin D Receptor

vdW – van der Waals

VLB – Vinblastine

CHAPTER 1 Introduction

1.1 Cancer

Cancer is a devastating disease that strikes millions of people with different age, sex and ethnicity. It occurs when healthy cells behave abnormally and start to proliferate out of control, thus spreading into surrounding tissues and causing tumors. According to the World Health Organization (WHO), 8.8 million people died from cancer in 2015 [1]. In Canada, cancer is the leading cause of deaths (30%) and estimated to affect half of Canadians in their lifetime [2, 3].

Although sometimes considered fatal, 30%-50% of cancer types are preventable, and many are curable. The probability of developing cancer is dependent upon factors such as age, sex and daily life habits such as smoking, alcohol and obesity. As the population in Canada is aging, the incidence of cancer is likely to increase by 79% in the following years. The most common types of cancer in Canada are prostate and breast cancer thus annually affects around 100,000 males and women, respectively [2, 3].

1.1.1 Treatment and Side Effects

Chemotherapy is the most common type of treatment for cancer, especially if the disease has metastasized. It is chosen either as a single therapy or in combination with other types of cancer treatments such as surgery and radiation [4].

Chemotherapy can be administered by different routes such as oral and intravenous (IV), which are the most used ones. Despite advances in its effectiveness, chemotherapy is well known to cause endless adverse drug reactions (ADRs) and thus decreases patient's

quality of life and sometimes delays the treatment. The most common ADRs during chemotherapy are nausea, vomiting, diarrhea, fatigue, alopecia, neuropathy, anemia, anorexia and rash [5, 6]. Among those, nausea is undeniably the most prevalent and unpleasant ADR reported by patients during chemotherapy [6-9]. According to a study conducted by Kuchuk *et al.*, 60 out of 100 patients have ranked nausea as the worst ADR during chemotherapy, thus even more unpleasant than fatigue, alopecia and motor neuropathy [9].

1.2 Vinblastine

Vinblastine (VLB) or vincaleukoblastine is an anticancer drug that was firstly isolated from the alkaloids of Madagascar periwinkle *(Catharantus roseus)* plant in 1960 in Canada [10]. (**Figure 1.1**)

Along with other alkaloids derived from periwinkle plant such as vinorelbine, vindesine and vincristine, VLB is one of the major agents with antitumor properties used in chemotherapy [11]. These drugs act by inhibiting the polymerization of the microtubules (MTs) due to binding to the tubulin heterodimer, thus preventing the mitotic spindle, and the cell proliferation process. Usually administered in combined therapy, VLB is effective against a number of cancers such as renal cell carcinoma [12], Hodgkin's lymphoma [13], small cell lung, breast and colon cancers [14].

Currently, the only route of administration of VLB is IV [15-19], by intermittent infusion over 1-15min [15, 20]. Interestingly, there have been studies showing the efficacy of VLB locally administered in patients with Kaposi's sarcoma (KS), a very common associated disease with AIDS and diabetes that leads to unpleasant oral lesions.

Intralesional injections of VLB seems to ameliorate the symptoms in patients with KS [21, 22]. However, it is strongly contraindicated by intrathecal route of administration due to its fatal risk. According to the Food & Drugs Administration (FDA), the pharmaceutical companies that manufacture VLB in the United States are Fresenius Kabi USA and West-Ward Pharms INT [23]. In Canada, VLB is commercialized by Pfizer and Sandoz pharmaceutical companies [17]. Further information is available through the most updated guide of drug information for health professionals and patients provided by BC Cancer Agency [15].

1.2.1 Physicochemical Properties of Vinblastine

VLB has a molecular weight (MW) of 812.99 g/mol and a chemical formula of $C_{46}H_{60}N_4O_9$, thus considered a large and complex structure. The catharantine portion (CT) of VLB (labelled C1′-C26′) has an unusual 9-membered ring named azacyclononane ring that contains a protonated and charged nitrogen atom at position 6′, a hydroxyl and methyl group at C4′, an ester group at C18′ and an indole ring. The vindoline portion (VD) of VLB (labelled N1-C30) is the major alkaloid from the periwinkle plant [24]. It also has an indole ring that contains an N-methyl at position 1 and a methoxy moiety at C16. It contains an ester and hydroxyl groups at C3, as well as an ester and ethyl groups at C4 and C5, respectively. According to the crystal structure of VLB, the molecule exists in dicationic form whereas the N6′ of catharantine portion and the N9 of vindoline portion are both protonated and positively charged [25]. (**Figure 1.1**)

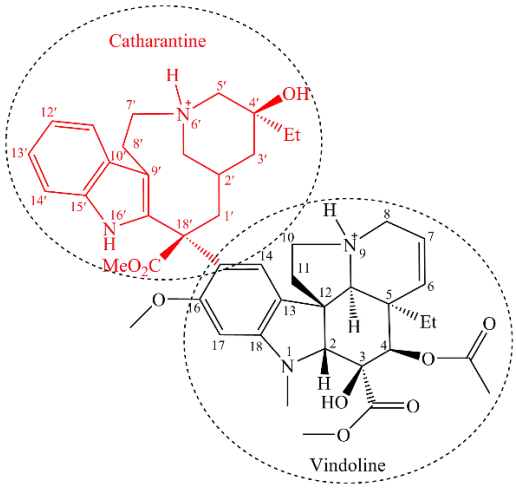

Figure 1.1: Chemical structure of vinblastine.

1.2.2 Vinblastine Target

1.2.2.1 Microtubules

The microtubules (MTs) are one of the main filaments of the cytoskeleton. They are responsible for a variety of intracellular mechanisms such as the transport of proteins, cellular signaling, maintenance of cell structure, segregation of chromosomes, protein trafficking and mitosis [26, 27]. The latter feature gained attention in the chemotherapeutic field as the MTs play a fundamental role in the mitotic spindle function during cell division, hence they could affect the cellular proliferation of cancer cells [28]. Therefore, the mechanism of action of drugs that target the MTs could inhibit the mitotic spindle, as well. The dynamics of the MTs are defined by the polymerization (assembly) and depolymerization (disassembly) states that in turn determine the cellular division [26].

Drugs that bind to the MTs are divided into two main classes of MT stabilizers and destabilizers agents. These drugs have different classifications and bind to different sites

in tubulin heterodimer. VLB is a microtubule-destabilizing agent whose binding site is located at the inter-dimer interfaces of α- and β-subunits of tubulin. Residues of helix H10 of α-subunit of tubulin play a major role in the interactions with VLB and thus causes depolymerization of MTs [29]. (**Figure 1.2**)

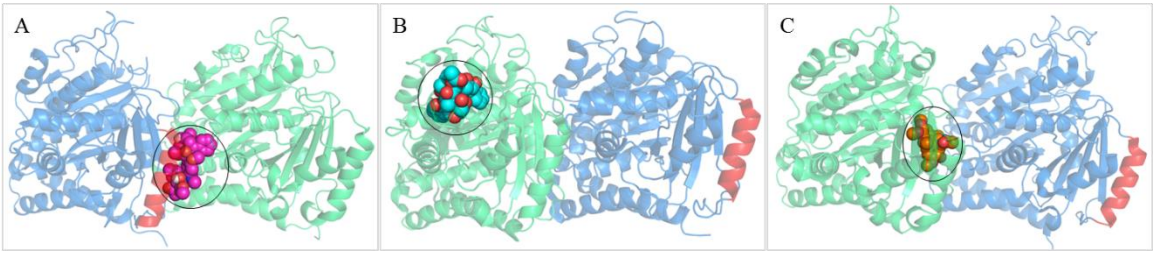

Figure 1.2: Drugs that bind to the tubulin heterodimer. Subunits α- and β-tubulin are shown in blue and green, respectively. Drugs are shown in spheres within a circle. Helix H10 is shown in red. A) VLB (PDB entry 4EB6); B) Paclitaxel (PDB entry 1JFF), and C) Colchicine (PDB entry 4O2B).

1.2.2.2 Vinblastine Binding Site

The binding site of VLB is located in the inter-dimer interface of α- and β-subunits of tubulin, which is also known as the vinca site. In the β-tubulin subunit, the drug interacts with the carboxy-terminal of helix H6, loop T5 and helix H7. In the α-tubulin subunit, it binds to loop T7, helix H10 and strand S9 [27, 28]. Residues Phe351 and Val353 of α-tubulin and residues Lys176 (loop T5) and Tyr208 (helix H6) of β-tubulin make hydrogen bonds (H-bonds) with VLB [28]. Furthermore, residues Ala247, Leu248, Asn249, Pro325, Asn329, Lys352 of α-tubulin and residues Lys174 and Pro220 of β-tubulin interact through hydrophobic interactions with VLB [28].

1.2.3 Absorption, Distribution, Metabolism, Excretion and Toxicity Properties of Vinblastine

VLB is known to be highly distributed throughout the body. A study of combined therapy (Adriamycin, Bleomycin, Vinblastine and Dacarbazine) using VLB administered by IV injection in patients with Hodgkin's lymphoma has shown that VLB reaches a maximum plasma concentration (C_{max}) and maximum time (T_{max}) of 7.95 μg/ml and 0.08 h, respectively [13]. This is due to the rapid plasma availability of VLB upon IV administration [13]. High C_{max} and T_{max} values lead VLB to have a very high area under the curve (AUC) as well as a long half-life ($t_{1/2}$), thus increasing the renal elimination time from the body [13, 24]. Another contribution of slow excretion comes from the high percentage of drug bound to plasma proteins, to which VLB is 99% bound [15, 17]. Due to the high metabolism rate by the hepatobiliary system, the concentration of VLB is found 50 to 100 times higher in the bile than in blood samples [30]. It seems that VLB does not undergo glucoronidation or sulfation during phase II drug metabolism [31]. Drug-drug interactions have been reported with epipodophyllotoxin, a class of anticancer drugs such as etoposide [31], CYP3A4 inhibitors and substrates, phenytoin and mitomycin [15].

1.2.4 Vinblastine Adverse Drug Reactions

It has been more than fifty years since VLB was approved, but the ADRs caused by the high drug toxicity remain poorly understood. The most common ADRs of VLB are nausea, vomiting, diarrhea, alopecia, myelosuppression and anemia [18, 24]. According to Lohr [32], Jordan *et al.* [33] and Shankar *et al.* [34], VLB has a minimal emetogenic risk of less

than 10%. On the other hand, the Clinical Guide to Antineoplastic Therapy [35], suggests that VLB is a moderate emetogenic agent as it occurs in 30%-60% of patients.

1.3 Metabolites of Vinblastine

Due to its molecular complexity, VLB is likely to form a variety of metabolites and hence lead to a variety of ADRs. However, the research for the identification of VLB metabolites and their elucidated chemical structures is still developing. The majority of the experiments regarding the identification of metabolites of VLB are performed *in vivo*, but lack the chemical elucidation of the possible compounds formed during the VLB metabolism.

Three most recent studies have proposed a possible fragmentation of VLB. Twenty chemical structures were indicated as metabolites of VLB and elucidated *in vitro* through mass spectrophotometry technique [36-38]. (**Figure 1.3**)

Moreover, an *in vivo* study of the metabolism of vinorelbine, an analog of VLB, has found possible metabolites for the anticancer drug [39]. The chemical structure of vinorelbine only differs from VLB in the catharantine portion which lacks the hydroxyl group observed in position C20′ of VLB. (**Figure 1.1**)

de Grave *et al.* have identified ten products formed *in vivo* during the metabolism of vinorelbine [39]. Interestingly, a metabolite of vinorelbine which undergoes oxidation and cyclization in the vindoline unit was also previously elucidated by Elmarakby *et al.* as a possible metabolite of VLB [40], thus suggesting that vinorelbine and VLB may go through the same metabolic reactions. Moreover, de Grave *et al.* have considered two metabolic reactions for one metabolite of vinorelbine formed [39]. As the *in vivo* metabolic reactions of VLB have not been fully characterized yet, each metabolic reaction is

considered for one metabolite formed, thus totalizing fifteen metabolites of VLB formed *in vivo*. By saying that, there are thirty-five known metabolites of VLB identified up to date. (**Figure 1.3**)

1.3.1 Vinblastine Metabolic Reactions

VLB mainly undergoes hydroxylation, demethylation and hydrolysis reactions during its metabolism. The metabolites of VLB have their molecular mass varying from 353.44 g/mol to 828.99 g/mol, whereas only a minority of those have their MW increased due to aromatic hydroxylation [36-39]. The VD of VLB is more susceptible to metabolic reactions due to a high number of functional groups prone to metabolism. (**Figure 1.3** and **Table 1.1**)

1.4 Drug Administration, Distribution, Metabolism, Excretion and Toxicology

1.4.1 Solubility, Log P, Log D and Human Jejunal Effective Permeability

The predicted administration, distribution, metabolism, excretion and toxicology (ADMET) is based on different parameters related to the physicochemical properties of drugs. The measured solubility of drug-like compounds is obtained from three different fluid states: fasted state gastric fluid (FaSSGF), fasted state intestinal fluid (FaSSIF) and fed intestinal state fluid (FeSSIF). These fluids mimic the possible environments that a drug would encounter upon oral administration. According to Jantradid *et al.*, a different pH, that corresponds to the *in vivo* characteristics, is calculated for each state fluid such as pH 1.6, 6.5 and 5.8 for FaSSGF, FaSSIF and FeSSIF, respectively [41].

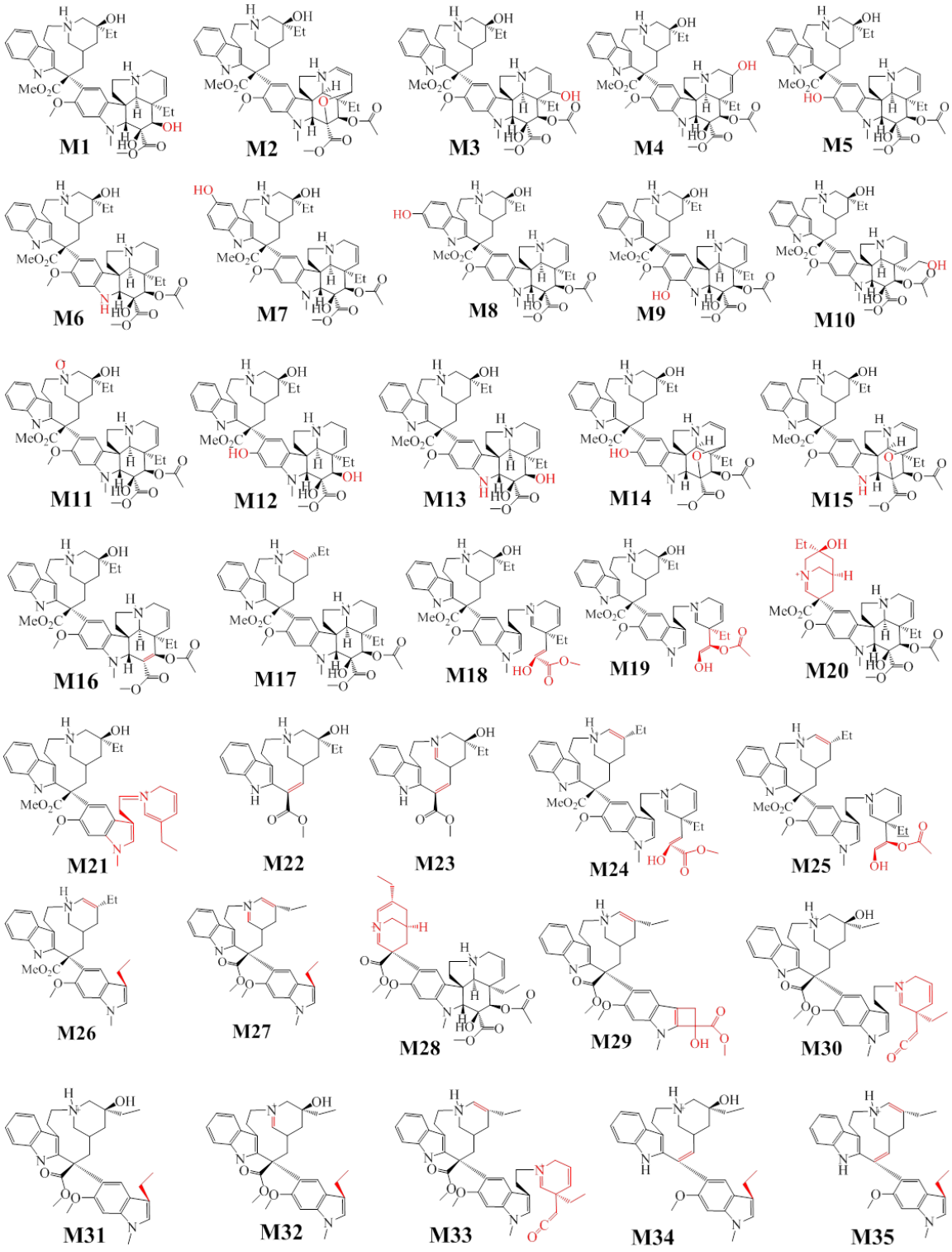

Figure 1.3: Metabolites of VLB.

Table 1.1: Metabolites of VLB, their metabolism reaction, location of reaction, and molecular weight.

Metabolite	Location	Metabolic Reaction	MW(g/mol)	Ref.
MTB1	C4 (VD)	Ester hydrolysis	770.95	
MTB2	C3 (VD)	Deprotonation, oxidation, cyclisation	810.97	
MTB3	C6 (VD)	Ollefin Hydroxylation	828.99	
MTB4	C7 (VD)	Ollefin Hydroxylation	828.99	
MTB5	C16 (VD)	O-demethylation	798.96	
MTB6	N1 (VD)	N-demethylation	798.96	
MTB7	C12′ (CT)	Aromatic Hydroxylation	828.99	
MTB8	C13′ (CT)	Aromatic Hydroxylation	828.99	[39]
MTB9	C17 (VD)	Hydroxylation	828.99	
MTB10	C20 (VD)	Hydroxylation	828.99	
MTB11	N6′ (CT)	N-oxidation	827.98	
MTB12	C16 (VD)	O-demethylation	756.93	
MTB13	N1 (VD)	N-demethylation	756.93	
MTB14	C16 (VD)	O-demethylation	796.95	
MTB15	N1 (VD)	N-demethylation	796.95	
MTB16	C3 (VD)	Dehydration/(17)C-3-dehydration	794.98	
MTB17	C4′ (CT)	Dehydration	794.98	
MTB18	C3 (VD)	Hydrolysis of ester	752.94	
MTB19	C4 (VD)	Hydrolysis of ester/	752.94	
MTB20	C18′ (CT)	Unknown	664.81	
MTB21	(VD)	Retro Diels–Alder	651.86	
MTB22	C18′ (CT)	Hydrolysis/Dehydration	354.44	
MTB23	C18′ (CT)	Hydrolysis/Dehydration	353.44	
MTB24	C4′ (CT)	Dehydration	734.92	
MTB25	C4′ (CT)	Dehydration	734.92	[36-
MTB26	C10 (VD)	Unknown	526.6	38]
MTB27	C10 (VD)	Unknown	524.67	
MTB28	(CT)	Dehydration	664.81	
MTB29	(VD)	Unknown	598.71	
MTB30	(VD)	Oxidation	692.89	
MTB31	(VD)	Unknown	544.70	
MTB32	(VD)	Unknown	542.69	
MTB33	C4′ (CT)	Dehydration	675.88	
MTB34	C18′ (CT)	Hydrolysis of ester	484.65	
MTB35	C4′ (CT)	Dehydration	466.64	

*CT: catharantine portion. VD: vindoline portion.

FaSSIF is correlated with the degree of drug hydrophobicity measured by log P, which is an octanol-water partition coefficient tool useful to measure the lipophilicity and hydrophilicity of a compound. If a compound has a high solubility rate in the intestines, it is likely to have a low log P, meaning that it is very hydrophilic. Very hydrophilic compounds are not able to successfully permeate the membranes as they lack a moderate hydrophilic/lipophilic balance, thus failing to be absorbed into the blood circulation and not achieving effectiveness. Therefore, drugs that have a low permeability across the intestinal membrane, known as the human jejunal effective permeability (P_{eff}) are likely to be rapidly excreted from the body as they are not likely to cross the cell membrane and be absorbed by the body [42].

Log P is strongly related to many physicochemical properties that plays a role in the solubility, absorption, distribution, metabolism and clearance of drugs. The Rule of Five (RO5) proposed by Lipinski [43, 44], states that the log P should be less than 5 for a drug-likeness compound. Drugs with a low log P (<5) are considered hydrophilic compounds due to their polarity. They are also more prone to interact with plasmatic proteins and undergo to phase II metabolic conjugation reactions. On the other hand, structures with too many hydrophobic groups are expected to have a high log P (>5) [42, 43]. The number of rotatable bonds (RB) and Log D value also play a role in the intestinal bioavailability for drug-like oral compounds [44]. A chemical drug with more than 10 RB and a log D higher than 0 and lower than 3 have low intestinal absorption [45].

1.4.2 Volume of Distribution and Plasma Proteins

The ratio of the amount of drug administered to the concentration that reaches to plasma or blood is defined as the volume of distribution (V_d). Thus, the V_d of a drug is useful to estimate the dose required to reach the plasma concentration determined for drug effectiveness. The prediction of the V_d is important as the dose required can vary depending on the height, weight and amount of fat tissue of each individual [46].

Once the drugs reach the ideal plasma concentration in the blood system, they enter into the organs and tissues to encounter their respective target. However, if they have an affinity to bind to plasma proteins they remain in the blood circulation, and thus fail or take long to reach their target. Drugs that are more likely to bind to plasma proteins have polar functional groups in their structures and last a long time in the body due to their slow release time. The percentage of drug that is not bound to plasma protein is the free form of the drug which is able to reach its target [42].

1.4.3 P-glycoprotein and Human ether-à-go-go-related gene

Among the most studied off-target receptors in drug discovery and in clinical research are permeability-glycoprotein (P-gp), human ether-à-go-go-related gene receptor (hERG) and cytochrome P450 complex [47]. P-gp belongs to the ABC transporters family as it is involved in drug cell efflux by using the energy produced by ATP hydrolysis [47]. P-gp is a transmembrane protein able to recognize a variety of xenobiotics due to its location at many different sites in the body such as the liver, intestine, brain and kidneys [48]. P-gp along with cytochrome P450 are the main enzymes that influence the pharmacotherapy

effectiveness as they are able to control cell efflux transporter and drug metabolism, respectively [49].

hERG is involved in the normal action potential of cardiac cells. The blockage of this receptor by xenobiotics is associated with many cardiovascular toxicities such as angina and ischemic events [50, 51].

1.4.4 Cytochrome P450 Complex

Cytochrome P450 complex is a superfamily of heme-containing enzymes that uses nicotinamide adenine dinucleotide phosphate (NADPH) as a co-factor to metabolize more than 90% of drugs. The main reactions that CYPs catalyze are hydroxylation, dealkylation, and heteroatom oxidation. From fifty-seven CYP isoforms, only nine are clinically relevant such as CYP1A2, CYP2A6, CYP2B6, CYP2C8, CYP2E1, CYP2C9, CYP2C19, CYP2D6 and CYP3A4. These metabolizing enzymes have more than 55% of sequence similarity and metabolize a great number of endogenous and exogenous compounds, either by oxidizing or reducing them [52].

CYP3A4 is the main enzyme of CYP450 complex as it is responsible for the metabolism of 50% of drugs [47, 48, 53]. Usually, most of the drugs which are substrates and/or inhibitors of P-gp are also considered the same for CYP3A4 and vice-versa [54]. Essentially, drugs that are substrates of both P-gp and CYP3A4 are extremely important because these proteins are located in the hepatocytes and enterocytes, cells that are crucial for absorption and metabolism of drugs [55]. As part of phase I reactions, CYP450 enzymatic complex is the main route by which drugs are metabolized. Compounds that undergo reactions with this complex aim to become more soluble for easier excretion from

the body. However, these enzymes can also trigger metabolic reactions that turn drugs and its metabolites into reactive compounds that can further bind to off-target sites [56].

1.4.4.1 CYP1A2, CYP2C8 and CYP2C9

CYP1A2 have been described to facilitate the metabolism of certain class of medicines such as tricyclics antidepressants, antipsychotics, antihypertensive, and antiemetic drugs as ondansetron [57]. Ondansetron is a selective serotonin (5-HT3) receptor antagonist of nausea associated receptors and commonly used to treat nausea during chemotherapy. It is administered as a prophylactic treatment on the onset of symptoms [58, 59]. As a substrate of CYP1A2, ondansetron is also an inhibitor and substrate of CYP3A4 [60].

CYP2C8 is responsible for the metabolism of 35% of drugs due to its ability to accommodate large structures despite their hydrophobic character. The active site of this isoform is quite unique as it can, for instance, interact with anionic groups present in steroids and retinoid drugs [53].

CYP2C9 is responsible for the metabolism of common and widely used class of drugs such as antidepressants and anti-inflammatories [57]. This isoenzyme is the most second abundant in the small intestine, only behind CYP3A4 [61].

1.4.4.2 CYP2D6

CYP2D6 accounts for less than 2% of the isoforms of CYP450 complex. However, it is known to metabolize more than 25% of the drugs. Its endogenous substrates are hydroxytryptamines and neurosteroids [62, 63] which are metabolized into serotonin, dopamine and testosterone [62]. Ligands having a lipophilic character contain a planar

hydrophobic component such as an aromatic ring. Drugs containing nitrogen atoms are likely to be protonated in the physiological pH and can also play a role in this enzyme [63]. It is noteworthy that this is a matter of chemical conformation and structure specificity within the active site of CYP2D6. Wang *et al.* have demonstrated that substrates of this enzyme are likely to have a nitrogen atom in 5-7 Å distant from the site of oxidation. Moreover, CYP2D6 triggers a variety of metabolic reactions such as demethylation, hydroxylation and oxidation [62]. The active site of CYP2D6 has an area of 540 $Å^2$ and contains nearly 28 residues which are located around the heme group [64].

1.4.4.3 CYP3A4

The isoform CYP3A4 plays the greatest role in drug metabolism. It is found in the intestine and liver in high amounts, while its natural substrates include retinoic acids, steroids and bile acids [53]. CYP3A4 is considered the largest human enzyme of the CYP complex, formed by 502 residues (57.29 kDa). It has a reasonable variability among individuals due to differences in gender hormones, environment and genetic factors [65, 66].

Because more than 60% of drugs are metabolized by CYP3A4, this enzyme is of extremely importance in drug-drug interactions caused by competition of CYP3A4. This can further account for a decrease of drug plasma concentration and poor treatment efficacy [65].

CYP3A4 is located in the apex of enterocytes cells, a unique site that enhances the chances of this enzyme to meet xenobiotics that probably explains its main role in the metabolism first-pass effect [53]. The likelihood of binding of drugs is easily favored to

the CYP3A4 due to its active site being much larger than CYP2D6 (1385 $Å^2$ vs. 540 $Å^2$) [62, 66].

1.5 Molecular Simulation

1.5.1 Molecular Docking

The pharmaceutical research field makes use of technologies based on structure-activity relationship (SAR) and structure-based drug design (SBDD) for the prediction of drug pharmacodynamics and pharmacokinetics (PK) properties, drug development and repositioning/repurposing, and protein-ligand molecular recognition [67]. Advances in protein purification, crystallography methods and nuclear magnetic resonance spectroscopy have vastly contributed to the medicinal chemistry research field due to the availability of knowledge of target protein structures and protein-ligand interactions [67, 68]. In addition, developments within computational experiments as part of SBDD approaches have aided in the elucidation of the behavior of small molecules in the protein active site as well as protein-protein interactions in atomistic levels [67, 68]. One of the most useful and used applications in SBDD strategies is molecular docking techniques.

Molecular docking is a key *in silico* tool that aims to predict the best conformation of the ligand into the binding pocket of a protein by calculating the binding energy of the ligand [67-69]. It requires two step process known as the conformational pose of the ligand in the protein binding site accessed by a sampling algorithm, and prediction of the binding affinity which is achieved by a scoring function [67, 68]. Thus, molecular docking experiments involve searching for the best conformation and scoring conformations based on their binding energy (i.e. a representation of affinity to the receptor). Koshland conceptualized the theory involving ligand-protein binding by suggesting that the interaction should be considered in flexible mode [70]. The “induced-fit” theory suggests

that as the ligand binds to the receptor, the protein active site changes its shape to fit the ligand [69, 70]. Thus, this theory defines that both receptor and ligand are flexible [68].

Widely known software programs that adopt the flexible ligand docking include *FlexX* [69] and *AutoDock* [71]. Molecular docking programs are based on different sampling algorithms such as matching, genetic and incremental construction algorithms [67]. In addition, the best binding energy of the ligand predicted by molecular docking programs is calculated with different scoring functions such as knowledge-based, empirical and force-field-based [67, 68]. However, they all search for the best orientation pose and molecular interactions by considering all the inter-atomic forces between a ligand and its surrounding environment in the binding site. In particular, *FlexX* (used in this project), a commercial software package developed by BioSolveIT, is frequently utilized in the drug discovery field of small molecules and analysis of ligand-protein interactions.

1.5.1.1 *FlexX* Algorithm and Scoring Function

The search for the best conformation of a small molecule into the binding site of a protein depends on the torsional, translational and rotational degrees of freedom of the ligand as well as the interaction types and strength between a ligand and the binding site [67, 68]. Therefore, a great number of possible conformations can be adapted by either the ligand/protein or ligand-protein complex. Despite advances in the computer-aided drug discovery, it still takes a large amount of CPU time to generate all possible conformations. Thus the use of sampling algorithms is required to optimize this issue [68].

FlexX uses an incremental construction algorithm that searches for the energetically favorable conformations of the ligand for their optimized binding to the protein target [69].

Initially, it selects one of the fragments of the ligand by breaking the rotatable bonds and setting its moiety as a base-fragment in the binding site. Then it adds the remaining moieties of the ligand to the base-fragment [68, 69]. The order that the remaining fragments are added to the base-fragment depends on their favorable binding energies and orientation. For instance, those which are more prone to form H-bonds or salt bridges are added first. This is because these interactions are more geometrically and directionally stable [69]. The algorithm of *FlexX* constructs the ligand in an incremental fashion by finding the best binding mode of the ligand in the binding site of a protein and providing the total Gibbs energy of the ligand-protein complex.

The foundation set for the best conformation of the ligand is based on the sum of all binding interactions between a ligand and the target receptor which mainly include hydrogen bonds (H-bond(s)) and hydrophobic interactions, electrostatic interactions, and van der Waals (vdW) forces [69, 72].

Electrostatic interactions exist in both intramolecular and intermolecular forces. They comprise hydrogen bonds and ionic interactions, and follow Coulomb's law, V_c. The sum of interactions among atoms i and j with two charges q_i and q_j and distance r is given below [73]:

$$V_c(r_{ij}) = \frac{1}{4\pi\varepsilon_0}\frac{q_i q_j}{\varepsilon_r r_{ij}} \qquad (\boldsymbol{Equation\ 1.1})$$

Where ε_0 is the electric constant or the vacuum permittivity that relates the units of electric charges to mechanical quantities; ε_r is the relative permittivity that is a decreased

factor relative to the vacuum due to the electric field between the charges, and π, which is the log (P_x / P_H) for a substituent X relative to a hydrogen substituent [73].

Van der Waals (vdW) force involves repulsive and attractive forces and is best known through the *Lennard-Jones 12-6 function*, V_{LJ}. The intermolecular distance defined as r_{ij}, separates the interaction among atoms *i* and *j*, and thus vdW forces are calculated as given below [73]:

$$V_{LJ}(r_{ij}) = 4\varepsilon\left[\left(\frac{\sigma}{r_{ij}}\right)^{12} - \left(\frac{\sigma}{r_{ij}}\right)^{6}\right] \qquad (\boldsymbol{Equation\ 1.2})$$

Where $(r_{ij})^{12}$ and $(r_{ij})^{6}$ are defined as the distance between atoms *i* and *j*, ε corresponds to the depth of the potential well, and σ is the finite distance at which the inter-particle potential is zero [73].

The output docking solutions for the ligands are ranked according to their total binding energy based on Böhm empirical scoring function [69, 72, 74, 75]. The Böhm scoring function, used in *FlexX* tool, estimates the free binding energy for the protein-ligand complex, which is known as Gibbs energy ($\Delta G_{binding}$) [72]. Thus, the best binding energy is the lowest binding energy (first rank) or the highest binding affinity.

The approach used by Böhm which involves hydrogen bonding, ionic and hydrophobic interactions as well as the loss of internal degrees of freedom of the ligand as a result of binding is shown below:

$$\Delta G_{binding} = \Delta G_0 + \Delta G_{hb} \sum_{h-bonds} f(\Delta R, \Delta\alpha) + \Delta G_{ionic} \sum_{ionic\ interactions} f(\Delta R, \Delta\alpha) + \Delta G_{lipo} \left|A_{lipo}\right| + \Delta G_{rot} NROT \qquad (\boldsymbol{Equation\ 1.3})$$

Where ΔG_0 is the overall change in Gibbs rotational/translational degree of free energy; ΔG_{hb} is the contribution of hydrogen bonds which is multiplied by a penalty function $f(\Delta R, \Delta\alpha)$ derived from large geometric deviations such as distances and angles from an ideal hydrogen bond; the same is applied for ΔG_{ionic} function; hydrophobic interactions which are defined as ΔG_{lipo}, are supposed to be proportional to the lipophilic contacts among ligand and protein, and is expressed by A_{lipo}. Finally, $\Delta G_{rot} NROT$ is the loss of Gibbs energy caused by the number of rotatable bonds of the ligand when it is bound to protein [72, 73].

1.6 Bibliography

1. WHO, *World Health Organization - Cancer Fact Sheets*. **2018**.
2. Statistics, C.C.S.s.A.C.o.C., *Canadian Cancer Statistics 2017*. **2017**: Toronto, ON.
3. WHO. *World Health Organization - Facts about cancer*. **2017** [cited 2018 Jan 30]; Available from: http://www.who.int/en/.
4. Miller, K.D., et al., *Cancer treatment and survivorship statistics, 2016.* CA Cancer J Clin, **2016**. 66(4): p. 271-89.
5. Holt, K., *Common side effects and interactions of colorectal cancer therapeutic agents.* J Pract Nurs, **2011**. 61(1): p. 7-20.
6. Sun, C.C., et al., *Rankings and symptom assessments of side effects from chemotherapy: insights from experienced patients with ovarian cancer.* Support Care Cancer, **2005**. 13(4): p. 219-27.
7. Beusterien, K., et al., *Use of conjoint analysis to assess breast cancer patient preferences for chemotherapy side effects.* Oncologist, **2014**. 19(2): p. 127-34.
8. Colagiuri, B., et al., *Does assessing patients' expectancies about chemotherapy side effects influence their occurrence?* J Pain Symptom Manage, **2013**. 46(2): p. 275-81.
9. Kuchuk, I., et al., *Preference weights for chemotherapy side effects from the perspective of women with breast cancer.* Breast Cancer Res Treat, **2013**. 142(1): p. 101-7.

10. Johnson, I.S., et al., *The Vinca Alkaloids: A New Class of Oncolytic Agents.* Cancer Res, **1963**. 23: p. 1390-427.

11. Moudi, M., et al., *Vinca alkaloids.* Int J Prev Med, **2013**. 4(11): p. 1231-5.

12. Long, Q.Z., et al., *Interaction of CCN1 with alphavbeta3 integrin induces P-glycoprotein and confers vinblastine resistance in renal cell carcinoma cells.* Anticancer Drugs, **2013**. 24(8): p. 810-7.

13. Malik, M.Z., et al., *Pharmacokinetic evaluation of anticancer drugs in Hodgkin's lymphoma patients after their simultaneous administration.* Pak J Pharm Sci, **2016**. 29(6): p. 2079-2082.

14. Auyeung, K.K., P.C. Law, and J.K. Ko, *Combined therapeutic effects of vinblastine and Astragalus saponins in human colon cancer cells and tumor xenograft via inhibition of tumor growth and proangiogenic factors.* Nutr Cancer, **2014**. 66(4): p. 662-74.

15. *BC Cancer Agency Cancer Drug Manual - Vinblastine*. **2015**.

16. Hong, A., et al., *Distinct Fragmentation Pathways of Anticancer Drugs Induced by Charge-Carrying Cations in the Gas Phase.* J Am Soc Mass Spectrom, **2016**.

17. *Pfizer Product Monography - Vinblastine Sulfate Injection.* **2017**.

18. *Cancer Care Ontario - Vinblastine.* **2016**.

19. *Micromedex*. **2017**; Available from: http://www.micromedexsolutions.com/micromedex2/librarian/.

20. Leveque, D. and F. Jehl, *Molecular pharmacokinetics of catharanthus (vinca) alkaloids.* J Clin Pharmacol, **2007**. 47(5): p. 579-88.

21. Vassallo, C., et al., *Intralesional vinblastine injections for treatment of classic Kaposi sarcoma in diabetic patients.* Cutis, **2015**. 95(5): p. E28-34.

22. Ramirez-Amador, V., et al., *Intralesional vinblastine vs. 3% sodium tetradecyl sulfate for the treatment of oral Kaposi's sarcoma. A double blind, randomized clinical trial.* Oral Oncol, **2002**. 38(5): p. 460-7.

23. Administration, U.F.D. *Vinblastine sulfate*. **2017** [cited 2017 Aug 15]; Available from: https://www.fda.gov/.

24. Zhou, X.J. and R. Rahmani, *Preclinical and clinical pharmacology of vinca alkaloids.* Drugs, **1992**. 44 Suppl 4: p. 1-16; discussion 66-9.

25. R. Bau, K.K.J., *Cystal structure of vinblastine.* The Royal Society of Chemistry, **2000**: p. 2079-2082.

26. Stanton, R.A., et al., *Drugs that target dynamic microtubules: a new molecular perspective.* Med Res Rev, **2011**. **31**(3): p. 443-81.

27. Gigant, B., et al., *Structural basis for the regulation of tubulin by vinblastine.* Nature, **2005**. 435(7041): p. 519-22.

28. Li, Z. and L. Alisaraie, *Microtubules dual chemo and thermo-responsive depolymerization.* Proteins, **2015**. 83(5): p. 970-81.

29. Ranaivoson, F.M., et al., *Structural plasticity of tubulin assembly probed by vinca-domain ligands.* Acta Crystallogr D Biol Crystallogr, **2012**. 68(Pt 8): p. 927-34.

30. Zhou, X.J., et al., *In vivo and in vitro pharmacokinetics and metabolism of vincaalkaloids in rat. II. Vinblastine and vincristine.* Eur J Drug Metab Pharmacokinet, **1990**. 15(4): p. 323-32.

31. Owellen, R.J., C.A. Hartke, and F.O. Hains, *Pharmacokinetics and metabolism of vinblastine in humans.* Cancer Res, **1977**. 37(8 Pt 1): p. 2597-602.

32. Lohr, L., *Chemotherapy-induced nausea and vomiting.* Cancer J, **2008**. 14(2): p. 85-93.

33. Jordan, K., et al., *International antiemetic guidelines on chemotherapy induced nausea and vomiting (CINV): content and implementation in daily routine practice.* Eur J Pharmacol, **2014**. 722: p. 197-202.

34. Shankar, A., et al., *Prevention of Chemotherapy-Induced Nausea and Vomiting in Cancer Patients.* Asian Pac J Cancer Prev, **2015**. 16(15): p. 6207-13.

35. Magee, M., *Clinical Guide to Antineoplastic Therapy - A Chemotherapy Handbook*. 3rd Edition ed. **2014**: Oncology Nursing Society.

36. Beni, Z., et al., *Structure elucidation of indole-indoline type alkaloids: a retrospective account from the point of view of current NMR and MS technology.* J Pharm Biomed Anal, **2012**. 69: p. 106-24.

37. Dubrovay, Z., et al., *NMR and mass spectrometric characterization of vinblastine, vincristine and some new related impurities - part I.* J Pharm Biomed Anal, **2013**. 84: p. 293-308.

38. Hada, V., et al., *NMR and mass spectrometric characterization of vinblastine, vincristine and some new related impurities--part II.* J Pharm Biomed Anal, **2013**. 84: p. 309-22.

39. de Graeve, J., et al., *Metabolism pathway of vinorelbine (Navelbine) in human: characterisation of the metabolites by HPLC-MS/MS.* J Pharm Biomed Anal, **2008**. 47(1): p. 47-58.

40. Elmarakby, S.A., M.W. Duffel, and J.P. Rosazza, *In vitro metabolic transformations of vinblastine: oxidations catalyzed by human ceruloplasmin.* J Med Chem, **1989**. 32(9): p. 2158-62.

41. Jantratid, E., et al., *Dissolution media simulating conditions in the proximal human gastrointestinal tract: an update.* Pharm Res, **2008**. 25(7): p. 1663-76.

42. Graham, L.P., *Introduction to Medicinal Chemistry* Fifth ed. **2013**: Oxford.

43. Lipinski, C.A., et al., *Experimental and computational approaches to estimate solubility and permeability in drug discovery and development settings.* Adv Drug Deliv Rev, **2001**. 46(1-3): p. 3-26.

44. Chagas, C.M., S. Moss, and L. Alisaraie, *Drug metabolites and their effects on the development of adverse reactions: Revisiting Lipinski's Rule of Five.* Int J Pharm, **2018**. 549(1-2): p. 133-149.

45. Lipinski, C.A., *Lead- and drug-like compounds: the rule-of-five revolution.* Drug Discov Today Technol, **2004**. 1(4): p. 337-41.

46. Smith, D.A., et al., *Volume of Distribution in Drug Design.* J Med Chem, **2015**. 58(15): p. 5691-8.

47. Broccatelli, F., et al., *A novel approach for predicting P-glycoprotein (ABCB1) inhibition using molecular interaction fields.* J Med Chem, **2011**. 54(6): p. 1740-51.

48. Silva, R., et al., *Modulation of P-glycoprotein efflux pump: induction and activation as a therapeutic strategy.* Pharmacol Ther, **2015**. 149: p. 1-123.

49. Staud, F., et al., *Expression and function of p-glycoprotein in normal tissues: effect on pharmacokinetics.* Methods Mol Biol, **2010**. 596: p. 199-222.

50. Rosa, G.M., et al., *Update on cardiotoxicity of anti-cancer treatments.* Eur J Clin Invest, **2016**. 46(3): p. 264-84.

51. Diaz, G.J., et al., *The [3H]dofetilide binding assay is a predictive screening tool for hERG blockade and proarrhythmia: Comparison of intact cell and membrane preparations and effects of altering [K+]o.* J Pharmacol Toxicol Methods, **2004**. 50(3): p. 187-99.

52. de Groot, M.J., et al., *Understanding CYP2D6 interactions.* Drug Discov Today, **2009**. 14(19-20): p. 964-72.

53. DeLisle, R.K., J. Otten, and S. Rhodes, *In silico modeling of p450 substrates, inhibitors, activators, and inducers.* Comb Chem High Throughput Screen, **2011**. 14(5): p. 396-416.

54. Rubio-Gonzalez, B., et al., *Pathogenesis and treatment options for chemotherapy-induced alopecia: a systematic review.* Int J Dermatol, **2018**.

55. Kim, R.B., *Drugs as P-glycoprotein substrates, inhibitors, and inducers.* Drug Metab Rev, **2002**. 34(1-2): p. 47-54.

56. Stachulski, A.V., et al., *The generation, detection, and effects of reactive drug metabolites.* Med Res Rev, **2013**. 33(5): p. 985-1080.

57. Chandrani, G., *Drug Metabolism & Pharmacokinetics in Drug Discovery: A Primer for Bioanalytical Chemists, Part I.* Current Separations, **2000**. 19:1.

58. Soukop, M., et al., *Ondansetron compared with metoclopramide in the control of emesis and quality of life during repeated chemotherapy for breast cancer.* Oncology, **1992**. 49(4): p. 295-304.

59. Wenzell, C.M., et al., *Pilot study on the efficacy of an ondansetron- versus palonosetron-containing antiemetic regimen prior to highly emetogenic chemotherapy.* Support Care Cancer, **2013**. 21(10): p. 2845-51.

60. Youssef, A.S., H.P. Parkman, and S. Nagar, *Domperidone interacts with pioglitazone but not with ondansetron via common CYP metabolism in vitro.* Xenobiotica, **2014**. 44(9): p. 792-803.

61. Zhou, S.F., et al., *Substrates, inducers, inhibitors and structure-activity relationships of human Cytochrome P450 2C9 and implications in drug development.* Curr Med Chem, **2009**. 16(27): p. 3480-675.

62. Wang, B., et al., *New insights into the structural characteristics and functional relevance of the human cytochrome P450 2D6 enzyme.* Drug Metab Rev, **2009**. 41(4): p. 573-643.

63. Zhou, S.F., J.P. Liu, and X.S. Lai, *Substrate specificity, inhibitors and regulation of human cytochrome P450 2D6 and implications in drug development.* Curr Med Chem, **2009**. 16(21): p. 2661-805.

64. Rowland, P., et al., *Crystal structure of human cytochrome P450 2D6.* J Biol Chem, **2006**. 281(11): p. 7614-22.

65. Zhou, S.F., *Drugs behave as substrates, inhibitors and inducers of human cytochrome P450 3A4.* Curr Drug Metab, **2008**. 9(4): p. 310-22.

66. Yano, J.K., et al., *The structure of human microsomal cytochrome P450 3A4 determined by X-ray crystallography to 2.05-A resolution.* J Biol Chem, **2004**. 279(37): p. 38091-4.

67. Ferreira, L.G., et al., *Molecular Docking and Structure-Based Drug Design Strategies.* Molecules, **2015**. 20(7): p. 13384-13421.

68. Meng, X.Y., et al., *Molecular docking: a powerful approach for structure-based drug discovery.* Curr Comput Aided Drug Des, **2011**. 7(2): p. 146-57.

69. Rarey, M., et al., *A fast flexible docking method using an incremental construction algorithm.* J Mol Biol, **1996**. 261(3): p. 470-89.

70. Koshland, D.E., Jr., *Correlation of Structure and Function in Enzyme Action.* Science, **1963**. 142(3599): p. 1533-41.

71. Osterberg, F., et al., *Automated docking to multiple target structures: incorporation of protein mobility and structural water heterogeneity in AutoDock.* Proteins, **2002**. 46(1): p. 34-40.

72. Bohm, H.J., *The development of a simple empirical scoring function to estimate the binding constant for a protein-ligand complex of known three-dimensional structure.* J Comput Aided Mol Des, **1994**. 8(3): p. 243-56.

73. Leach, A.R., *Molecular Modelling: Principles and Applications*. 2nd ed ed. **2001**: Prentice Hall.

74. Rarey, M., B. Kramer, and T. Lengauer, *Multiple automatic base selection: protein-ligand docking based on incremental construction without manual intervention.* J Comput Aided Mol Des, **1997**. 11(4): p. 369-84.

75. Rarey, M., B. Kramer, and T. Lengauer, *Docking of hydrophobic ligands with interaction-based matching algorithms.* Bioinformatics, **1999**. 15(3): p. 243-50.

CHAPTER 2 Effects of Vinblastine and its Metabolites on Nausea Associated Receptors

2.1 Introduction

2.1.1 Chemotherapy-Induced Nausea and Vomiting

Chemotherapy-induced nausea and vomiting (CINV) is the most common and unpleasant ADR during cancer treatment [1-4]. CINV is classified into three categories: i) acute onset, ii) delayed onset, and iii) anticipatory nausea and vomiting. This is, the onset of symptoms that can occur either in the first 24h, in the first five days or after a completed cycle of chemotherapy [1].

The emetogenic profile of chemotherapeutic agents is defined as the relative percentage of the drug to induce emesis during chemotherapy. It is classified in four potential risks such as minimal (<10%), low (10-30%), moderate (30-90%) and high (>90%) [1, 5, 6]. CINV does not only impact the patient's quality of life but can also lead to disease complications such as dehydration and malnutrition [1]. There are many prophylactic interventions to avoid or attenuate CINV with antiemetic drugs such as olanzapine, ondansetron or a combination of other nausea associated receptor antagonists [1, 7]. The American Society of Clinical Oncology provides the most updated guideline for antiemetics used in oncology [8]. However, CINV still remains an issue for the healthcare system and cancer patients.

2.1.2 Nausea Associated Receptors

Nausea is stimulated by a variety of mechanisms in our body. For instance, the chemoreceptor trigger zone is located in the fourth ventricle and is a very vulnerable area found outside the blood brain barrier (BBB) [9]. This zone sends signals to the vomiting center when stimulated by xenobiotics such as the antineoplastic drugs, thus activates neurotransmitters such as dopamine and serotonin. The vestibular system responsible for the sense of balance and spatial orientation is mediated by the neurotransmitters acetylcholine (ACh) and histamine and it is also involved in nausea-induced symptoms. Other mechanisms such as the gastrointestinal (GI) tract and the cerebral cortex can also stimulate the vomiting center and cause emesis [9]. Flynn *et al.* have thoroughly investigated the main neurotransmitters involved in nausea and how this symptom is highly associated with anticancer drugs through the activation of nausea associated receptors [10].

Dopamine, histamine, ACh and serotonin are the main neurotransmitters known to play important roles in emesis [10]. These molecules bind specifically to nausea associated receptors such as dopaminergic (D_1, D_2, D_3, D_4, D_5), histaminic (H_1, H_2, H_3, H_4), muscarinic (M_1, M_2, M_3, M_4 and M_5) and serotoninergic (5-HT_1-5-HT_7), respectively. They belong to the largest membrane bound family of proteins known as G-coupled protein receptors (GCPRs), which are responsible for a variety of mechanisms within the cell such as signaling, transport and response. Moreover, cannabinoid, corticosteroid, neurokinin-1, GABAminergic and opioids are also receptors included in nausea pathway, however, they are not discussed in this study [6, 9, 10].

2.1.2.1 Dopaminergic Receptors

Dopaminergic receptors are classified into five different subtypes: D_1, D_2, D_3, D_4 and D_5. These receptors share a high homology but distinct pharmacological features in between. For instance, D_1R with D_5R, as well as D_2R with D_3R and D_4R share structure similarity, but they have different drug responses due to differences in their amino acid sequence. They are comprised of seven-transmembrane domains and their molecular mechanisms involve regulation of cAMP (cyclic adenosine monophosphate), which triggers a variety of biological signaling. Dopamine is the endogenous substrate of these receptors, known to play an important role in neurological dysfunctions such as Parkinson's disease and schizophrenia. In particular, antagonists of dopaminergic receptors have been extensively studied for the treatment of nausea and psychological disorders [11]. These drugs act by inhibiting dopamine to bind to its receptor, thus prevent its activation. Osinski *et al.* have shown that D_2R and D_3R trigger emesis process in ferrets treated with specific receptor agonists [12].

2.1.2.2 Histaminic Receptors

A variety of mechanisms involved mainly in allergy and inflammation are unleashed through the activation of histaminic receptor subtypes H_1, H_2, H_3 and H_4 by its natural substrate, histamine. This endogenous compound also plays an important role in regulating the mucosa immunity, motility, neurotransmission and visceral nociception of the GI tract. The synthesis of the endogenous substrate occurs mainly in the mast cells, platelets and basophils cells via decarboxylation of histidine [13-15].

Sullivant *et al.* have shown that the presence of subtypes H_1, H_2, and H_3 are more highly expressed throughout the GI tract of dogs with canine inflammatory bowel disease than the subtype H_4 [15]. This is in agreement with previous research performed in humans that demonstrates similar distribution of histaminic receptors in the GI tract [16]. In particular, H_1R is extensively distributed in the smooth muscle and gastric mucosa, and H_3R is mainly found at the myenteric plexus, a major nerve supply also involved in motility [15, 16]. Therefore, the histaminic receptors, which are mainly involved in causing nausea are H_1R and H_3R.

Among the antagonists of H_1R, a class of drugs known as piperazines are often prescribed to control nausea symptoms in patients with cancer. A case report of 2008 in United Kingdom shows that cyclizine, a second generation of antagonists H_1R, is effective in managing nausea induced by chemotherapy [17]. Studies of H_1R antagonists have also demonstrated that this class of drugs are also effective in postoperative nausea and vomiting [18].

2.1.2.3 Muscarinic Receptors

The identified muscarinic receptors are divided into five subtypes: M_1, M_2, M_3, M_4 and M_5, which all of them exhibit high sequence similarity with each other. Highly expressed in the parasympathetic system, these receptors regulate functions of the GI tract, endocrine and cardiac systems. The muscarinic receptors, also known as cholinergic receptors are expressed in the central nervous system. Thus, they are involved in memory, learning and cognitive functions, as well [19].

The endogenous substrate responsible for the activation of muscarinic receptors, ACh, exerts physiological effects in hormonal and neuronal pathways. As ACh is found both in the vestibular and GI systems, antagonists of the natural ligand are useful drugs to treat nausea induced by different mechanisms. Anticholinergic agents such as scopolamine, a non-specific antagonist of muscarinic receptors, has been extensively studied for the relief of nausea caused by chemotherapy and/or postoperative situations [20]. More specifically, M_1R and M_5R antagonists have been reported as effective drug targets during nausea induced by cancer treatment [21, 22].

2.2 Material and Method

2.2.1 Energy minimization

A library consisting of the structures of VLB and its thirty-five known metabolites were built up using SYBYL®-X 2.1.1, a commercial molecular modelling and simulation package developed by Certera™. Metabolites were minimized step-wise using Pullman atomic charges and Tripos force field starting from 1.0 kJ/mol to 0.001 kJ/mol energy gradient each through 1000 iterations. In addition, the chemical structures of the natural substrates histamine, dopamine, and ACh were set to correct protonation states for molecular docking.

2.2.2 Molecular Docking

The natural endogenous substrates as well as the library of VLB and metabolites were docked into the binding pocket of each nausea associated receptors H_1, H_3, D_2, M_1, M_4 and M_5. These individual *in silico* experiments were carried out using *FlexX* program embedded in the LeadIT software package (version 2.1.8). Our laboratory has previously

performed studies with these nausea associated receptors. The homology modelling of the protein structures H_3R, D_2R, M_1R, M_4R and M_5R used here have already been modelled and described elsewhere [10]. The crystalized structure of H_1R was retrieved from the PDB entry 3RZE [14] where water molecules were removed, side chains and atom charges were calculated, and protonation states were adjusted for further energy minimization with AMBER7 FF99 force field.

The binding pocket of H_1R can accommodate two different charge states of the agonist histamine, dicationic with a protonated imidazole ring and monocationic with a neutral imidazole ring [23]. According to previous studies, all endogenous substrates of the nausea receptors have the amine group in the protonated state and are positively charged [23-26]. (**Figure 2.1**)

H_1R: The binding pocket of H_1R (PDB 3RZE), comprised of hydrophobic residues, is formed by three α-helices: α3 (residues 96-130), α5 (188-216) and α6 (408-441) [10, 14]. The crystal structure used for H_1R contains the antagonist doxepin that was used as a reference ligand for the docking experiments into H_1R. A spherical region with a radius of 20 Å surrounding doxepin was chosen as the target site for molecular docking of histamine, VLB and metabolites.

H_3R: The binding pocket of H_3R (UniProtKB Q9Y5N1) is also formed by hydrophobic interactions that involves helices α3, α4 and α5 which respectively comprise residues 104-137, 141-178 and 196-225 [10, 13, 27]. A spherical region with a radius of 20 Å around residue Asp114 located at α3 was selected as the target site for docking VLB, its metabolites and histamine into the binding site of homology model of H_3R.

D_2R: The binding pocket of D_2R (UniProtKB P14416) is located between helices α3 (residues 104-137), α4 (151-171), α5 (187-220) and α6 (336-369), while residue Asp114 is involved in an H-bond with the endogenous substrate dopamine [10, 28-30]. Thus, a spherical region with a radius of 20 Å around Asp114 was defined as the target site for docking the library of metabolites, VLB and dopamine into D_2R.

M_1R: The hydrophobic pocket located at helices α2, α6 and α7 are involved in the binding of ACh and antagonists into M_1R (UniProtKB P11229), whereas α3, α4, α5, α6 and α7 interact with the anticholinergic agents. To define the binding site of M_1R, a spherical region with a radius of 20 Å around residue Asp105 was chosen as the target site for docking VLB, its metabolites and ACh. This residue is involved in the binding of agonists and antagonists of M_1R through electrostatic interactions [10, 31, 32].

M_4R: For the binding pocket of M_4R (UniProtKB P08173), a spherical region with a radius of 20 Å around residue Tyr113 was defined as the target site for docking VLB, its metabolites and ACh [32, 33].

M_5R: The binding site of M_5R (UniProtKB P08912) is located between α2 (residues 62-93), α3 (99-133), α4 (142-166), α5 (189-215), α6 (435-467) and α7 (472-495). A spherical region with a radius of 20 Å surrounding residue Asp109, which is involved in the agonist and antagonist interactions within M_5R, was chosen as the target site for docking the natural substrate, VLB and its metabolites [10, 34].

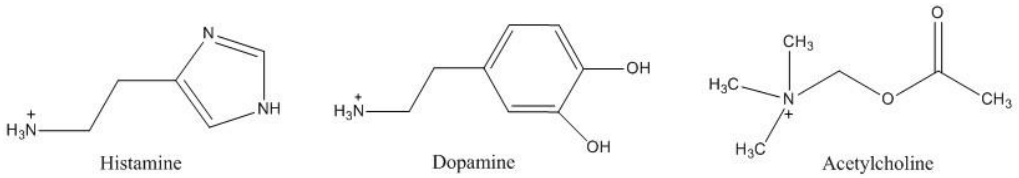

Figure 2.1: Chemical structures of main neurotransmitters involved with the nausea associated receptors.

2.2.3 *In silico* Prediction of Absorption, Distribution, Metabolism, Excretion and Toxicology Properties

ADMET Predictor™ (version 7.2) [35] is a state-of-the-art software package developed by Simulation Plus, which predicts the Absorption, Distribution, Metabolism, Excretion and Toxicology (ADMET) properties of drugs or lead compounds with respect to their chemical structure. ADMET is used to calculate the pharmacokinetics and pharmacodynamics of molecular compounds by mimicking physiological conditions under pH 7.4. The parameters predicted by ADMET Predictor are based on pre-existing *in vitro* and *in vivo* data [35]. This software provides *in silico* data for over 140 PK parameters such as the gastric and intestinal solubility, log P, and the likelihood of drugs crossing the blood-brain barrier (BBB). In addition, it calculates the affinity for a diverse number of proteins/enzymes or receptors involved in drug effectiveness and drug-drug interactions, such as P-glycoprotein, plasma proteins, human ether-à-go-go-related gene channel (hERG), as well as phase I and II metabolism. This is performed by assessing the likelihood of compounds binding to CYP450 enzymes and glucuronosyltransferases (UGT).

Our research group have recently investigated the ADMET properties of tamoxifen and its metabolites providing satisfactory results which are in agreement with previous *in vivo* and *in vitro* research [10]. In addition, other research such as El-Saadi *et al.* have demonstrated in-depth characterization of ADMET profile of promising analogs of fusarochromanone, a novel anticancer drug [36]. Through the use of ADMET Predictor, the authors have identified a few problematic areas that required further investigation for potential candidates for a drug-likeness compound, thus showing the software usefulness in predicting meaningful data prior to *in vitro* studies. Therefore, due to its accuracy and satisfactory results, ADMET Predictor was chosen as an *in silico* modeling tool for prediction of the PK of VLB and its metabolites.

2.3 Results and Discussion

VLB and its metabolites were docked into the nausea associated receptors D_2, H_1, H_3, M_1, M_4 and M_5 by means of molecular docking. The binding energy values and main binding interactions of VLB and its metabolites were compared to the known binding interactions of the endogenous substrates for each receptor, in order to evaluate their likelihood of inducing nausea during chemotherapy.

2.3.1 Dopaminergic D_2R

Dopamine, VLB and its metabolites were docked into the binding site of D_2R as described in the Materials and Method section of Chapter 2. (**Table 2.1**)

2.3.1.1 Dopamine Binding to D_2R

The natural substrate of D_2R, dopamine, interacts with residues Phe361 and Val115 through hydrophobic contacts. Additionally, the hydroxyl groups of dopamine makes H-bonds with residue Ser193 (1.9 Å and 1.8 Å), and the amine group makes a H-bond and ionic interactions with residue Asp114 (1.8 Å). Dopamine has a binding energy of -12.89 kJ/mol for the binding site of D_2R. (**Figure 2.2B**)

2.3.1.2 Vinblastine Binding to D_2R

The binding energy of VLB for D_2R is higher (-2.37 kJ/mol) than dopamine (-12.89 kJ/mol). VLB makes H-bonds with residues Glu181, Gln179, Glu95, and with the main chain of Leu94. Due to the binding affinity of VLB (-2.37 kJ/mol) for D_2R and a lack of involvement with residues that bind to the natural substrate, it is suggested that the anticancer drug would not compete with dopamine for the binding site of D_2R. (**Figure 2.2C**)

Table 2.1: Binding energies of VLB, its metabolites and dopamine docked into D_2R. The energy value of the metabolite with the lowest binding energy is shown in bold.

D_2R	$\Delta G_{binding}$ (kJ/mol)
Dopamine	-12.89
VLB	-2.37
MTB1	-5.54
MTB2	-4.28
MTB3	-10.17
MTB4	-5.31
MTB5	-9.61
MTB6	-5.19
MTB7	-1.61
MTB8	-6.46
MTB9	-0.89
MTB10	-2.90
MTB11	1.17
MTB12	-8.02
MTB13	-15.57
MTB14	-9.65
MTB15	-6.25
MTB16	-5.29
MTB17	-0.70
MTB18	-17.51
MTB19	-10.94
MTB20	-0.78
MTB21	-10.90
MTB22	-17.07
MTB23	-15.40
MTB24	-13.26
MTB25	-9.34
MTB26	-14.12
MTB27	-10.05
MTB28	-3.07
MTB29	-13.11
MTB30	-14.17
MTB31	-9.68
MTB32	-6.03
MTB33	-7.94
MTB34	**-17.58**
MTB35	-12.45

2.3.1.3 Metabolites Binding to D_2R

The majority of metabolites of VLB would not play a role in the binding site of D_2R due to their binding energies. However, metabolite 34 interacts stronger than the dopamine for D_2R, with a binding energy of -17.58 kJ/mol compared to -12.89 kJ/mol, respectively. The protonated nitrogen atom from the azacyclononane ring as well as the hydroxyl group establish H-bonds with the binding site of D_2R through residues Glu95 and Leu94. Metabolite 34 makes hydrophobic interactions with residues Asn367, Ile183, Phe110 and Tyr379. Therefore, it is suggested that metabolite 34 competes with dopamine for the binding site of D_2R due to its binding energy (-17.58 kJ/mol). (**Table 2.1** and **Figure 2.2D**)

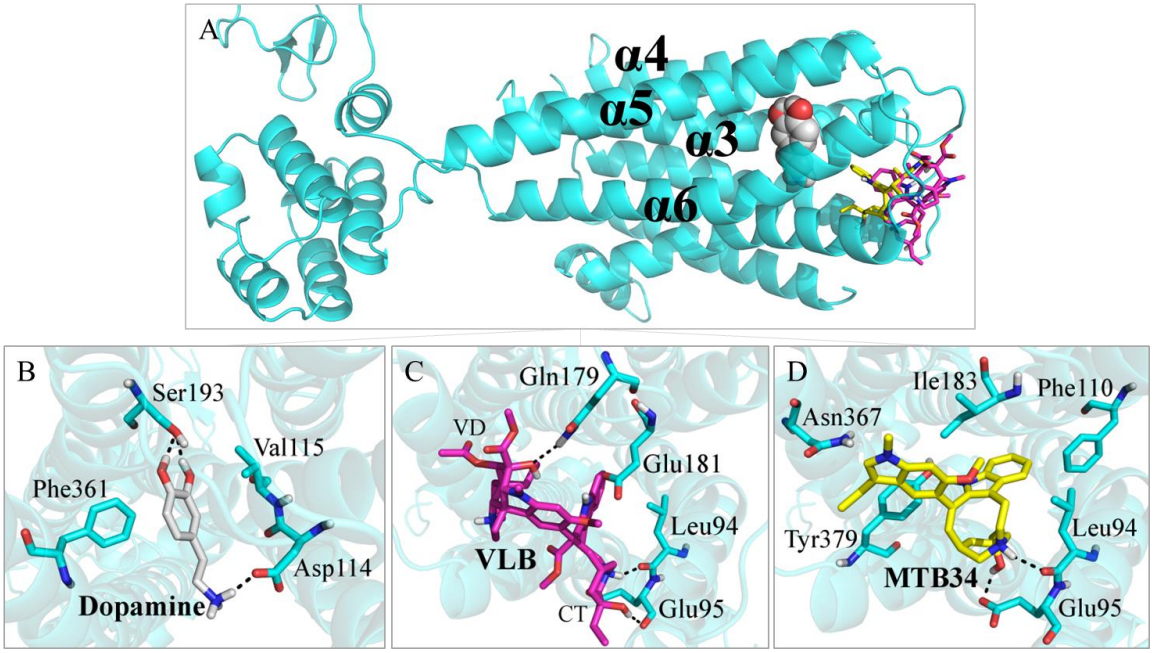

Figure 2.2: A) Pose view of dopamine docked into D_2R. B) Binding interactions of dopamine; C) VLB, and D) Metabolite 34. Hydrogen bonds are shown in dashed lines.

2.3.2 Histaminic H_1R

VLB, its metabolites and histamine were docked into the binding pocket of H_1R as described in the Materials and Method section of Chapter 2. The docking results of histamine, VLB and its metabolites into the binding site of H_1 receptor demonstrates that only three metabolites (metabolites 22, 23 and 35) have a strong binding energy for the binding pocket of the natural substrate, whereas metabolite 22 has the lowest binding energy of -18.10 kJ/mol. (**Table 2.2**)

2.3.2.1 Histamine Binding to H_1R

The imizadole ring of histamine makes H-bonds with residues Asp178 (2.2 Å) and the protonated amine makes ionic interactions and H-bonds with Asp107 (1.9 Å and 2.3 Å) within the binding site of H_1R. Moreover, histamine also interacts with residues Ile454 and Tyr431 through hydrophobic contacts with a binding energy of -14.40 kJ/mol for H_1R. (**Table 2.2** and **Figure 2.3B**)

2.3.2.2 Vinblastine Binding to H_1R

The binding energy of VLB in the binding pocket of H_1R is -0.17 kJ/mol. VLB makes H-bonds with residues Arg175, Arg97 and Trp93, whereas both methyl groups of esters and the hydroxyl group are involved in these interactions. Although VLB is able to interact with H_1R, it would not play a role in this receptor. This is because VLB does not interact with the same residues involved in the binding of the natural substrate and has a binding energy of only -0.17 kJ/mol for H_1R. (**Figure 2.3C**)

Table 2.2: Binding energies of VLB, its metabolites and histamine docked into H_1R. The energy value for the metabolite with the lowest binding energy is shown in bold.

H_1R	$\Delta G_{binding}$ (kJ/mol)
Histamine	-14.40
VLB	-0.17
MTB1	0.82
MTB2	13.98
MTB3	0.37
MTB4	-0.08
MTB5	-2.15
MTB6	2.83
MTB7	4.25
MTB8	-2.65
MTB9	4.19
MTB10	0.32
MTB11	-0.96
MTB12	0.82
MTB13	-7.90
MTB14	-3.42
MTB15	5.24
MTB16	0.92
MTB17	-2.71
MTB18	-12.23
MTB19	-7.05
MTB20	-6.83
MTB21	-8.84
MTB22	**-18.10**
MTB23	-15.13
MTB24	-7.64
MTB25	-7.62
MTB26	-6.99
MTB27	-8.29
MTB28	-0.20
MTB29	-12.00
MTB30	-8.10
MTB31	-9.49
MTB32	-7.53
MTB33	-7.11
MTB34	-13.35
MTB35	-15.30

2.3.2.3 Metabolites Binding to H_1R

The metabolites of VLB that are more likely to display a significant role in the functionality of H_1R are metabolite 22, metabolite 23 and metabolite 35 due to their binding energies. (**Table 2.2**)

Metabolite 22 has a binding energy of -18.10 kJ/mol when docked into H_1R. It interacts with residues from helices α5 and α6 of H_1R such as Asp183. Hydrogen bonds are observed with residues Asp183 (2.0 Å and 1.9 Å) and Arg175 (1.7 Å), and hydrophobic interactions with residues Phe184, Tyr185 and Arg97. Therefore, metabolite 22 competes with histamine for its binding site due to its binding energy for H_1R (-18.10 kJ/mol). Thus, it is suggested that metabolite 22 may account for nausea during chemotherapy with VLB through interaction with H_1R. (**Figure 2.3D**)

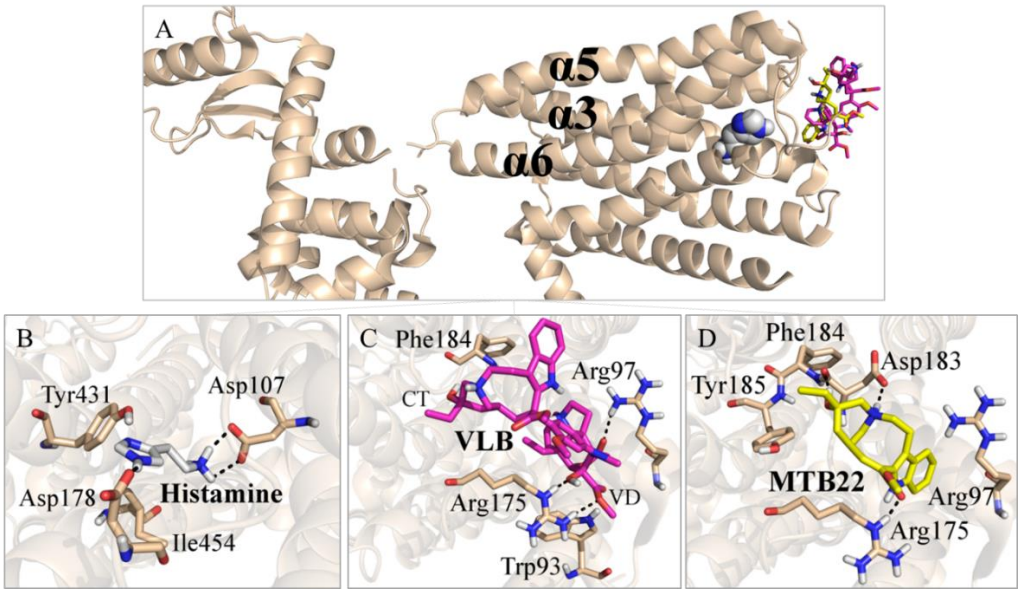

Figure 2.3: A) Pose view of histamine docked into H_1R. Binding interactions of B) Histamine; C) VLB; and D) Metabolite 22. Hydrogen bonds are shown in dashed lines.

2.3.3 Histaminic H_3R

Histamine, VLB and its metabolites were docked into the binding pocket of H_3R as described in the Materials and Method section of Chapter 2. (**Table 2.3**)

2.3.3.1 Histamine Binding to H_3R

Histamine has a binding energy calculated of -13.42 kJ/mol when docked into H_3R. The imidazole ring makes an H-bond with residue Asp114 (2.1Å), the charged amine makes H-bonds with residues Ser121 and Asp80 (2.1 Å and 1.8 Å, respectively). Moreover, hydrophobic interactions are seen among the aliphatic chain of histamine and residue Trp371. (**Table 2.3** and **Figure 2.4B**)

2.3.3.2 Vinblastine Binding to H_3R

In the binding site of H_3R, VLB has a binding energy of -13.78 kJ/mol, whereas the azacyclononane ring makes an H-bond with the main chain of residue Cys188 (1.8 Å). Residues Tyr194, Phe193, Tyr115, Arg381 and Tyr94 also participate in interactions with VLB within the binding site of H_3R. VLB and histamine have very close binding energies (-13.78 kJ/mol vs. -13.42 kJ/mol). Although they do not interact with the same residues, it is possible that VLB competes with histamine for the binding site of H_3R. (**Table 2.3** and **Figure 2.4C**)

2.3.3.3 Metabolites Binding to H_3R

All of the metabolites of VLB have some degree of binding affinity for H_1R. Metabolite 18 has the lowest binding energy among the metabolites of VLB (-19.67 kJ/mol vs. to -13.42 kJ/mol) docked into H_3R. Similar to VLB, metabolite 18 is located at the entrance of the binding pocket. (**Table 2.3** and **Figure 2.4A**)

Table 2.3: Binding energies of VLB, its metabolites and histamine docked into H_3R. The energy value for the metabolite with the lowest binding energy is shown in bold.

H_3R	$\Delta G_{binding}$ (kJ/mol)
Histamine	-13.42
VLB	-13.78
MTB1	-12.97
MTB2	-11.07
MTB3	-11.97
MTB4	-12.30
MTB5	-15.95
MTB6	-13.42
MTB7	-12.23
MTB8	-11.11
MTB9	-6.71
MTB10	-9.35
MTB11	-8.36
MTB12	-16.19
MTB13	-13.77
MTB14	-12.36
MTB15	-15.00
MTB16	-15.40
MTB17	-11.77
MTB18	**-19.67**
MTB19	-16.74
MTB20	-9.70
MTB21	-16.81
MTB22	-18.49
MTB23	-13.44
MTB24	-15.29
MTB25	-13.94
MTB26	-12.42
MTB27	-17.74
MTB28	-11.97
MTB29	-17.39
MTB30	-19.55
MTB31	-14.86
MTB32	-13.63
MTB33	-13.62
MTB34	-17.96
MTB35	-17.46

Metabolite 18 makes H-bonds with residues Tyr115, Cys188 and Arg381, whereas residue Tyr115 binds to the carbonyl group of ester, and the main chain of Cys188 interacts with the hydroxyl group of the vindoline unit. In addition, residues Tyr94 and Tyr194 interact through hydrophobic contacts with metabolite 18. Therefore, due to the binding energy of metabolite 18 (-19.67 kJ/mol), this metabolite competes with histamine for the binding pocket of H_3R. However, it mainly interacts with the residues in proximity of those interacting with histamine, similar to VLB. (**Figure 2.4D**)

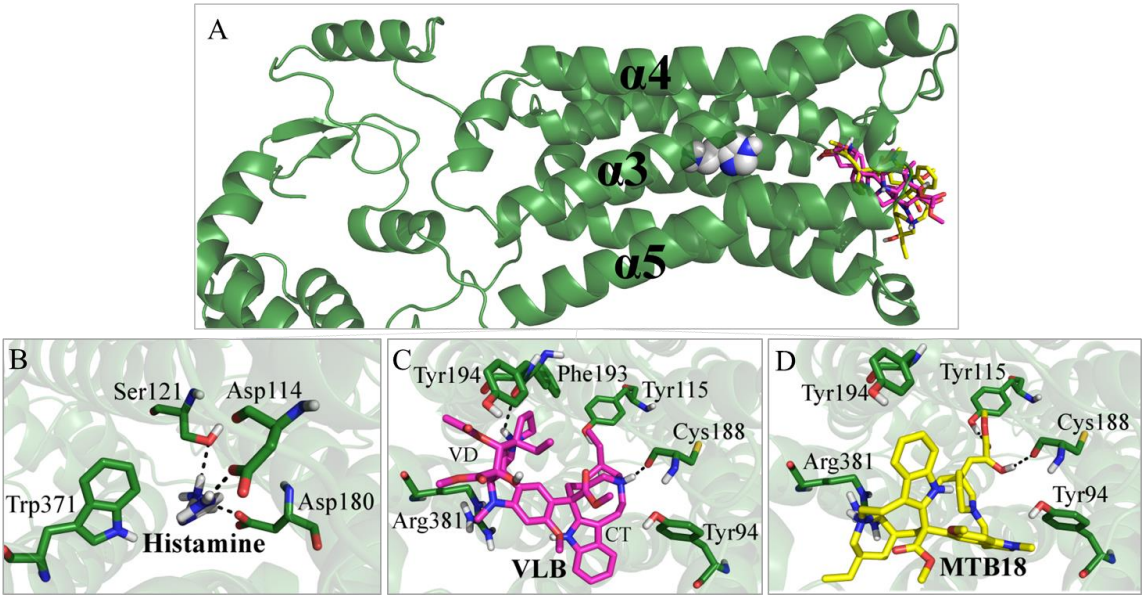

Figure 2.4: A) Pose view of histamine docked into H_3R. B) Binding interactions of histamine; C) VLB; and D) Metabolite 18. Hydrogen bonds are shown in dashed lines.

2.3.4 Muscarinic M_1R

VLB, its metabolites and acetylcholine were docked into the binding pocket of M_1R as described in the Materials and Method section of Chapter 2. (**Table 2.4**)

2.3.4.1 Acetylcholine Binding to M_1R

Acetylcholine (ACh) has a binding energy of -4.79 kJ/mol in the binding site of M_1R, whereas it makes H-bonds with residues Tyr404 and Tyr106, within a distance of 2.2 Å and 2.4 Å, respectively. Hydrophobic interactions are seen among the N-trimethyl group of ACh and residues Asp105 and Tyr381. (**Figure 2.5B**)

2.3.4.2 Vinblastine Binding to M_1R

VLB has a lower binding affinity than ACh for M_1R (binding energies of -3.77 kJ/mol vs. -4.79 kJ/mol, respectively). H-bonds are seen with residues Leu183 and Ser388 with the catharantine portion of VLB. Moreover, residue Gln177 interacts with the ester group at C4 of vindoline portion, and residues Trp400, Tyr404 and Tyr179 make hydrophobic interactions with VLB. VLB interacts hydrophobically with residue Tyr404 which is also involved in the binding of ACh, thus it may contribute to nausea during chemotherapy. (**Figure 2.5C**)

2.3.4.3 Metabolites Binding to M_1R

The metabolites of VLB that would play major role in the activation of M_1R are metabolites 22 and 23 due to their binding energies for the binding site of M_1R (-18.10 kJ/mol and -16.86 kJ/mol, respectively) and similar interaction profiles as of ACh.

Table 2.4: Binding energies of VLB, its metabolites and acetylcholine docked into M_1R. The energy value for the metabolite with the lowest binding energy is shown in bold.

M_1R	$\Delta G_{binding}$ (kJ/mol)
Acetylcholine	-4.79
VLB	-3.77
MTB1	-6.65
MTB2	-4.19
MTB3	-2.70
MTB4	-4.61
MTB5	-3.58
MTB6	-6.43
MTB7	-2.48
MTB8	-1.89
MTB9	-3.44
MTB10	-6.24
MTB11	-4.78
MTB12	-6.30
MTB13	-8.47
MTB14	-12.17
MTB15	-8.07
MTB16	-7.17
MTB17	-1.73
MTB18	-17.01
MTB19	-14.27
MTB20	-5.33
MTB21	-13.52
MTB22	**-18.24**
MTB23	-16.86
MTB24	-15.14
MTB25	-14.63
MTB26	-13.84
MTB27	-15.51
MTB28	-4.72
MTB29	-16.00
MTB30	-17.73
MTB31	-13.47
MTB32	-11.67
MTB33	-13.62
MTB34	-17.90
MTB35	-14.96

Metabolite 22 has the lowest binding energy among the metabolites of VLB docked into M_1R, calculated as -18.24 kJ/mol. The binding energy of metabolite 22 is more than three times stronger than the binding energy of ACh (-4.79 kJ/mol). (**Table 2.4**)

Metabolite 22 makes a H-bond with residue Asn382 within a distance of 1.6 Å and interacts hydrophobically with residues Ala193, Tyr381, Tyr106 and Phe197. Metabolite 22 shares common residues (Tyr106 and Tyr381) with ACh within the binding pocket of M_1R. Thus, it is suggested that metabolite 22 may induce nausea during chemotherapy with VLB due to its binding energy (-18.24 kJ/mol) for M_1R and similar interaction profile as of ACh (Tyr106 and Tyr381). (**Figure 2.5D** and **Figure 1.3-M22**)

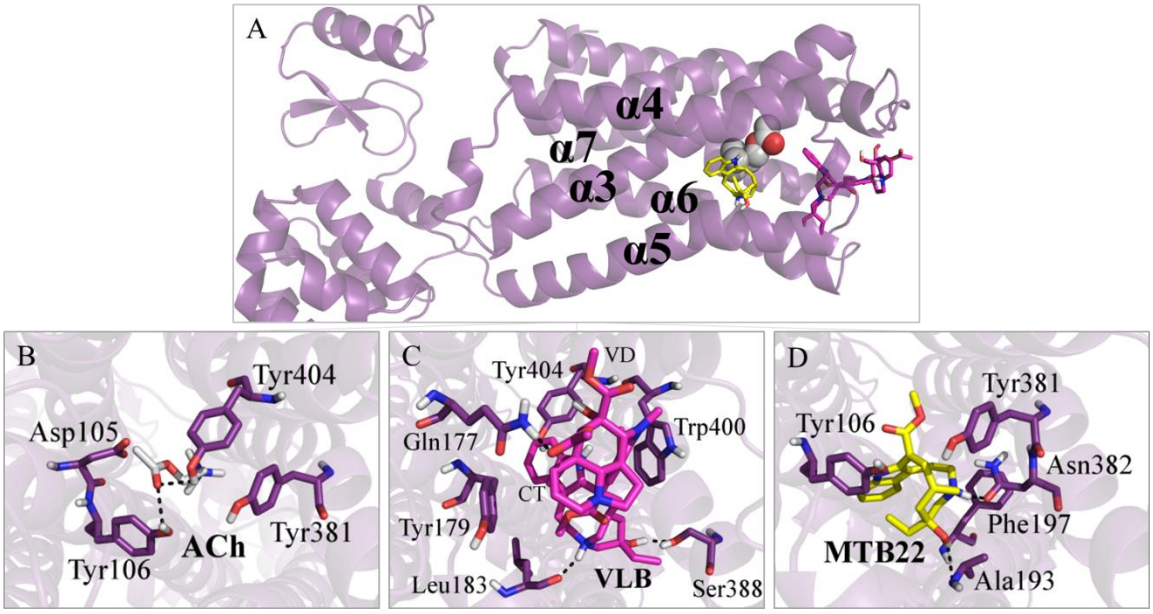

Figure 2.5: A) Pose view of acetylcholine docked into M_1R. Binding interactions of B) ACh; C) VLB, and D) Metabolite 22. Hydrogen bonds are shown in dashed lines.

Residues Tyr106 and Tyr404 which are involved in the binding of ACh into the binding site of M_1R, also interact with metabolite 23. A H-bond is observed among residue Tyr106 and the ester group of metabolite 23, within a distance of 1.7 Å. This interaction is 0.7 Å shorter than the binding of ACh with residue Tyr106 (2.4 Å). Moreover, residue Tyr404 interacts with the protonated nitrogen of indole ring at a distance of 1.6 Å, 0.6 Å shorter than ACh and Tyr404 (2.2 Å). Besides stronger H-bonds with residues Tyr106 and Tyr404 (1.7 Å and 1.6 Å) with M_1R than the natural substrate (2.4 Å and 2.2 Å), metabolite 23 also makes H-bonds with the main chains of residues Leu183 and Ile180. Therefore, due to binding energy of metabolite 23 as well as similar interaction profile as of ACh, it is suggested that this metabolite may contribute to nausea during chemotherapy with VLB through activation of M_1R. (**Figure 2.6** and **Figure 1.3-M23**)

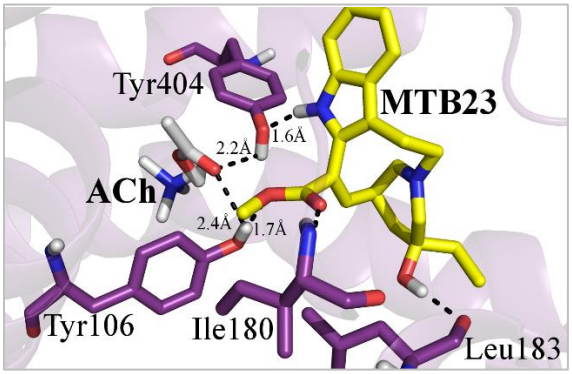

Figure 2.6: Binding interactions of metabolite 23 (yellow) docked into the binding site of M_1R and similar interaction profile as of ACh (white). Hydrogen bonds are shown in dashed lines.

The remaining metabolites of VLB also bind to the binding site of M_1R, however, they do not show the same interaction profile as of ACh, which suggests that those metabolites are less likely to activate the receptor during nausea. Nevertheless, metabolites 22 and 23 have significant binding affinities for M_1R, and share similar binding interactions as of ACh (Tyr106, Tyr404 and Tyr381), hence could induce for nausea during treatment with VLB.

2.3.5 Muscarinic M_4R

VLB, its metabolites as well as ACh were docked into the binding site of M_4R as described in the Materials and Method section of Chapter 2. (**Table 2.5**)

2.3.5.1 Acetylcholine binding to M_4R

ACh interacts with residues Tyr439, Tyr113 and Asp112 in the binding site of M_4R through hydrophobic contacts and H-bonds. The carbonyl of ester group of ACh makes an H-bond with Tyr439 (3.0 Å) and Tyr113 (2.2 Å), and contributes to a binding energy of -7.65 kJ/mol for ACh docked into M_4R. (**Figure 2.7A** and **2.7B**)

2.3.5.2 Vinblastine Binding to M_4R

VLB has a binding energy of -3.90 kJ/mol docked into M_4R and interacts with residue Tyr92 through an H-bond. In addition, residues Ile93 and Gln184 make hydrophobic interactions with VLB. However, due to its binding energy of -3.77 kJ/mol vs. -7.65 kJ/mol for ACh, as well as having similar binding profile to ACh, VLB would not play a role in the binding site of M_4R. (**Figure 2.7C**)

Table 2.5: Binding energies of VLB, its metabolites and acetylcholine docked into M_4R. The energy value for the metabolite with the lowest binding energy is shown in bold.

M_4R	$\Delta G_{binding}$ (kJ/mol)
Acetylcholine	-7.65
VLB	-3.90
MTB1	-9.98
MTB2	-15.14
MTB3	-6.71
MTB4	-4.09
MTB5	-9.15
MTB6	-4.16
MTB7	-3.85
MTB8	-4.02
MTB9	-5.58
MTB10	-10.16
MTB11	-6.82
MTB12	-10.28
MTB13	**-20.65**
MTB14	-17.36
MTB15	-14.52
MTB16	-10.18
MTB17	-6.14
MTB18	-17.19
MTB19	-18.63
MTB20	-10.87
MTB21	-10.87
MTB22	-16.71
MTB23	-16.63
MTB24	-14.88
MTB25	-15.48
MTB26	-12.38
MTB27	-18.40
MTB28	-6.79
MTB29	-17.66
MTB30	-14.96
MTB31	-11.31
MTB32	-14.72
MTB33	-12.53
MTB34	-17.09
MTB35	-13.74

2.3.5.3 Metabolites Binding M_4R

Some metabolites of VLB have significant binding affinities for M_4R. For instance, metabolite 13 has the strongest binding affinity among the metabolites, according to its binding energy of -20.65 kJ/mol when docked into the binding site of M_4R. The binding energy calculated is more than twice that of ACh (-7.65 kJ/mol). Metabolite 13 makes H-bonds with residues Ile187, Gln427 and Asn423. In addition, residue Tyr439, which is also involved in the binding of ACh, makes hydrophobic interactions with the ethyl group of metabolite 13. Moreover, residues Phe186, Leu190 and Cys185 also interact hydrophobically with metabolite 13. Therefore, metabolite 13 could potentially contribute to nausea during chemotherapy with VLB due to its binding affinity for M_4R (-20.65 kJ/mol). (**Figure 2.7D**)

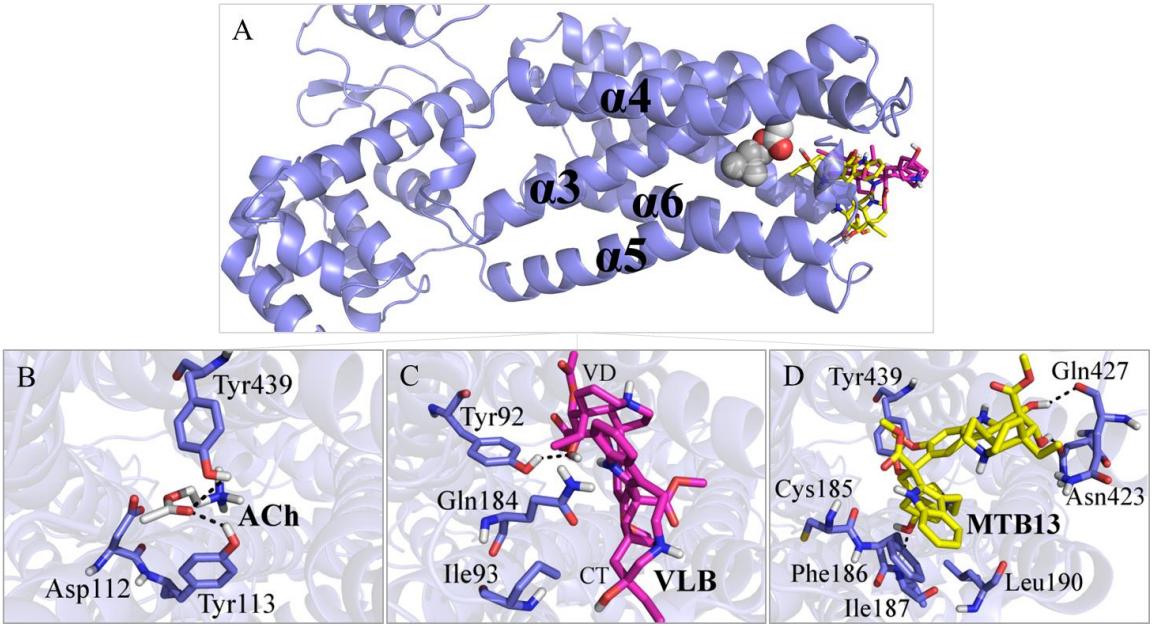

Figure 2.7: A) Pose view of ACh docked into M_4R. Binding interactions of B) ACh; C) VLB, and D) Metabolite 13. Hydrogen bonds are shown in dashed lines.

Many of VLB metabolites have better binding energies for M_4R than ACh, however their interaction profile are different from ACh, which could result in different induced effect during the signaling process. The metabolites that have binding affinities for M_4R and display similar interaction profiles to that of ACh are metabolite 19, metabolite 18, metabolite 34, metabolite 22, metabolite 23 and metabolite 10. Thus, it is suggested that these metabolites could trigger the onset of nausea during chemotherapy with VLB.

Metabolite 19 has binding energy of -18.63 kJ/mol docked into M_4R. Its affinity is mainly due to hydrophobic interactions and a H-bond with residue Tyr439 which is also involved in the binding of ACh. Residue Tyr439 interacts with metabolite 19 within a distance of 2.2 Å, 0.8 Å shorter than ACh (3.0 Å). Hydrophobic contacts are seen with Trp435 and Cys185. Therefore, metabolite 19 contributes to nausea during chemotherapy with VLB due to its binding affinity for M_4R (-18.63 kJ/mol) and a similar interaction profile. (**Figure 2.8A**)

Metabolite 18 also binds to residue Tyr113 within a distance of 2.1 Å, which is 0.1 Å shorter than of that by ACh (2.2 Å). In addition, it makes H-bonds with residues Asn423 and Ile187, and contributes to a binding energy of -17.19 kJ/mol and its likelihood of activating M_4R during treatment with VLB. (**Figure 2.8B**)

Metabolite 34 has a binding energy of -17.10 kJ/mol when docked into the binding site of M_4R. It also makes a H-bond with residue Tyr439 within a distance of 2.2 Å, which is 0.8 Å shorter than the natural substrate (3.0 Å). In addition, it interacts with Asp432 and Trp435, suggesting that metabolite 34 may trigger nausea symptoms during chemotherapy with VLB. (**Figure 2.8C**)

Metabolite 22 has a calculated binding affinity of -16.71 kJ/mol for M_4R. It makes hydrophobic interactions with residues Tyr113 and Tyr439, which are involved with the binding of ACh. This interaction is different than between Tyr113 and ACh. However, metabolite 22 has additional interactions with the binding pocket of M_4R, as it interacts with residues Asn417, Trp413 and Ser116, which in turn contribute to its binding energy. Metabolite 22 competes with ACh for binding to M_4R and potentially activates the receptor during nausea. (**Figure 2.8D**)

Metabolite 23 has a binding energy of -16.63 kJ/mol, more than double the binding energy of ACh (-7.65 kJ/mol) for M_4R. Residues Tyr113 and Tyr439 which are involved in the binding of ACh, interact with the ester group and the protonated nitrogen of the indole ring of metabolite 23, respectively. Although the distance between residue Tyr113 and metabolite 23 (2.7 Å) is 0.5 Å longer than that of ACh (2.2 Å), this metabolite is 1.4 Å closer than ACh in the binding of residue Tyr439 (1.6 Å vs. 3.0 Å). Because metabolite 23 interacts with the same residues as ACh in M_4R, it is suggested that this metabolite may induce nausea during chemotherapy with VLB. (**Figure 2.8E**)

Metabolite 10 (20-hydroxy-VLB) has a binding energy of -10.16 kJ/mol and also interacts with residues Tyr439 and Tyr113. The protonated nitrogen of azacyclononane ring makes one H-bond with Tyr439 within a distance of 1.8 Å. This interaction is 1.2 Å shorter than of that with the natural substrate (3.0 Å). Tyr113 makes hydrophobic contacts with metabolite 10 instead of an H-bond seen with ACh. Hydrophobic interactions are seen with Trp435, Gln427 and Phe186. Therefore, due to the binding affinity of metabolite 10 for M_4R and similar involving residues (Tyr113 and Tyr439) in the binding of the natural

substrate, this metabolite may activate nausea symptoms during treatment with VLB. (**Figure 2.8F**)

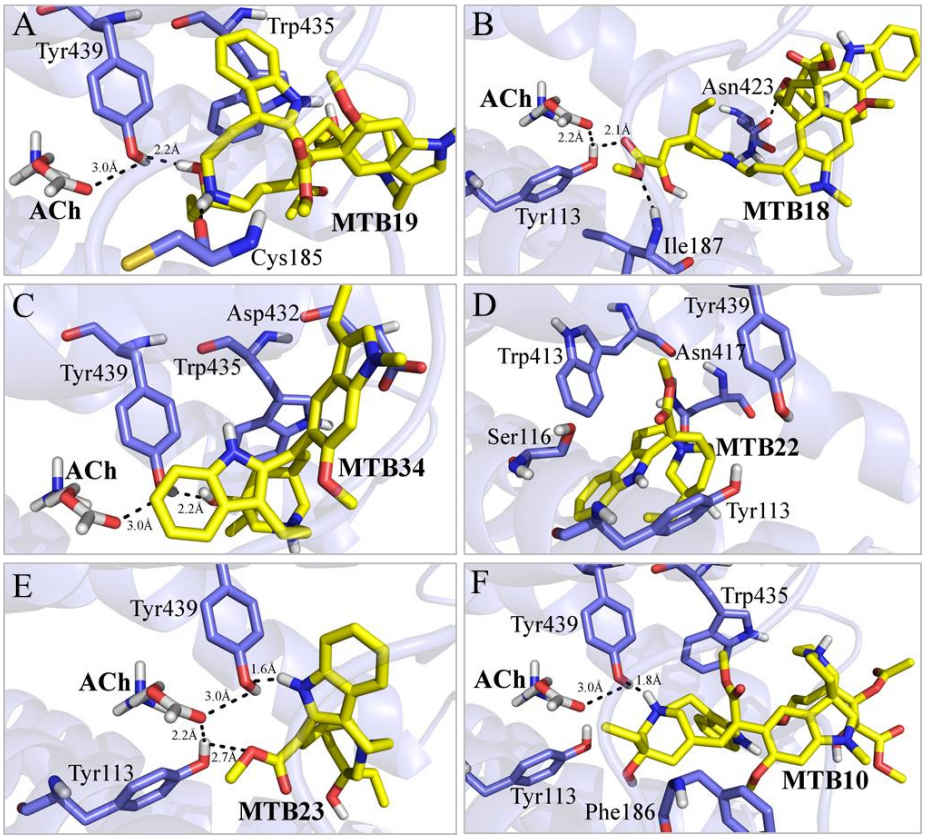

Figure 2.8: Binding interactions of A) Metabolite 19; B) Metabolite 18; C) Metabolite 34; D) Metabolite 22; E) Metabolite 23, and F) Metabolite 10 docked into M_4R. Hydrogen bonds are shown in dashed lines.

2.3.6 Muscarinic M_5R

ACh, VLB and its metabolites were docked into the binding site of M_5R as described in the Materials and Method section of Chapter 2. (**Table 2.6**)

2.3.6.1 Acetylcholine Binding to M_5R

The binding energy calculated for ACh docked into M_5R is -4.51 kJ/mol. ACh binds to residues Tyr480, Tyr110 and Tyr457. The carbonyl group of ACh makes H-bonds with residues Tyr480 and Tyr110 within a distance of 2.6 Å and 2.2 Å, respectively. Hydrophobic interactions are seen with residues aforementioned as well as with Tyr457 and Asp109. (**Figure 2.9B**)

2.3.6.2 Vinblastine Binding to M_5R

VLB has a binding energy of -9.28 kJ/mol for M_5R, approximately ~4 kJ/mol lower than that of ACh (-4.51 kJ/mol). VLB makes H-bonds with residues Asp468 and Gln183. The hydroxyl group and the protonated nitrogen both make H-bonds with Asp468, within a distance of 1.6 Å and 1.9 Å, respectively. The charged nitrogen atom in the azacyclononane ring of VLB also makes an ionic interaction with Asp468. In addition, Gln183 interacts with the carbonyl ester group (2.2 Å). Hydrophobic interactions among the aforementioned residues (Asp468 and Gln183) as well as with Trp476 and Val473 are observed. Although VLB does not bind to the same residues involved with ACh in M_5R, its binding energy is stronger than that of ACh (-9.28 kJ/mol vs. -4.51 kJ/mol). (**Figure 2.9C**)

Table 2.6: Binding energies of VLB, its metabolites and acetylcholine docked into M_5R. The energy value for the metabolite with the lowest binding energy is shown in bold.

M_5R	$\Delta G_{binding}$ (kJ/mol)
Acetylcholine	-4.51
VLB	-9.28
MTB1	-11.17
MTB2	-10.60
MTB3	-7.88
MTB4	-7.88
MTB5	-8.65
MTB6	-10.04
MTB7	-5.76
MTB8	-11.67
MTB9	-7.32
MTB10	-6.44
MTB11	-9.71
MTB12	-10.05
MTB13	-15.05
MTB14	-10.04
MTB15	-10.79
MTB16	-11.88
MTB17	-4.34
MTB18	**-18.68**
MTB19	-12.25
MTB20	-4.19
MTB21	-15.33
MTB22	-18.40
MTB23	-14.11
MTB24	-13.63
MTB25	-15.15
MTB26	-11.07
MTB27	-15.31
MTB28	-8.86
MTB29	-12.40
MTB30	-14.84
MTB31	-12.08
MTB32	-15.26
MTB33	-15.13
MTB34	-17.93
MTB35	-16.06

2.3.6.3 Metabolites Binding to M_5R

As seen with muscarinic M_1 and M_4 receptors, many of VLB metabolites bind to the M_5 receptor stronger than ACh, and often interact with the same residues involved with ACh binding, such as Tyr480 and Tyr110. (**Table 2.4**, **2.5** and **2.6**)

The binding energy of metabolite 18 is -18.68 kJ/mol when docked into the binding site of M_5R. It interacts with residues Asp468, Lys469 and Gln183 through H-bonds. The amide group of Gln183 interacts with the carbonyl ester (2.0 Å) and with the indole ring (1.7 Å) of metabolite 18. Metabolite 18 also makes hydrophobic interactions with Val473 and Trp476. Although metabolite 18 does not interact with exact the same residues involved in ACh binding, it binds better than the natural substrate to M_5R due to its binding energy (-18.68 kJ/mol). (**Figure 2.9D**)

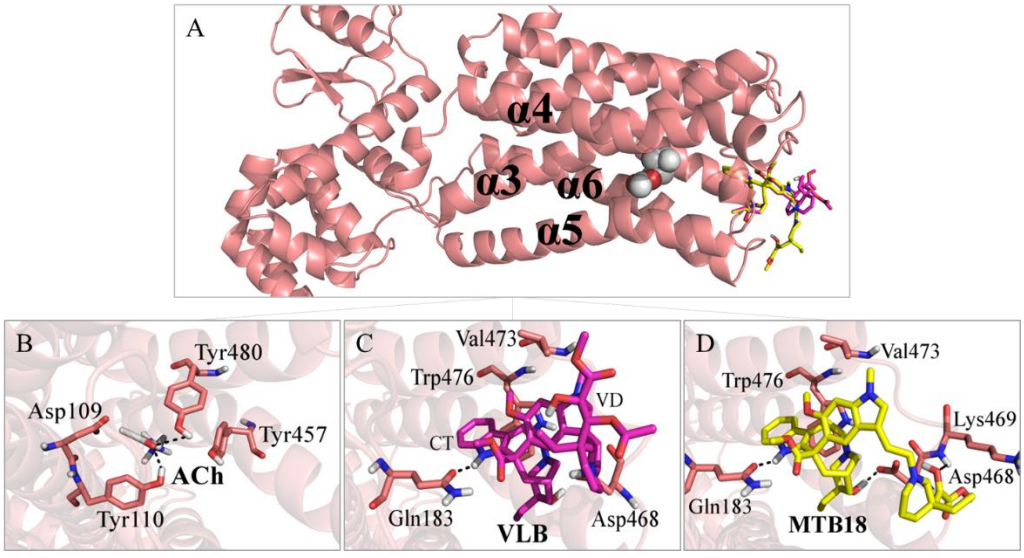

Figure 2.9: A) Pose view of acetylcholine docked into M_5R. Binding interactions of B) ACh; C) VLB, and D) Metabolite 18. Hydrogen bonds are shown in dashed lines.

Metabolite 23 interacts with the binding site of M_5R more than three times stronger than ACh (-14.11 kJ/mol and -4.51 kJ/mol) and binds to two of four residues such as Tyr110 and Tyr480 involved in interactions with the natural substrate. The hydroxyl group makes H-bonds with these residues within a distance of 2.5 Å for both interactions. Although the distance among residue Tyr110 and metabolite 23 is 0.3 Å longer than the one observed with ACh (2.5 Å vs. 2.2 Å), this metabolite has an extra H-bond with residue Thr193 (2.2 Å, not shown here). Thus, it is suggested that metabolite 23 may induce nausea through activation of M_5R. (**Figure 2.10A**)

Residue Tyr480 which makes an H-bond with the endogenous substrate ACh (2.6 Å), makes H-bonds with the hydroxyl group of metabolite 22 within a distance of 1.9 Å. These interactions are 0.7 Å shorter than the one seen with the substrate (1.9 Å vs. 2.6 Å). Metabolite 22 has a binding energy of -18.41 kJ/mol docked into M_5R, more than three times stronger than the binding energy of ACh (-4.51 kJ/mol). Metabolite 22 binds to the same residues involved with ACh in the binding pocket of M_5R, and can similarly trigger the onset of nausea during chemotherapy with VLB. (**Figure 2.10B**)

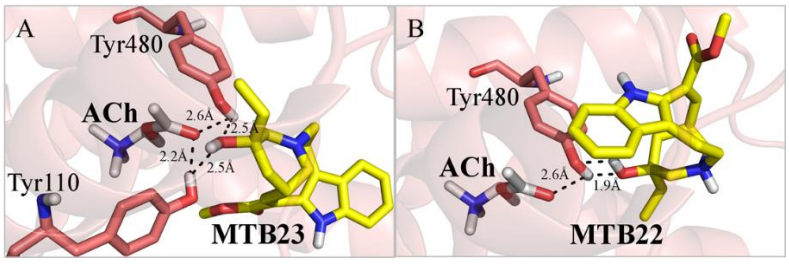

Figure 2.10: Binding interactions of A) Metabolite 23 and B) Metabolite 23 docked into M_5R. Hydrogen bonds are shown in dashed lines.

2.3.7 *In silico* Prediction of Absorption, Distribution, Metabolism, Excretion and Toxicology Properties of Vinblastine and its Metabolites

2.3.7.1 Solubility, Log P and Human Jejunal Effective Permeability

The gastric solubility (FaSSGF) of VLB is higher than the intestinal solubility in the fasted state (FaSSIF) and fed state (FeSSIF) (4.61 mg/mL vs. 4.61 x 10^{-2} mg/mL and 3.12 x 10^{-2} mg/mL, respectively). (**Table 2.7**)

A drug possessing a high solubility does not necessarily have a high rate of bioavailability that depends on the route of administration and a variety of other physicochemical properties such as molecular weight and structural flexibility affecting the drug effectiveness [37].

An orally administered drug must pass through many organs before it reaches the blood circulation. On the other hand, IV administered drugs go directly into the blood system, and thus achieve 100% of bioavailability. As orally administered drugs, IV administered drugs can go to the gut upon absorption and encounter similar pathways to be eliminated as well. Thus, IV administered drugs are also able to be reabsorbed in the gut or liver and then go back to the blood circulation before excreted through the kidneys [38]. In the case of IV administered drugs, only a small amount of the drug in the blood flow would be reabsorbed by the stomach, while the main portion of it would go back into the intestines [37].

The human jejunal effective permeability (P_{eff}) of VLB is calculated to be 0.58 cm/s x 10^{4}. *In vivo* studies performed by Ogihara *et al.* [39], have demonstrated that

VLB has an intestinal permeability of less than 1.0 x 10^{-6} cm/s. The authors have also shown that VLB is absorbed from the duodenum and ileum, but not from the jejunum in the intestinal segments of wild-type mice [39]. Compounds with a P_{eff} lower than 0.5 cm/s x 10^4 have low permeability [35]. Although VLB has a P_{eff} higher than 0.5 cm/s x 10^4 (0.58 cm/s x 10^4), it is still considered to be poorly absorbed by the intestines as it is administered by IV route. (**Table 2.7**)

Metabolite 23 has an intestinal solubility of 3.70 mg/mL in the fasted state (FaSSIF). Having the highest intestinal solubility among the metabolites (3.70 mg/mL vs. 0.01 mg/mL), metabolite 23 is likely to be absorbed back into the blood circulation system. However, considering its log P value of 0.22 and P_{eff} through the small intestine (0.36 cm/s x 10^4), metabolite 23 is probably not reabsorbed into the portal circulation in the liver. This is because compounds with a P_{eff} less than 0.5 cm/s x 10^4 and a low log P (<1) have low permeability and are too hydrophilic to cross the cellular membrane [35]. (**Table 2.7**)

Very hydrophilic compounds with poor membrane permeability (less than 0.5 x 10^{-4} cm/s) are more likely to be excreted through the kidneys or remain in the intestines rather than be reabsorbed in the blood system [37]. Thus, it is expected that metabolite 23 remains in the intestines or is excreted by renal route. If the former is the case, metabolite 23 would be able to interact with H_1R, M_1R, M_4R and M_5R as these receptors are found throughout the body [40]. In addition, metabolite 23 binds to these receptors with stronger affinities (-15.13 kJ/mol, -16.86 kJ/mol, -16.63 kJ/mol and -14.11 kJ/mol, respectively) than the natural substrates histamine and ACh (-14.40 kJ/mol,

-4.79 kJ/mol, -7.65 kJ/mol and -4.51 kJ/mol, respectively). Therefore, due to the ADMET findings for metabolite 23 in addition to its likelihood of interaction with nausea associated receptors, the metabolite could cause nausea symptoms during chemotherapy with VLB. (**Tables 2.2**, **2.4**, **2.5** and **2.6**)

Moreover, metabolite 26, metabolite 29, metabolite 31, metabolite 34 and metabolite 35 all have poor intestinal solubility (values close to 0.0 mg/mL) in the fed or fasted states (gastric and intestinal). They have high log P (>5.0) and high P_{eff} (>0.5 cm/s x 10^4), with values ranging from 4.93 to 7.04, and 1.08 to 4.73 cm/s x 10^4, respectively. These three parameters (solubility, log P and P_{eff}) can be useful for considering whether or not a compound could reach the blood circulation. For instance, there is a higher possibility for these metabolites (26, 29, 31, 34 and 35) than metabolite 23 to cross the intestinal membranes and to be reabsorbed into the blood system due to their P_{eff} and log P values. If these metabolites are reabsorbed into the blood system, they might account for further off-target interactions with proteins or receptors and cause adverse drug reactions. In addition, metabolite 22 and metabolite 34 have a high P_{eff} (1.99 cm/s x 10^4 and 2.22 cm/s x 10^4) compared to the P_{eff} calculated for the other metabolites, and have a high likelihood to cross the BBB due to their ability to cross the membrane. These are physicochemical properties that facilitate promiscuous off-target binding. In addition, metabolite 22 and metabolite 34 display affinities for all nausea associated receptors studied in this work (H_1R, H_3R, D_2R, M_1R, M_4R and M_5R), thus have increased potential of causing ADRs. (**Table 2.7**)

Table 2.7: Solubility in fed and fasted gastric/intestinal fluids, log P and human jejunal effective permeability (P_{eff}) of VLB and its metabolites.

Drug & Metabo-lites	Solubility in simulated fasted state gastric fluid FaSSGF (mg/mL)	Solubility in simulated fasted state intestinal fluid FaSSIF (mg/mL)	Solubility in simulated fed state intestinal fluid FeSSIF (mg/mL)	Log P	Human jejunal effective permeability (cm/s x 10^4)
VLB	4.61	0.05	0.03	3.95	0.58
MTB1	12.89	0.14	0.03	3.61	0.53
MTB2	4.19	0.01	0.03	4.57	0.57
MTB3	3.94	0.11	0.03	3.26	0.41
MTB4	3.91	0.10	0.03	3.31	0.43
MTB5	5.06	0.14	0.03	3.48	0.48
MTB6	0.43	0.05	0.07	3.73	0.47
MTB7	3.80	0.08	0.05	3.56	0.46
MTB8	3.78	0.12	0.05	3.60	0.46
MTB9	4.16	0.07	0.03	3.81	0.60
MTB10	4.65	0.11	0.03	2.99	0.43
MTB11	77.43	0.70	0.08	1.62	0.21
MTB12	12.76	0.40	0.04	3.12	0.43
MTB13	2.69	0.17	0.07	3.36	0.42
MTB14	4.88	0.03	0.03	4.09	0.46
MTB15	0.31	0.02	0.06	4.34	0.45
MTB16	2.16	0.02	0.03	4.71	0.84
MTB17	2.46	0.01	0.02	5.00	0.95
MTB18	30.79	0.04	0.00	3.99	0.30
MTB19	35.07	0.15	0.00	3.71	0.30
MTB20	217.19	0.29	0.30	0.77	0.24
MTB21	5.79	0.05	0.00	3.96	0.27
MTB22	3.12	0.90	0.63	2.40	1.99
MTB23	6.44	3.70	0.57	0.22	0.36
MTB24	22.01	0.05	0.00	4.50	0.35
MTB25	26.62	0.07	0.00	4.50	0.38
MTB26	0.03	0.01	0.07	6.41	3.67
MTB27	2.56	0.11	0.07	3.93	0.43
MTB28	183.45	0.15	0.24	1.45	0.27
MTB29	0.02	0.01	0.02	5.11	1.08
MTB30	39.10	0.05	0.00	3.92	0.25
MTB31	0.34	0.07	0.08	4.93	1.44
MTB32	5.02	0.23	0.08	3.09	0.35

MTB33	21.88	0.03	0.00	4.70	0.30
MTB34	0.48	0.04	0.09	5.69	2.22
MTB35	0.07	0.01	0.08	7.04	4.73

The predicted ADMET properties of VLB compares to two of the RO5 criteria, as it has a log P 3.95 and three HBD groups within the criteria suggested by Lipinski (log P and number of HBD groups both <5) [41]. Even though VLB has a desired log P value for a drug likeness according to Lipinski's rules (<5.0), it is poorly absorbed via the oral route as mentioned before. This is due to its extensive binding to plasma proteins and to P-glycoprotein (P-gp) transporter which are contributing factors to poor oral bioavailability. In this case, a drug takes longer to reach its target as it is bound to plasma proteins, and once it binds to the cell target, it is effluxed out of the cell by P-gp [37]. Therefore, the poor oral bioavailability of VLB may be due to its gastric and intestinal solubility, P_{eff} and affinity for both P-gp and plasma proteins. Moreover, VLB has a MW of 812.99 g/mol, which ~300 g/mol exceeds the acceptable magnitude according to the RO5 and thus influences the low likelihood of oral drug bioavailability [42]. (**Tables 2.7** and **2.8**)

Large and complex molecules similar to VLB also have low membrane permeability. Therefore, VLB physicochemical properties do not match to RO5 and thus it is reasonable that it is not administered orally. Furthermore, VLB has 12 rotatable bonds and a log D value of 3.37 that are in correlation with drug solubility. The RO5 is usually followed as a guideline for compounds for oral use, and not intravenously administered as

VLB. Many anticancer drugs including VLB were discovered around 1960, and the RO5 was introduced more than 30 years later, in 1997 [41]. (**Table 2.8** and **Figure 2.11**)

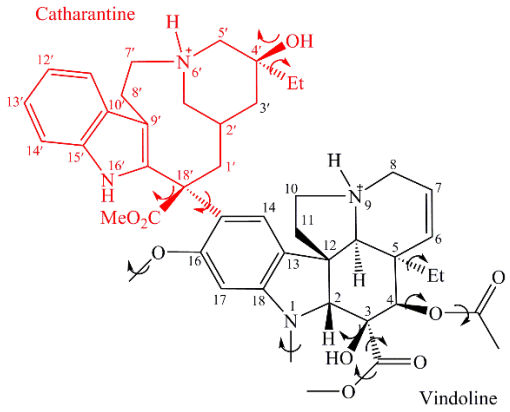

Figure 2.11: Rotatable bonds of VLB.

2.3.7.2 Volume of distribution, Plasma Proteins, Log D and BBB

The first possible interaction of VLB and the blood protein human serum albumin (HSA), was demonstrated *in vitro* in 1973 [43], suggesting that the biological effects of the drug are increased compared to other anticancer agents with biological effects diminished in the presence of albumin [43, 44]. Pandya *et al.* demonstrated that although VLB was seen bound to HSA with an affinity of -7.6 kJ/mol, the binding affinity of the drug for its target tubulin was stronger (-10.0 kJ/mol) [45]. The *in silico* results show that VLB is 89.22% bound to plasma proteins due to its hydrophilic character and affinity for these proteins. Therefore, only ~10.78% of the drug is in the free form and available to interact with its target tubulin. (**Table 2.8**)

The V_d of VLB is calculated to be 13.41 L/kg, suggesting that it is highly distributed throughout the body. This is in agreement with previous research stating that vinca

alkaloids such as VLB have significant V_d [46, 47], that could explain why VLB has a long half-life of 35h compared to other anticancer drugs [48] as it is dispersed throughout the body, thus taking a long time to be excreted. (**Table 2.8**)

Among the metabolites of VLB, metabolite 23 has the highest amount of unbound plasma proteins (~77.2%), indicating that the metabolite is more available in the blood system than the others. However, it also has a V_d of 0.59 L/kg which indicates that it is not scattered throughout the tissues. Although metabolite 23 has a low predicted P_{eff} (0.36 cm/s $x10^4$), it is known that the less a molecule is bound to the plasma proteins, and the smaller it is, the easier can traverse the cell membrane and be considered active to interact with protein-receptors [37]. It is noteworthy to point out that this metabolite has a low MW (< 400 g/mol) and low affinity for plasma proteins (< 20% bound). As it was shown earlier, it has affinity for all nausea associated receptors in this study, and supporting the idea that metabolite 23 can induce the onset of nausea during chemotherapy of VLB (**Tables 2.7** and **2.8**)

Metabolite 11 and metabolite 20 are found in high amounts in the body as their *in silico* predicted values of V_d is calculated as of 0.46 L/Kg and 0.72 L/Kg, respectively. However, neither of these metabolites display a significant interaction with any of the nausea associated receptors in this study. Therefore, more research needs to be done to evaluate other possible interactions during their clearance to identify other off-targets receptors. (**Table 2.5**)

Table 2.8: Volume of distribution, percentage of unbound plasma proteins, log D, and log BBB coefficient partition of VLB and its metabolites.

Drug & Metabolites	Volume of Distribution V_d (L/kg)	% of unbound to plasma proteins	Log D	Log BBB partition coefficient
VLB	14.02	10.78	3.37	-0.95
MTB1	11.25	12.23	2.96	-0.89
MTB2	17.60	7.13	4.08	-0.77
MTB3	17.65	15.80	2.76	-1.26
MTB4	17.26	15.06	2.82	-1.40
MTB5	12.21	13.56	2.91	-1.09
MTB6	5.55	11.91	3.14	-0.87
MTB7	2.78	13.13	3.04	-1.16
MTB8	2.80	13.27	3.04	-1.08
MTB9	13.59	11.35	3.28	-0.90
MTB10	12.43	18.83	2.43	-1.29
MTB11	0.46	46.06	-1.71	-1.43
MTB12	9.74	15.71	2.48	-1.04
MTB13	4.34	13.81	2.70	-0.82
MTB14	15.81	9.09	3.61	-0.93
MTB15	6.58	8.02	3.83	-0.66
MTB16	18.81	5.90	4.18	-0.59
MTB17	13.57	3.00	4.80	-0.80
MTB18	0.49	11.93	3.25	-1.13
MTB19	0.36	16.81	1.04	-1.20
MTB20	0.72	55.70	0.72	-1.10
MTB21	0.46	13.86	0.78	-0.30
MTB22	1.67	15.90	1.89	-0.25
MTB23	0.59	77.22	-0.85	-0.79
MTB24	0.42	10.45	2.02	-1.02
MTB25	0.38	9.99	2.16	-1.07
MTB26	1.53	0.46	6.28	0.16
MTB27	0.49	9.46	1.31	-0.29
MTB28	2.95	45.32	1.39	-0.81
MTB29	1.47	1.12	4.93	-0.45
MTB30	1.18	15.40	0.80	-0.66
MTB31	1.58	2.20	4.22	-0.10
MTB32	0.57	16.59	0.86	-0.68
MTB33	0.96	9.09	1.62	-0.51
MTB34	1.43	1.06	5.13	0.17

MTB35	1.22	0.60	6.79	0.43

Metabolite 17, metabolite 26, metabolite 29, metabolite 31, metabolite 34 and metabolite 35 have high affinities for the plasma proteins (< 3% unbound). Even though metabolite 17 does not have an affinity for M_5R (-4.34 kJ/mol vs. -4.51 kJ/mol for ACh), all of the aforementioned metabolites have stronger binding energies than ACh for M_5R (-11.07 kJ/mol, -12.40 kJ/mol, -12.08 kJ/mol, -17.93 kJ/mol and -16.06 kJ/mol vs. -4.51 kJ/mol). This is useful to compare the binding affinity of these metabolites against the muscarinic receptors and plasma proteins as the former receptors are also present in the blood circulation. Therefore, more research is required to investigate the binding profile of the aforementioned metabolites with respect to the plasma proteins. (**Table 2.6**)

Drugs capable of crossing the blood-brain barrier (BBB) must be lipophilic enough to be absorbed by the cell membranes and enter into the brain [37]. The likelihood of VLB to cross the BBB is calculated to be log -0.95. VLB has a partial hydrophilic character with charged atoms such as the protonated nitrogen atoms at N6′ and N9 that make difficult the entrance of VLB through the endothelial cells of the central nervous system [49]. Therefore, VLB does not cross the BBB. (**Table 2.7** and **2.8**)

2.3.7.3 P-glycoprotein and Human ether-à-go-go-related gene

VLB and its metabolites are all transported by P-gp, whereas a majority of them can also inhibit this protein according to the *in silico* results. The metabolites transported out of the cell by P-gp are metabolite 11, metabolite 20, metabolite 22, metabolite 23, metabolite 27, metabolite 28 and metabolite 32. Horio *et al.* have explained that VLB is actively

transported by P-gp in Hodgkin's disease cells (KB cells) with a transport affinity of 2 μM for P-gp [50]. Previous studies have shown that VLB is also an inhibitor and inducer of P-gp [47, 51-53]. This is, VLB is transported out of the cell by P-gp and inhibit the functionality of this protein and/or induce its activity to transport other xenobiotics.

Metabolite 22 and metabolite 23 have a high probability to cross the BBB (-0.25 and -0.79) and are transported by P-gp. If drugs capable of crossing the BBB are taken in concomitantly with VLB, metabolites 22 and 23 are likely to compete with them for interaction with P-gp in the brain. If metabolite 22 and metabolite 23 are better binders to P-gp than the concomitant drugs, it would be expected an increase of blood concentration of either metabolite or of the concomitant drugs in the brain. Therefore, as these metabolites are transported out of the cell membrane due to their P-gp affinity, the chances of off-targets events and thus drug-drug interactions induced by these compounds are increased within the brain environment. (**Table 2.8**)

The human ether-à-go-go-related gene receptor (hERG), a potassium channel receptor responsible for the action potential of myocardiocytes, is also an important enzyme in pharmacokinetic studies due to its cardiotoxicity induced by a drug inhibitory effect [54]. Compounds with an inhibitory concentration (IC_{50}) less or equal to 10 μM have an affinity for hERG potassium channel and thus block the receptor [35]. In agreement with previous research [55], the *in silico* predicted ADMET data shows that VLB does not interact with hERG receptor, but some of its metabolites such as metabolite 19, metabolite 21, metabolite 27, metabolite 30, metabolite 31, metabolite 32, metabolite 34 and metabolite 35 have an affinity to the receptor. Their predicted inhibitory concentration

(pIC_{50}) for hERG inhibition is 6.25, 6.07, 6.09, 6.03, 6.18, 6.02, 6.88 and 6.71 mol/L, respectively. Therefore, the metabolites aforementioned block hERG channel could cause cardiovascular complications post chemotherapy with VLB. Previous research has shown that tubulin-binding drugs have a probability to induce cardiotoxicity during cancer treatment through damage of endothelial cells of the myocardium, however, the mechanism is not yet fully known [56]. Thus, further research is required to evaluate detailed mechanism of triggering cardiotoxic events during the clearance of VLB.

2.3.7.4 Cytochrome P450 complex

2.3.7.4.1 CYP1A2, CYP2A6, CYP2B6, CYP2C8, CYP2E1, CYP2C9 and CYP2C19

As ondansetron, metabolite 22, metabolite 23, metabolite 34 and metabolite 35 are all metabolized by CYP1A2. Thus, it is suggested that the binding competition among the ondansetron and VLB or its metabolites for CYP1A2 can play a role in determining differences in plasma concentration whether used in concomitance during chemotherapy [57].

The predicted ADMET properties show that metabolite 2, metabolite 3, metabolite 15, metabolite 16, metabolite 17 and metabolite 34 are metabolized by CYP2C8. However, neither drug nor metabolites are metabolized by isoforms CYP2A6, CYP2B6, CYP2E1 and CYP2C19. In addition, metabolite 2, metabolite 15, metabolite 17, metabolite 20, metabolite 24, metabolite 25, metabolite 26 and metabolite 27 are able to inhibit CYP2C9, whereas only metabolite 35 is metabolized by CYP2C9. Interestingly, metabolite 35 has similar chemical structure to the compounds metabolized by CYP2C9 due to the heteroatoms and aromatic rings in its molecule [58].

2.3.7.4.2 CYP2D6

The *in silico* results have shown that VLB and all of its metabolites could inhibit CYP2D6, but not all of them are metabolized by this enzyme, this is, they are not substrates (NB) of CYP2D6. (**Table 2.9**)

VLB and metabolites that are metabolized by CYP2D6 might have drug-drug interactions with inhibitors of this enzyme, such as quinidine, cimetidine and ritonavir [59]. The concomitant intake of compounds that are metabolized by or inhibit CYP2D6 can potentially lead to an increase on the plasma concentration level of VLB. This is due to the lower metabolism rate of VLB trigged by enzymatic competition of CYP2D6. For instance, if VLB is taken along with the antiarrhythmic agent quinidine, an inhibitor of CYP2D6, the plasma concentrations of VLB are increased because CYP2D6 is inhibited by quinidine, and thus can cause drug toxicity [60].

VLB can also cause drug-drug interactions with drugs that are metabolized by CYP2D6 [61]. Ondansetron is an antiemetic agent often administered during cancer treatment [62]. Because it is metabolized by CYPD26 [63] similar to VLB, ondansetron would compete with VLB for metabolism with CYP2D6, thus probably causing drug-drug interactions because one of the two compounds would have its plasma concentrations increased.

Table 2.9: Kinetic and intrinsic parameters (K_m, V_{max} and CL_{int}) of VLB and its metabolites for CYP2D6.

Drug & Metabolites	Qualitative assessment of substrates of 2D6	Kinetic Michaelis-Menten K_m	Kinetic Michaelis-Menten V_{max}	Intrinsic clearance (CL_{int}) constants
VLB	Yes	1443.0	92.7	0.5
MTB1	Yes	3949.2	174.6	0.4
MTB2	Yes	262.0	26.8	0.8
MTB3	No	NB	NB	NB
MTB4	No	NB	NB	NB
MTB5	Yes	5125.5	133.1	0.2
MTB6	No	NB	NB	NB
MTB7	Yes	5408.1	170.7	0.3
MTB8	Yes	5250.9	82.1	0.1
MTB9	No	NB	NB	NB
MTB10	No	NB	NB	NB
MTB11	No	NB	NB	NB
MTB12	Yes	10276.2	265.2	0.2
MTB13	Yes	2502.8	232.8	0.7
MTB14	Yes	1714.9	67.4	0.3
MTB15	No	NB	NB	NB
MTB16	Yes	246.1	17.6	0.6
MTB17	No	NB	NB	NB
MTB18	No	NB	NB	NB
MTB19	No	NB	NB	NB
MTB20	No	NB	NB	NB
MTB21	Yes	6.5	18.9	23.4
MTB22	Yes	89.9	32.7	2.9
MTB23	Yes	15.1	10.4	5.5
MTB24	No	NB	NB	NB
MTB25	No	NB	NB	NB
MTB26	Yes	3.5	24.8	57.3
MTB27	No	NB	NB	NB
MTB28	Yes	137.1	29.8	1.7
MTB29	Yes	20.9	47.7	18.2
MTB30	No	NB	NB	NB
MTB31	Yes	31.1	48.8	12.6
MTB32	No	NB	NB	NB
MTB33	Yes	0.9	33.3	295.3
MTB34	Yes	24.6	13.0	4.2

MTB35	Yes	2.9	9.8	27.4

*K_m (μM). V_{max} (nmol/min^{-1}/$nmol^{-1}$). CL_{int}(μL/min/mg HLM protein), HLM: human liver microsomes (concentration of 0.5 mg/mL). NB: non substrate.

CYP3A4 plays the major role in the metabolism of VLB and its metabolites. Some VLB metabolites that are metabolized by both CYP3A4 and CYP2D6, such as metabolite 1, metabolite 2, metabolite 5, metabolite 7, metabolite 13 and metabolite 14. As these metabolites are preferentially bound to CYP3A4, they would interfere with the metabolism of the drugs binding to CYP3A4 whether other drug is taken in concomitance. (**Tables 2.9** and **2.10**)

2.3.7.4.3 CYP3A4

According to the *in silico* predictions, the metabolism of VLB and all of its metabolites is mediated by CYP3A4. However, the activity of CYP3A4 is also inhibited by all of them. (**Table 2.10**)

This is in agreement with the *in vitro* PK study of VLB that has shown that VLB is both a substrate [47, 64, 65], and an inhibitor of CYP3A4 [64, 66], which is the same observed for its metabolites. Levêque and Jehl have revised the PK of the main vinca alkaloids used to treat cancer and shown that VLB is highly metabolized by CYP3A4 in human liver microsomes [47]. In addition, Zhou-Pan *et al.* have demonstrated that the K_m and V_{max} constants of VLB are 6.82 ± 0.27 μM and 0.64 ± 0.06 nmol/min/mg P450, respectively [64]. The inhibitory effect of CYP3A4 caused by VLB was investigated by Baumhäkel *et al.*, which has shown that the IC_{50} of VLB was 20 and 44 μmol/L in two human liver microsome samples compared with the plasma concentrations of

antineoplastic drugs taken during chemotherapy [66]. Both inhibition of or metabolism by CYP3A4 is an important factor to explain treatment failures commonly seen with VLB as well as adverse drug reactions caused by drug-drug interactions whether co-administered with other drugs. (**Table 2.7**)

VLB has a Michaelis-Menten constant (K_m) of 19.9 μM and a maximum metabolic rate (V_{max}) of 25.2 nmol/min^{-1}/$nmol^{-1}$ P450. Even though it is also a substrate of CYP2D6, another important enzyme in drug metabolism, VLB has much higher K_m for CYP2D6 (1443.0 μM) than for CYP3A4 (19.9 μM), thus indicates a significant affinity for the latter enzyme. (**Table 2.9** and **2.10**)

Table 2.10: Kinetic and intrinsic parameters (K_m, V_{max} and CL_{int}) of VLB and its metabolites for CYP3A4.

Drug & Metabolites	Kinetic Michaelis-Menten K_m	Kinetic Michaelis-Menten V_{max}	Intrinsic clearance (CL_{int}) constants
VLB	19.9	25.2	299.1
MTB1	17.5	13.2	183.6
MTB2	26.3	24.8	345.0
MTB3	17.3	25.0	109.5
MTB4	14.8	26.7	82.1
MTB5	21.6	25.0	134.7
MTB6	21.8	23.1	239.7
MTB7	17.8	11.2	144.8
MTB8	18.9	12.9	154.8
MTB9	16.8	9.3	333.2
MTB10	17.6	27.7	140.0
MTB11	64.5	7.2	139.4
MTB12	19.4	13.3	75.2
MTB13	19.5	15.8	146.9
MTB14	30.0	25.3	156.9
MTB15	28.9	21.3	282.1
MTB16	32.8	76.8	327.3
MTB17	6.6	12.7	1107.9
MTB18	13.2	2.3	1871.7
MTB19	21.3	3.7	993.2
MTB20	28.7	6.4	183.2
MTB21	17.4	2.8	1781.9
MTB22	192.5	36.4	11.0
MTB23	326.2	3.8	19.5
MTB24	23.3	1.8	1614.7
MTB25	22.4	2.2	1952.1
MTB26	6.2	2.5	556.5
MTB27	67.0	0.7	503.9
MTB28	25.8	4.1	498.5
MTB29	6.3	3.1	149.2
MTB30	22.0	3.5	3507.8
MTB31	31.1	10.1	93.4
MTB32	72.8	1.4	187.9
MTB33	23.4	2.0	6361.0
MTB34	28.5	8.1	132.3
MTB35	11.4	1.8	592.5

*K_m (μM). V_{max} (nmol/min^{-1}/nmol^{-1}). CL_{int}(μL/min/mg HLM protein), HLM: human liver microsomes (concentration of 0.5 mg/mL). NB: non substrate.

2.3.7.5 Phase II Metabolism - Glucuronidation Reactions

VLB and its metabolites were screened against Uridine 5′-Diphosphate-Glucuronosyltransferase (UGT), an enzyme responsible for catalyzing glucuronidation reaction during Phase II drug metabolism [67]. In particular, the UGT isoforms UGT1A1, UGT1A3, UGT1A4, UGT1A6, UGT1A8, UGT1A9, UGT1A10, UGT2B7, and UGT2B15 were experimentally tested for VLB and metabolites in this work. The *in silico* data shows that VLB is not catalyzed by any of the UGT enzymes indicating that VLB is not conjugated through glucuronidation metabolism. This correlates with Owellen *et al.* results, that demonstrated VLB does not undergo glucuronide neither sulfate formation [68]. However, some of the metabolites undergo glucuronidation reactions with enzymes UGT1A3, UGT1A8 and UGT2B7 while the remaining metabolites do not undergo glucuronidation. (**Table 2.11**)

Table 2.11: Phase II of metabolites of VLB with isoenzymes UGT1A3, UGT1A8 and UGT2B7.

Qualitative model of glucuronidation by UGT1A3	Qualitative model of glucuronidation by UGT1A8	Qualitative model of glucuronidation by UGT2B7
MTB9 (45%) MTB26 (49%) MTB27 (49%) MTB32 (47%)	MTB19	MTB22 (61%) MTB23 (65%)

2.4 Conclusion

VLB and its metabolites were docked into nausea associated receptors D_2, H_1, H_3, M_1, M_4 and M_5 by means of molecular docking and their binding interactions were compared to that of dopamine, histamine and acetylcholine. Furthermore, the ADMET properties of VLB and its metabolites were predicted through *in silico* experiments. The potential for VLB and its metabolites to interact with receptors involved in nausea induced by chemotherapy was evaluated. The results have shown that VLB plays a role in the M_5R, and it might compete with histamine for the binding site of H_3R. On the other hand, the metabolites of VLB bind to all of the nausea associated receptors used in this study, and thus can trigger nausea during chemotherapy with VLB. The molecular docking has shown that the metabolites of VLB have binding affinities mainly for the muscarinic receptors along with similar binding interactions to that of ACh in the binding site of the target receptor.

In the binding pocket of M_1R, metabolite 22 and metabolite 23 interact with the same residues involved in the binding of ACh, such as Tyr106, Tyr404 and Tyr381. For instance, metabolite 23 makes stronger H-bonds with residues Tyr104 and Tyr404 than ACh (1.7 Å and 1.6 Å vs. 2.4 Å and 2.2 Å, respectively). Furthermore, metabolite 22 and metabolite 23 have both binding affinities stronger than that of ACh (-18.24 kJ/mol and -16.84 kJ/mol vs. -4.79 kJ/mol). Thus, it is evident that these metabolites display significant binding interactions with the binding pocket of M_1R, and could be involved in the onset of nausea through receptor activation. (**Table 2.4**)

The metabolites of VLB also display binding affinities for M_4R and thus may be involved with nausea during chemotherapy with VLB through this additional receptor. For instance, Tyr439 and Tyr113 of ACh binding site in the M_4R, also interact with metabolite 13, metabolite 19, metabolite 18, metabolite 34, metabolite 22, metabolite 23 and metabolite 10 by either hydrophobic contacts or H-bonds. Metabolite 13 has a binding energy of -20.65 kJ/mol, more than twice of ACh (-7.65 kJ/mol). Although it does not interact with any of the residues directly interacting with ACh, it can compete with the natural substrate for stronger interactions with M_4R. Moreover, metabolite 23 and metabolite 10 both have the same type of interactions as ACh and interact with the same residues in M_4R. For instance, metabolite 23 and metabolite 10 interact with residue Tyr439 within a distance of 1.6 Å and 1.8 Å, respectively, compared to 3.0 Å for ACh. Besides that, metabolites 23 and 10 (-16.63 kJ/mol and -10.16 kJ/mol) have stronger affinities than ACh (-7.65 kJ/mol) for M_4R, hence compete with ACh for activation of M_4R. Therefore, the *in silico* results have shown that the metabolites of VLB are likely to contribute to nausea through activation of M_4R, as well. (**Table 2.5**)

In respect to M_5R, metabolite 18, metabolite 22 and metabolite 23 have better binding affinities for the binding pocket of the receptor than the substrate. Residues Tyr110, Tyr480 and Tyr457 are involved in the binding of ACh to M_5R, whereas only Tyr110 and Tyr480 make H-bonds with the substrate. Metabolite 22 and metabolite 23 make H-bonds and hydrophobic interactions with all of the residues involved with ACh. For instance, metabolite 22 (1.9 Å) and metabolite 23 (2.5 Å) interact with residue Tyr480 in closer proximity than the substrate (2.6 Å), and both have binding affinities for M_5R

(-18.40 kJ/mol and -14.11 kJ/mol, respectively, vs. -4.51 kJ/mol for ACh). Furthermore, metabolite 23 also make a H-bond with Tyr110 within a distance of 2.5 Å, which is 0.3 Å longer than that of ACh (2.2 Å). However, it has an additional H-bond with residue Thr193, favoring its interaction with the receptor. Therefore, all of the aforementioned metabolites have binding affinities for M_5R and could compete with ACh for the binding to M_5R. Thus, it is evident that the metabolites of VLB such as metabolite 22 and metabolite 23 affect the function of M_5R during chemotherapy with VLB and could play a role in the development of nausea. (**Table 2.6**)

The ADMET results for VLB and metabolites have shown that all of them are inhibitors of CYP2D6 and CYP3A4. They could be metabolized by CYP3A4 and transported out of the cell by P-gp as well. This could explain why drug-drug interactions are seen with VLB when a variety of drugs are taken in concomitance. In addition, drugs that are metabolized by, or inhibit CYP2C8 and/or CYP2C9, and are taken concurrently with VLB, also account for drug-drug interactions during chemotherapy with VLB. This is because the metabolites of VLB can also be metabolized by or inhibit these two isoenzymes, thus an enzymatic competition is likely to occur. (**Tables 2.9** and **2.10**)

Among the VLB metabolites, metabolite 23 interacts well with nausea associated receptors. Its PK properties are of extremely importance for evaluation of how this metabolite behaves inside the body. It has an intestinal solubility (FaSSIF) of 3.70 mg/mL, and an affinity for plasma proteins with 77.2% of it unbound, therefore indicates its availability for off-targets binding. (**Tables 2.7** and **2.8**)

Moreover, the predicted results demonstrate that only a few metabolites of VLB undergo phase II metabolism through UGT. It is noteworthy that metabolite 22 and metabolite 23, which display strong binding affinities and similar binding profile to the substrates for all nausea associated receptors, can undergo glucuronidation through catalysis of UGT2B7. Therefore, their effect within the body must be investigated due to the fact that glucuronidation reaction can also cause toxicity [67]. In addition, a few metabolites of VLB block hERG receptor involved in cardiotoxic events and can cross the BBB, thus further investigation on the effects of these metabolites in different organ tissues is needed. (**Table 2.11**)

2.5 Bibliography

1. Shankar, A., et al., *Prevention of Chemotherapy-Induced Nausea and Vomiting in Cancer Patients.* Asian Pac J Cancer Prev, 2015. **16**(15): p. 6207-13.
2. Beusterien, K., et al., *Use of conjoint analysis to assess breast cancer patient preferences for chemotherapy side effects.* Oncologist, 2014. **19**(2): p. 127-34.
3. Holt, K., *Common side effects and interactions of colorectal cancer therapeutic agents.* J Pract Nurs, 2011. **61**(1): p. 7-20.
4. Kuchuk, I., et al., *Preference weights for chemotherapy side effects from the perspective of women with breast cancer.* Breast Cancer Res Treat, 2013. **142**(1): p. 101-7.
5. Jordan, K., et al., *International antiemetic guidelines on chemotherapy induced nausea and vomiting (CINV): content and implementation in daily routine practice.* Eur J Pharmacol, 2014. **722**: p. 197-202.
6. Lohr, L., *Chemotherapy-induced nausea and vomiting.* Cancer J, 2008. **14**(2): p. 85-93.
7. Yoodee, J., U. Permsuwan, and M. Nimworapan, *Efficacy and safety of olanzapine for the prevention of chemotherapy-induced nausea and vomiting: A systematic review and meta-analysis.* Crit Rev Oncol Hematol, 2017. **112**: p. 113-125.
8. Hesketh, P.J., K. Bohlke, and M.G. Kris, *Antiemetics: American Society of Clinical Oncology Clinical Practice Guideline Update Summary.* J Oncol Pract, 2017. **13**(12): p. 825-830.

9. O'Brien, C., *Nausea and vomiting.* Can Fam Physician, 2008. **54**(6): p. 861-3.

10. Flynn, M., K.A. Heale, and L. Alisaraie, *Mechanism of Off-Target Interactions and Toxicity of Tamoxifen and Its Metabolites.* Chem Res Toxicol, 2017. **30**(7): p. 1492-1507.

11. Salmas, R.E., et al., *Modeling and protein engineering studies of active and inactive states of human dopamine D2 receptor (D2R) and investigation of drug/receptor interactions.* Mol Divers, 2015. **19**(2): p. 321-32.

12. Osinski, M.A., et al., *Dopamine D2, but not D4, receptor agonists are emetogenic in ferrets.* Pharmacol Biochem Behav, 2005. **81**(1): p. 211-9.

13. Ishikawa, M., et al., *Investigation of the histamine H3 receptor binding site. Design and synthesis of hybrid agonists with a lipophilic side chain.* J Med Chem, 2010. **53**(17): p. 6445-56.

14. Shimamura, T., et al., *Structure of the human histamine H1 receptor complex with doxepin.* Nature, 2011. **475**(7354): p. 65-70.

15. Sullivant, A., et al., *Identification of histamine receptors in the canine gastrointestinal tract.* Vet Immunol Immunopathol, 2016. **182**: p. 29-36.

16. Thurmond, R.L., *Histamine inflammation. Preface.* Adv Exp Med Biol, 2010. **709**: p. vii-viii.

17. Bailey, F. and A. Davies, *The misuse/abuse of antihistamine antiemetic medication (cyclizine) by cancer patients.* Palliat Med, 2008. **22**(7): p. 869-71.

18. Doenicke, A.W., R. Hoernecke, and I. Celik, *Premedication with H1 and H2 blocking agents reduces the incidence of postoperative nausea and vomiting.* Inflamm Res, 2004. **53 Suppl 2**: p. S154-8.

19. Ishii, M. and Y. Kurachi, *Muscarinic acetylcholine receptors.* Curr Pharm Des, 2006. **12**(28): p. 3573-81.

20. Lochner, M. and A.J. Thompson, *The muscarinic antagonists scopolamine and atropine are competitive antagonists at 5-HT3 receptors.* Neuropharmacology, 2016. **108**: p. 220-8.

21. Zhong, W., et al., *Ca(2+) signaling and emesis: Recent progress and new perspectives.* Auton Neurosci, 2017. **202**: p. 18-27.

22. Golding, J.F. and J.R. Stott, *Comparison of the effects of a selective muscarinic receptor antagonist and hyoscine (scopolamine) on motion sickness, skin conductance and heart rate.* Br J Clin Pharmacol, 1997. **43**(6): p. 633-7.

23. Ratnala, V.R., et al., *Solid-state NMR evidence for a protonation switch in the binding pocket of the H1 receptor upon binding of the agonist histamine.* J Am Chem Soc, 2007. **129**(4): p. 867-72.

24. Lichman, B.R., et al., *'Dopamine-first' mechanism enables the rational engineering of the norcoclaurine synthase aldehyde activity profile.* FEBS J, 2015. **282**(6): p. 1137-51.

25. Schyman, P., et al., *The directive of the protein: how does cytochrome P450 select the mechanism of dopamine formation?* J Am Chem Soc, 2011. **133**(20): p. 7977-84.

26. Lioe, H., C.K. Barlow, and R.A. O'Hair, *How does acetylcholine lose trimethylamine? A density functional theory study of four competing mechanisms.* J Am Soc Mass Spectrom, 2009. **20**(2): p. 238-46.

27. Uveges, A.J., et al., *The role of transmembrane helix 5 in agonist binding to the human H3 receptor.* J Pharmacol Exp Ther, 2002. **301**(2): p. 451-8.

28. Durdagi, S., et al., *Binding Interactions of Dopamine and Apomorphine in D2High and D2Low States of Human Dopamine D2 Receptor Using Computational and Experimental Techniques.* ACS Chem Neurosci, 2016. **7**(2): p. 185-95.

29. Kalani, M.Y., et al., *The predicted 3D structure of the human D2 dopamine receptor and the binding site and binding affinities for agonists and antagonists.* Proc Natl Acad Sci U S A, 2004. **101**(11): p. 3815-20.

30. Platania, C.B., et al., *Homology modeling of dopamine D2 and D3 receptors: molecular dynamics refinement and docking evaluation.* PLoS One, 2012. **7**(9): p. e44316.

31. Peng, J.Y., et al., *The predicted 3D structures of the human M1 muscarinic acetylcholine receptor with agonist or antagonist bound.* ChemMedChem, 2006. **1**(8): p. 878-90.

32. Thal, D.M., et al., *Crystal structures of the M1 and M4 muscarinic acetylcholine receptors.* Nature, 2016. **531**(7594): p. 335-40.

33. Leach, K., et al., *The role of transmembrane domain 3 in the actions of orthosteric, allosteric, and atypical agonists of the M4 muscarinic acetylcholine receptor.* Mol Pharmacol, 2011. **79**(5): p. 855-65.

34. Huang, X., G. Zheng, and C.G. Zhan, *Microscopic binding of M5 muscarinic acetylcholine receptor with antagonists by homology modeling, molecular docking, and molecular dynamics simulation.* J Phys Chem B, 2012. **116**(1): p. 532-41.

35. Predictor, A., *ADMET Predictor User Manual*. March 13, 2017.

36. El-Saadi, M.W., et al., *Use of in-silico assays to characterize the ADMET profile and identify potential therapeutic targets of fusarochromanone, a novel anti-cancer agent.* In Silico Pharmacol, 2015. **3**(1): p. 6.

37. Graham, L.P., *Introduction to Medicinal Chemistry* Fifth ed. 2013: Oxford.

38. Rang, H.P., Flower, R.J., Henderson, G., Ritter, J.M., *Rang and Dale's Pharmacology*. 2015: Elsevier.

39. Ogihara, T., et al., *What kinds of substrates show P-glycoprotein-dependent intestinal absorption? Comparison of verapamil with vinblastine.* Drug Metab Pharmacokinet, 2006. **21**(3): p. 238-44.

40. Haga, T., *Molecular properties of muscarinic acetylcholine receptors.* Proc Jpn Acad Ser B Phys Biol Sci, 2013. **89**(6): p. 226-56.

41. Lipinski, C.A., et al., *Experimental and computational approaches to estimate solubility and permeability in drug discovery and development settings.* Adv Drug Deliv Rev, 2001. **46**(1-3): p. 3-26.

42. Chagas, C.M., S. Moss, and L. Alisaraie, *Drug metabolites and their effects on the development of adverse reactions: Revisiting Lipinski's Rule of Five.* Int J Pharm, 2018. **549**(1-2): p. 133-149.

43. Donigian, D.W. and R.J. Owellen, *Interaction of vinblastine, vincristine and colchicine with serum proteins.* Biochem Pharmacol, 1973. **22**(17): p. 2113-9.

44. Takahashi, I., et al., *Interaction of human serum albumin with anticancer agents in vitro.* Br J Cancer, 1980. **41**(4): p. 602-8.

45. Pandya, P., et al., *Molecular recognition pattern of cytotoxic alkaloid vinblastine with multiple targets.* J Mol Graph Model, 2014. **54**: p. 1-9.

46. *BC Cancer Agency Cancer Drug Manual - Vinblastine*. 2015.

47. Leveque, D. and F. Jehl, *Molecular pharmacokinetics of catharanthus (vinca) alkaloids.* J Clin Pharmacol, 2007. **47**(5): p. 579-88.

48. Malik, M.Z., et al., *Pharmacokinetic evaluation of anticancer drugs in Hodgkin's lymphoma patients after their simultaneous administration.* Pak J Pharm Sci, 2016. **29**(6): p. 2079-2082.

49. Daneman, R. and A. Prat, *The blood-brain barrier.* Cold Spring Harb Perspect Biol, 2015. **7**(1): p. a020412.

50. Horio, M., M.M. Gottesman, and I. Pastan, *ATP-dependent transport of vinblastine in vesicles from human multidrug-resistant cells.* Proc Natl Acad Sci U S A, 1988. **85**(10): p. 3580-4.

51. Sharom, F.J., *The P-glycoprotein multidrug transporter.* Essays Biochem, 2011. **50**(1): p. 161-78.

52. Silva, R., et al., *Modulation of P-glycoprotein efflux pump: induction and activation as a therapeutic strategy.* Pharmacol Ther, 2015. **149**: p. 1-123.

53. Long, Q.Z., et al., *Interaction of CCN1 with alphavbeta3 integrin induces P-glycoprotein and confers vinblastine resistance in renal cell carcinoma cells.* Anticancer Drugs, 2013. **24**(8): p. 810-7.

54. Diaz, G.J., et al., *The [3H]dofetilide binding assay is a predictive screening tool for hERG blockade and proarrhythmia: Comparison of intact cell and membrane preparations and effects of altering [K+]o.* J Pharmacol Toxicol Methods, 2004. **50**(3): p. 187-99.

55. DrugBank. *Vinblastine*. Aug, 2017; Available from: https://www.drugbank.ca/drugs/DB00570.

56. Mikaelian, I., et al., *Primary endothelial damage is the mechanism of cardiotoxicity of tubulin-binding drugs.* Toxicol Sci, 2010. **117**(1): p. 144-51.

57. Legha, S.S., C. Hodges, and S. Ring, *Efficacy of ondansetron against nausea and vomiting caused by dacarbazine-containing chemotherapy.* Cancer, 1992. **70**(7): p. 2018-20.

58. Zhou, S.F., et al., *Substrates, inducers, inhibitors and structure-activity relationships of human Cytochrome P450 2C9 and implications in drug development.* Curr Med Chem, 2009. **16**(27): p. 3480-675.

59. Chandrani, G., *Drug Metabolism & Pharmacokinetics in Drug Discovery: A Primer for Bioanalytical Chemists, Part I.* Current Separations, 2000. **19:1**.

60. Medscape, *Drug Interactions*. 2017.

61. Wang, B., et al., *New insights into the structural characteristics and functional relevance of the human cytochrome P450 2D6 enzyme.* Drug Metab Rev, 2009. **41**(4): p. 573-643.

62. Wenzell, C.M., et al., *Pilot study on the efficacy of an ondansetron- versus palonosetron-containing antiemetic regimen prior to highly emetogenic chemotherapy.* Support Care Cancer, 2013. **21**(10): p. 2845-51.

63. Youssef, A.S., H.P. Parkman, and S. Nagar, *Domperidone interacts with pioglitazone but not with ondansetron via common CYP metabolism in vitro.* Xenobiotica, 2014. **44**(9): p. 792-803.

64. Zhou-Pan, X.R., et al., *Involvement of human liver cytochrome P450 3A in vinblastine metabolism: drug interactions.* Cancer Res, 1993. **53**(21): p. 5121-6.

65. Rendic, S. and F.J. Di Carlo, *Human cytochrome P450 enzymes: a status report summarizing their reactions, substrates, inducers, and inhibitors.* Drug Metab Rev, 1997. **29**(1-2): p. 413-580.

66. Baumhakel, M., et al., *Screening for inhibitory effects of antineoplastic agents on CYP3A4 in human liver microsomes.* Int J Clin Pharmacol Ther, 2001. **39**(12): p. 517-28.

67. Sorich, M.J., et al., *The importance of local chemical structure for chemical metabolism by human uridine 5'-diphosphate-glucuronosyltransferase.* J Chem Inf Model, 2006. **46**(6): p. 2692-7.

68. Owellen, R.J., C.A. Hartke, and F.O. Hains, *Pharmacokinetics and metabolism of vinblastine in humans.* Cancer Res, 1977. **37**(8 Pt 1): p. 2597-602.

CHAPTER 3 Effects of Vinblastine and its Metabolites on Alopecia Associated Receptors

3.1 Introduction

3.1.1 Chemotherapy-Induced Alopecia

Chemotherapy-induced alopecia (CIA) remains one of the most unpleasant side effects during cancer treatment. The hair follicle (HF) is an unwanted target for anticancer drugs to affect, due to the fact that their matrix keratinocytes division rate can be higher than that of the neoplastic cells [1]. The occurrence of CIA is seen in 65% of the patients and depends on various factors. CIA leads to both psycho and physiological distress in patients with cancer. According to Patel *et al.*, around 50% of patients consider hair loss as the most traumatic experience during chemotherapy, and 8% of them would deny receiving chemotherapy [2]. Hair loss can begin anytime during chemotherapy, from days to a few weeks. Depending on the drug and therapy schedule, alopecia can occur during treatment or several weeks after the start of the first treatment and can progress gradually for 1 to 2 months [3-6]. The regrowth of hair usually occurs from 1 to 6 months after chemotherapy. Even though rare, permanent CIA is becoming more reported due to injury of the bulge and bulb hair, where stem cells are located. CIA can also affect the melanocytes, which can change the pigmentation color of the HF and its shape. Thus the hair can become either gray and/or curly after chemotherapy [7].

CIA can occur in more than 80% of the patients undergoing treatment with vinca alkaloids drugs and/or antimicrotubule agents. VLB is known to cause alopecia in cancer

patients [1, 5]. Interestingly, whilst VLB was under preliminary clinical trials, a study conducted by Crounse and Scott showed that it caused severe alopecia in treated-patient, in addition to the oral ulceration and myelosuppression [8].

Currently, the most effective treatment and/or prevention of alopecia during chemotherapy is the scalp cooling device. The cold cap constricts blood vessels and interrupts chemotherapeutic agent circulation in the scalp due to the low temperature setting. Some patients have headaches as a secondary effect when using the cold cap which is called brain freeze [9]. The rate of its effectiveness ranges from 50-80%. Despite advances with targeted therapies and radiotherapy, chemotherapy is still widely used and the scalp cooling device to reduce alopecia is not well received by most of patients going through the treatment [2, 10].

The amount of hair loss depends on the drug, dosage and route of administration. For instance, radiotherapy is delivered to a specific area and may cause hair loss only in the area receiving the treatment. In addition, hormonal therapy does not usually cause complete hair loss. Apart from the scalp cooling device, there are a variety of treatment options to alleviate or prevent alopecia during chemotherapy, but none of them have demonstrated significant success. Rubio-Gonzalez *et al.* have reviewed the most recent therapeutic approaches for CIA that include non-approved topical formulations of minoxidil, calcitriol, bimatoprost and others [5]. Similar to minoxidil, also spironolactone and finasteride may help the hair to regrow [2, 5]. CIA is defined as a diffuse nonscarring alopecia because it slowly reduces the hair growth and maintains the follicular ostia, where

the hair fibers grows from the skin. Alopecia caused by VLB can take up to 6 months for complete hair recovery [5].

Advances in the health care field to treat or prevent alopecia during chemotherapy include drug interventions and the use of an appropriate medical device system. However, physicochemical properties of the chemotherapeutic agents, which are the main cause of hair loss during cancer therapy, are yet to be studied.

3.1.2 Hair Follicle Cycle

Regulation of the hair cycle is obtained by the interchangeable interactions between the epithelial keratinocytes and the dermal papilla. The hair cycle is divided into three main phases known as anagen (growing), catagen (involution), and telogen (rest). During life, the keratinocytes or the proliferating matrix cells of the majority of HF are in the anagen phase (80-90%), while 5-10% are in the telogen phase and 1-3% in the catagen [5, 11]. The transition order of phases in the hair cycle occurs as anagen-to-catagen, catagen-to-telogen and telogen-to-anagen. The first phase is responsible to induce HF apoptosis when it is necessary in the natural cycle. Death of HF is a normal maintenance process of the hair cycle, but it can also be early induced during treatment of xenobiotics that target the proliferating matrix cells or the dermal papilla. The telogen-to-anagen transition phase causes the HF to exit quiescence or resting state, and to regrow again. These important HF transition states must be well coordinated and controlled to maintain cell survival and hair optimal conditions. An anagen cycle can last for many years, while the other two HF states last for a few days or months [12]. Different from mammals, human hair follows an asynchronous growth pattern. This miscellaneous or so-called mosaic pattern is

characterized by an independent HF growth, which no individual HF follows its neighbor hair cycle [13].

Signaling molecules such as bone morphogenic protein (BMP), Wingless (Wnt) and Hedgehog (Hh) are involved in the anagen onset pathway during embryonic and postnatal life cycles [7, 12]. The initiation process of the hair cycle occurs after nearly one month from the time a HF is in the telogen phase. The levels of Wnt antagonists such as Dickkopf (DKK1) and Secreted Frizzled-Related Protein 4 (SFRP4), as well as the levels of BMP2/4 signaling molecules, are decreased during the initiation of a hair cycle. The low expression of these antagonist ligands leads to the activation of Wnt signaling pathway, initiating anagen phase and hair growth. Another signaling molecule that positively controls the telogen-to-anagen phase is the fibroblast growth factor (FGF) 18, which is known to function as an antiproliferative protein that prolongs the duration of the HF in the refractivity telogen period. The deletion of FGF18 shortens the refractivity period of telogen by one week instead of one month, thus it normally works as a telogen inhibitory factor. In addition, overexpression of Noggin, an antagonist of BMP, reduces activity of BMP, thus initiates anagen more quickly. Another regulator of BMP during refractivity telogen phase is the transforming growth factor (TGF-β2) mediated via paracrine signaling during initiation of anagen [12]. Therefore, BMP signaling pathway must be inhibited during initiation of a hair cycle. Moreover, signaling molecules such as Notch proteins, sonic hedgehog (Shh), epidermal growth factor (EGF) and tumor necrosis factor (TNF) are also involved in the control of hair cycle [1, 5]. (**Figure 3.1** and **Table 3.1).**

3.1.3 The Hair Follicle on the Chemotherapy-Induced Alopecia

Chemotherapeutic agents likely damage the hair bulb of the anagen hair follicle. This is an area where the proliferative matrix of keranoticytes responsible for the formation of hair shaft and inner root sheath are located. Thus, anticancer drugs disturb the active growing of the hair follicle, interrupt the normal hair cycle and induce alopecia. The hair can regrow because the region of the arrector pilli muscle where the epithelial stem cells are located (i.e. bulge region) is not usually targeted by the anticancer drugs. If this area is affected, loss of stem cells interrupts formation of a new hair follicle [4].

Each HF follows its own full cycle, without any synchronized growing. However, as most of the HF are in the anagen phase (80-90%), CIA is often referred to as dystrophic anagen effluvium [3, 5]. Thus anagen HF and their pigmentary system are the main targets during chemotherapy. The melanocytes produces lots of melanin during anagen phase that are transferred to the keratinocyte populations to form the hair-shaft. The HF vasculature and sebaceous gland also are affected by chemotherapy, and probably that occurs to the mesenchyme, too. Apparently, the anagen HF have mechanisms to self-repair and resist against damage during chemotherapy such as an increase in proliferative activity to overcome the HF injury. This explains why some patients do not experience baldness and for those who have alopecia, once the treatment is completed, the hair grows back to normal again [4]. CIA is irreversible only after treatment with busulfan chemotherapy and bone marrow transplantation. Dystrophic anagen effluvium is induced by vinca alkaloids where the amount of hair loss depends on the dose, route and schedule [2].

During chemotherapy, there are two main pathways by which alopecia can be induced, the dystrophic anagen and the dystrophic catagen. The former is defined as a less severe follicular damage where the pigmented hair shaft changes and the HF undergoes two recovery phases, thus it is considered a long recovery process. The latter causes a more severe damage, with no pigmentation changes and a short recovery process [4]. Paus *et al.* have demonstrated that the CIA of cyclophosphamide-treated mice results from a dystrophic catagen alopecia with shortened telogen phase, but more severe damage of the HF is observed [14]. Total hair loss generally occurs in the frontal and occipital hairlines. The alopecia induced by chemotherapy is usually reversible, but it depends on the degree of the damage in epithelial hair follicle stem-cell. Besides all the undesired side effects caused by chemotherapy such as nausea, fatigue, myelosuppression, etc. [15], the psychological stress behind this condition is considered a relevant reason for the inhibition of hair growth/maintenance. Physiological stress is highly associated with the release of inflammatory mediators such as corticotropin-releasing hormone, substance P, an undecapeptide, and nerve growth factor. These mediators inhibit hair growth of follicles and promote catagen phase development followed by telogen effluvium [4].

Drugs are known to induce hair loss by different mechanisms such as the telogen effluvium, anagen arrest, and accentuation of androgenetic alopecia by androgens [2]. If drugs cause telogen effluvium or anagen arrest, the HF undergoes an early and unexpected entrance to the catagen phase that leads to hair loss. This early transition to the catagen phase is the direct accumulation of any xenobiotic on the HF cells during the anagen phase. This effect then leads to the interruption of mitotic activity, known to induce the HF to

entry the catagen phase. The hair fiber is hence broken because the growing hair shaft is only partially keratinized [4, 5].

CIA is believed to cause toxicity to both the proliferative matrix keratinocytes cells and the follicular pigmentary system of the HF. This off-target event causes acceleration in the transition of anagen-to-catagen of the HF [5-7]. The HF that enters early dystrophic catagen state undergoes uncontrolled apoptosis, thus compromising the integrity of the hair shaft and eventually making the hair to break and fall out. The specific molecular mechanisms of the HF that are either activated or inhibited during chemotherapy remain largely unknown. Paus *et al.* have elucidated the pathobiology involved in CIA, and how DNA damage caused by chemotherapeutic drugs leads to apoptosis, cell-cycle arrest and/or senescence, and thus alopecia [4].

Hussein *et al.* have introduced the first mouse model undergoing chemotherapy with cyclophosphamide, which has shown that keratinocytes of the outer and inner root sheaths, as well as melanocytes have abnormal excessive death of First Apoptosis Signal Receptor (FAS) and p55TNFR [16]. Furthermore, an upregulation of pro-apoptotic protein, Bcl-2-lymphoma-like protein 4 (BAX), in the HF and uncoordinated apoptosis have been demonstrated [16, 17]. Transcriptional factor p53 mediates DNA damage responses and involves upregulation of BAX and β-cell lymphoma 2 (BCL-2) proteins. It predisposes the HF cells to apoptosis either in normal conditions or during chemotherapy. In mice model with p53 deficient, neither apoptosis nor hair loss were observed in the keratinocytes matrix after chemotherapy [17]. P21 is a p53 target gene that is upregulated during DNA damage. Accumulation of p21 leads to binding and inactivation of Cyclin-Dependent Kinase 2

(CDK2)/cycling E complex, resulting in G1/S phase inhibition. P21 is not found in hair keratinocytes, however, CDK2 inhibitors have shown reduced hair loss induced by chemotherapy. In addition, p53 inhibitors may suppress hair loss during chemotherapy [17]. Therefore, it is well known that the HF undergo apoptosis during chemotherapy due to the activation of p53 transcription factor [3, 4, 7, 18, 19]. A study of cyclophosphamide-treated mice has shown that proteins involved in the p53 signaling pathway, such as pro-apoptotic BAX and anti-apoptotic Bcl-2, have increased and decreased expression levels, respectively [20]. Moreover, FAS and c-Kit proteins, involved in the p53 cycle activation, have been also shown to induce HF apoptosis induced by chemotherapy [21]. Inhibition of p53 through MDM2 controller, a negative regulator of p53, promotes HF survival after chemotherapy, indicating that apoptosis through activation of MDM2-p53 complex is indeed a mechanism that results in HF lost [4].

Hair-bulb melanocytes affected by chemotherapy can either express FAS that induces apoptosis, or c-Kit receptor that sends signals to proliferative cells to migrate towards the epidermis. The latter causes shrinkage of the hair and indicates a negative effect induced by FAS and c-Kit. However, studies have shown that c-Kit neutralizing antibody can avoid shrinkage of the hair, thus working as a positive regulator of the HF [4].

In normal hair cycle, the induction of apoptosis is the transition anagen-to-catagen is triggered by a variety of molecules such as FGF7, Interferon (IFN)-γ, substance P, estrogens; etc. [1]. Molecules identified during apoptosis and induced by chemotherapy include FGF7, ABC transporters, vitamin D receptor (VDR), parathyroid hormone (PTH),

EGF receptor (EGFR), and cyclin-dependent kinase 2 (CDK2) [4, 7]. Skrok *et al.* have thoroughly illustrated the proteins and their signaling pathways expressed in the HF and also those which have been postulated as modulators of the hair cycle [22]. Several proteins have been identified being activated or inhibited during CIA, depending on their own normal function in the HF. Important pathways responsible for the hair development, differentiation, proliferation and cycle which are unregulated during chemotherapy include Wnt/β-catenin, Shh, Notch and BMP/Noggin signaling. Additionally, a great variety of protein receptors involved in hormone regulation and apoptosis are expected to participate during CIA process [5, 22]. CIA is a complex mechanistic adverse effect that requires further in-depth investigation of its relevant signaling pathways. (**Figure 3.1** and **Table 3.1**)

Table 3.1: Main signaling pathways involved in the development, differentiation, proliferation and maintenance of the HF and their receptor, ligand, location in the HF, likelihood of activated or inhibited states as well as their PDB entry.

	Protein Signaling	Ligand	Location in the HF	Normal role in the HF	In CIA	PDB entry	Ref.
Hair Follicle Control	Wnt	Frizzled	Outer root sheath	Development, proliferation, differentiation	-	3S2K	[23, 24]
	Shh (SMO)	Cyclo-pamine LY2940680 Anta XV	Dermal papilla	Development, proliferation, differentiation	-	4O9R 4JKV 4QIM	[11, 25-27]
	Notch	Jagged1/2DL L1/3/4	Proliferating matrix, outer root sheath	Development, proliferation, differentiation	-	4XBM	[28, 29]
	BMP	Noggin	Dermal papilla	Development, proliferation, differentiation	+	1M4U	[11]
Hormones-Related	PTH1R	PTH PTHrP	Dermal sheath and papilla	Proliferation, differentiation	+	3C4M 3H3G	[22, 30]
	Vitamin D Receptor	Calci-triol TEI-9647	Dermal papilla and outer root sheath	Anagen initiation and differentiation	-	1DB1 3A2J	[31]
	FGFR1	FGF5	Dermal papilla	Induces anagen-to-catagen	+		[32]
	FGFR	FGF7	Dermal papilla, keratinocytes	Inhibits free radicals to induce apoptosis	-		[4, 33, 34]
	Androgen Receptor	Testos-terone DHT Bicalu-tamide	Dermal papilla	Inhibits Wnt/β-catenin pathway	+	2AM9 2AMA 1Z95	[35]
	EGFR	EGF	Hair matrix	Up-regulates p53	+		[36]

	ABC Transp.		Outer root sheath of the lower isthmus (insertion of arrector pili muscle)	Use energy from ATP hydrolysis to move substrates from the cell. May protect HF keratinocytes	-	6C0V	[4]
	FAS	FASL	Hair matrix, melanocytes; outer and inner root sheath	Apoptosis (pro-apoptotic)	+	4MSV 3TJE	[1, 4, 37]
Cellular Control	p53	MDM2	Hair matrix; outer root sheath	MDM2 forms a complex with p53. If apoptosis is required, MDM2 is inhibited and p53 gets free	+	1YCR	[1, 4]
	MDM2	Nutlins	Hair matrix; outer root sheath	Inhibition of MDM2 leads to p53 activation hence apoptosis	-	1RV1	[38]
	BAX		Hair matrix;	Apoptosis (pro-apoptotic)	+		[1, 4]
	BCL-2		Melanocytes; hair matrix; dermal papilla	Anti-apoptotic	-		[1, 4]
	CDK2	Cyclin A Stauros-porine	Post-mitotic keratinocytes	Stimulates cell-cycle arrest	+	1FIN 1AQ1	[4, 37, 39]

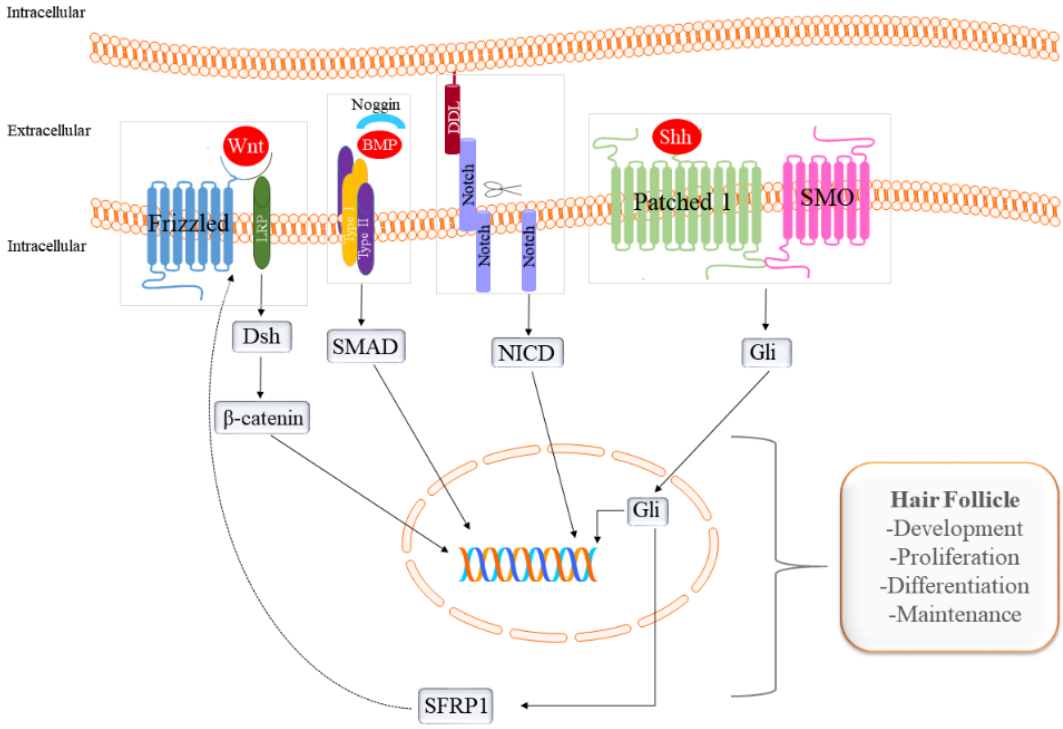

Figure 3.1: Signaling pathways involved in the development, proliferation and maintenance of the adult hair follicle.

3.1.4 Signaling Molecules Involved in Chemotherapy-Induced Alopecia

3.1.4.1 Hormones-Related

3.1.4.1.1 Testosterone

Testosterone is a steroid hormone that mainly contributes to the male reproductive system development, but it is also secreted by the ovaries. It binds and activates androgen receptor (AR), that among a great diversity of functions, regulates the skin physiology and the HF development. It is suggested that AR activation leads to inhibition of Wnt/β-catenin signaling in murine HF, thus negatively controlling the hair cycle pathway. However, the

exact mechanism by which activation of AR inhibits hair growth remains to be elucidated [35, 40].

One of the proposed mechanism of AR inducing catagen in the HF it that expression of 5α-dihydroxytestosterone (DHT), a metabolite of testosterone, in the dermal papillae leads to an increase of interleukin (IL) 6 and glycoprotein 130 expression. These molecules are known to be involved in the transition of anagen-to-catagen [22]. DHT is a stronger activator of AR than testosterone and indirectly inhibits the matrix cell proliferation leading to hair shaft shortening [11]. (**Table 3.1**)

The AR is classified as a nuclear receptor superfamily as it posses a N-terminal domain (NTD), a conserved DNA-binding domain (DBD) and more importantly, a ligand-binding domain (LBD), where testosterone or DHT bind to. It is known that the binding site of AR is highly hydrophobic and that the LBD adopts a sandwich α-helical conformation, a known feature of nuclear receptors. Despite the polar residues at the extremities of the binding pocket, the recognition of AR is mediated by hydrophobic residues that confers selectivity and stability of the substrate. The AR structure is comprised of 11 α-helices and 4 β-strands, whereas residues of helices H3, H4, H5, H11 and β-strand among H5 and H6 comprise the flexible LBD. One essential residue required for activation of AR is Arg752 that makes a H-bond with the ketone group of androgen ligands [41]. The natural substrates of AR, testosterone and DHT both have four cycles named A, B, C and D. These steroid-based structures have a ketone at position C3 and a hydroxyl group at position 17β in cycle D (cyclopentanol), respectively. They only differ by a cyclohexanone present at cycle A of testosterone. This structural difference among

testosterone and DHT changes the orientation of the ketone group at C3 of DHT, increasing its strength in the binding interaction with residue Arg752 [41]. (**Figure 3.2**)

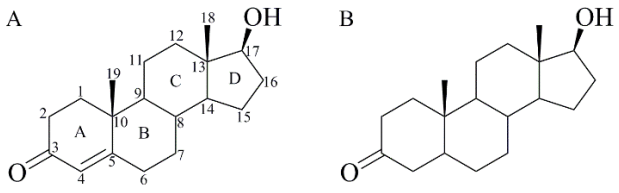

Figure 3.2: Chemical structures of the endogenous substrates of androgen receptor. A) Testosterone and B) DHT.

3.1.4.1.2 Prostaglandins

Prostaglandin (PG) subtype D_2 (PGD_2) and its metabolite 15-deoxy-Δ(12,14)-prostaglandin J2 (15-dPGJ2) have been shown to be involved in HF growth inhibition. High concentrations of 15-dPGJ2 in human HF cultured cells are induces apoptosis in HF and cause alopecia [42]. Upregulation of PGD_2 which is synthesized through an enzyme mechanism induced by testosterone has been suggested to be involved in androgenetic alopecia. This signaling pathway could be activated during chemotherapy, however, this hypothesis has not been confirmed [43]. Interestingly, during chemotherapy there is an increase in the expression of cyclooxygenase-2 (COX-2) that induces synthesis of PGs, especially prostaglandin E_2, suggesting its possible role during alopecia [44]. However, the mechanism by which either PGD_2 or PGE_2 can dysregulate the hair cycle is still unclear.

3.1.4.1.3 Parathyroid

Parathyroid hormone (PTH) is considered an inhibitor of hair development. PTH has been shown to function as an inducer of anagen-to-catagen transition phase in the HF [22, 30]. As a response of low levels of calcium, PTH is synthesized to promote calcium reabsorption in the kidneys and to synthesize 1,25-dihydroxyvitamin D_3 [45]. Also a polypeptide, the PTH related protein (PTHrP) shares 70% homology with the N-terminal of PTH. Both molecules and their receptor, the parathyroid hormone receptor (PTH1R) are all expressed in the hair, mainly in the dermal sheath and dermal papilla. It seems that the activation of PTH1R leads to induction of the anagen-to-catagen transition on the HF [22, 30].

The mechanism by which activation of PTH1R is suggested to be involved in CIA requires at least the binding of PTH or any other agonist in the transmembrane (7TM) of the receptor. However, the specific residues of PTH1R responsible for the PTH/PTHrP interaction hence induction of activation remain to be elucidated. Shimizu *et al.* have reported that PTH lacks the C-terminal fragment (15-34) and with the N-terminal modified is able to antagonize the receptor [46]. However, there is no further details about which N-terminal modifications are required for PTH1R antagonism effect, neither how the binding interactions take place. (**Table 3.1**)

3.1.4.1.4 Vitamin D

Vitamin D receptor (VDR) regulates the levels of calcium and phosphate that are responsible for bone development and maintenance. When vitamin D is synthesized into its active form, the seco-steroid hormone 1α,25-dihydroxyvitamin D3 ($1,25(OH)_2D$), also

known as calcitriol, it activates VDR which is expressed in different cellular tissues such as skin and hair. Resistance of VDR is related to rickets, a hereditary disease that is caused by a receptor mutation that leads to hypocalcemia, osteomalacia and alopecia. However, treatments for rickets cannot only suppress alopecia. This indicates that VDR is required in postnatal hair growth and maintenance as it is expressed in two fundamental communicable regions for the hair cycle regulation, namely dermal papillae and keratinocytes cells [31].

In vitro studies have shown that VDR is found in high concentrations during late anagen and catagen phases which are characterized by a decrease in cell division and an enhancement in differentiation. It is suggested that the lack of VDR expression might be the cause for observed alopecia. In addition, studies have been demonstrating that VDR is also somehow correlated with Hairless (Hr) gene, retinoid X receptor (RXR) and Wnt signaling [47]. For instance, it is thought that VDR regulates Hr expression due to high levels of Hr detected in VDR knockout mice, but not in the wild-type mice [47]. The heterodimerization formed by VDR and RXR is essential for maintenance of the hair cycle as RXR knockout mice exhibit similar alopecia patterns compared with VDR knockout. Therefore, the involvement of VDR with these protein receptors may be a reasonable explanation for alopecia induced by deregulation of VDR as many other signaling pathways are involved in CIA [47]. Topical application of VDR is a proposed treatment to reduce the activity of chemotherapy agents which are ABCB1 substrates in the HF [4]. (**Table 3.1**)

VDR belongs to the NR superfamily and its activation is mediated by the binding of 1,25-$(OH)_2D$. The VDR is comprised of 13 α-helices and 3 β-sheets, which residues of H3 and H5 are involved in the ligand binding domain activation by 1,25-$(OH)_2D$. In particular, residues Arg274 (H5), His305 (loop H6-H7) and His397 (H12) promote the receptor ligand affinity and activity [48]. A derivative of calcitriol, the antagonist (23S)-25-dehydro-1α-hydroxyvitamin D_3-26,23-lactone (TEI-9647) is found to inactive VDR by interacting with residues His397, Tyr143, Ser237, Arg274 and Ser278. Among those interactions, TEI-9647 binds to residue His397 and changes the conformation of H12 in a way that allows a covalent bond formation among residues Cys403 or Cys410. The presence of either cysteine residues at the C-terminal of VDR confers antagonism of the receptor [49]. Therefore, the binding of TEI-9647 to VDR requires interaction with residue His397 to initiate antagonism of the receptor, whereas the binding of calcitriol requires interaction mainly with residue His305 for receptor activation [48, 49].

The structure of the antagonist TEI-9647 only differs in the C23 position of calcitriol, whereas the 25-OH is replaced by a bulky lactone ring that prevents the closure of helix 12 of the VDR, a remarkable feature for receptor activation. Other mechanism proposed is that the methylene group attached at the C25 group of lactone ring can react with either Cys403 or Cys410 residues, thus inactivating VDR [49]. (**Figure 3.3**)

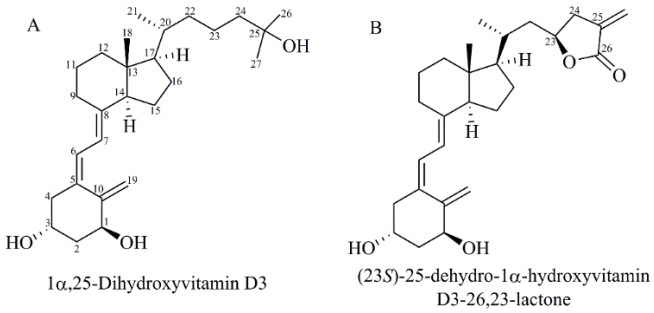

Figure 3.3: Chemical structures of endogenous substrate of vitamin D receptor A) 1α,25-(OH)D_3 and B) Antagonist TEF-9647.

3.1.4.1.5 Fibroblast-Growth Factor

Fibroblast-growth factor (FGF) is a ligand protein that interacts with FGF receptor (FGFR). There are at least 22 different FGFs that are divided into subfamilies that bind to four types of FGFRs (1-4) [50]. Beenken *et al.* [50] and Ornitz *et al.* [51] have thoroughly illustrated the classification, biology, pathophysiology, therapy and signaling cascade of FGF-FGFRs complex. They reviewed that the activation of FGF-FGFR complex protein is mainly mediated by the recruitment and binding of heparin sulphate glycosaminoglycan that strengths protein-protein interaction. After coupling, the ligand-receptor interact with another ligand-receptor to form a 2:2 FGF-FGFR-heparin complex dimer required for downstream signal transduction responses [50, 51]. Once the FGF-FGFR-heparin complex is formed, the activation of the receptor occurs upon ATP binding to and phosphorylation of the tyrosine kinase domain, a region that contains different residues from those participating in the heparin binding [52].

FGF5 has been strongly related with a negative controlling of the hair length. Its activation induces the HF to undergo an earlier catagen phase, thus diminishing the length of the hair. Studies have been shown that FGF5 knockout in mice increases the hair length [53, 54]. Overexpression of FGF5 in the dermal papilla cells of cashmere goats leads to an increase in BMP4 expression and to a decrease in noggin levels. This demonstrates the negative effect on the HF induced by FGF5 as BMP4 itself also induces early catagen and apoptosis in the HF [32]. Moreover, FGF7 also known as KGF (keratinocyte growth factor), is thought to protect the HF from CIA through regulation/stimulation of BCL2 and PI3K. FGF7 inhibits free radicals to induce apoptosis, but the exactly mechanism is not yet known [3, 4, 33]. (**Table 3.1**)

3.1.4.1.6 Epidermal Growth Factor

Epidermal growth factor (EGF) is involved in cell differentiation and proliferation. The signaling of epidermal growth factor receptor (EGFR) is negatively correlated with the hair cycle maintenance. Activation of EGFR is likely to induce early catagen phase transition within the HF as EGFR inhibition by gefitinib reduced alopecia in breast cancer patients [36]. Bichsel *et al.* have tested both cyclophosphamide-chemotherapy in EGFR knockout mice and in EGFR inhibitor-treatment and showed that alopecia was not developed in any model [36]. The mechanism behind EGFR effect is that if the receptor is knockdown, less cell proliferation in the hair follicle is observed, thus preventing or diminishing alopecia development [36]. (**Table 3.1**)

3.1.4.2 Cellular Control Pathways

Cancer is caused by many dysregulated cell functions such as upregulated mitosis and impaired apoptosis. For instance, after uncontrolled cell proliferation, cells accumulate in the cellular tissue due to an imbalance of pro-apoptotic and anti-apoptotic factors. The p53 transcriptional factor is known as a fundamental factor causing of alopecia induced by chemotherapy as it is related to cellular stress level and apoptosis [3, 4, 7, 18, 19].

3.1.4.2.1 Pro- and Anti-Apoptotic Proteins

During cancer treatment, p53 is normally found in high concentrations to promote upregulation of pro-apoptotic proteins First-Apoptosis Signal Receptor (FAS) and B-cell lymphoma-2-like protein 4 (BAX), and downregulation of anti-apoptotic protein B-cell lymphoma-2 (BCL-2). In the HF, increased levels of p53 in chemotherapy-treated mice are specifically seen in the outer and inner root sheaths. The high levels of p53 induces increased levels of FAS and BAX, and decreased levels of BCL-2, that potentially leads to the death of HF and alopecia during chemotherapy [3, 4, 17-19, 37]. (**Table 3.1**)

Sharov *et al.* have demonstrated that mice receiving cyclophosphamide but treated with anti-FAS ligand-neutralizing antibody did not result in alopecia [37]. The endogenous substrate of FAS, FAS ligand (FASL), exists in a trimeric form. FAS is a transmembrane protein type I and FASL is a transmembrane protein type II that belongs to the tumor necrosis factor superfamily (TNFSF). The interaction among ligand and receptor recruits a FAS-associated protein with death domain (FADD) that in turn activates caspase-8 to trigger apoptosis. Residues at the C-terminal loop of FASL seem to play a crucial role in

the binding of FAS [55]. Schneider *et al*. have shown that for one molecule of FAS, two of FASL are required for protein-protein interaction and activation of FAS signaling [56].

3.1.4.2.2 p53 Factor and Murine Double Minute 2 Homolog

p53 transcriptional factor is mainly regulated by murine double minute 2 homolog (MDM2), an E3 ubiquitin ligase protein that forms a complex with p53 [57]. Under normal cell stress conditions, MDM2-p53 complex is broken causing release of p53 to initiate apoptosis. In cancer cells, however, there is an overexpression of MDM2 that leads to inactivation of p53 function, thus impairing the normal apoptotic mechanism regulated by p53 [17, 58]. The activation of p53 pathway is controlled by an auto-regulatory feedback loop of MDM2 which inhibition of MDM2 leads to disruption of the complex and activation of p53. Thus, an inhibitor of MDM2 could promote apoptosis-induced by p53 [38, 59]. (**Table 3.1**)

Kussie *et al.* have identified the interaction among p53 and MDM2 in human species [57]. The transcriptional factor p53 is a small helical peptide of 15 residues that interacts with the hydrophobic cleft of MDM2 [57]. MDM2 is a protein of 85 amino acids length which structure is divided in two similar portions consisted of repeated β strands and α helices. The transcriptional factor p53 interacts with both α2 helix and β-sheet of MDM2 through VDW contacts and H-bonds [57].

The findings above has aroused special attention in the oncology field for the development of small molecules that could inhibit MDM2 hence activate p53 function. A virtual screening of cis-imidazole analogs called nutlins, have shown to have the same type of interactions seen among p53 and MDM2. More specifically, nutlins can mimic the

binding interactions of Phe19, Trp23 and Leu26, known residues of p53 that are involved in the binding of MDM2. Thus these small molecules can potentially inhibit MDM2 that in turn leads to the activation of p53 hence apoptosis [38]. (**Table 3.1**)

A number of hydrophobic residues are involved in the binding of nutlin-2 within the binding pocket of MDM2. In particular, the main chain of residue Gln72 of MDM2 makes one H-bond with the HBD group of hydroxyl of nutlin-2 [38]. Essentially, the bromo-substituent phenyl rings and the ethyl moiety of the ligand sits where Trp23, Leu26 and Phe19 residues of p53 are located. Nutlin-2 has a chemical formula of $C_{31}H_{34}Br_2N_4O_4$ with a MW of 686.45 g/mol [38, 60]. (**Figure 3.4**)

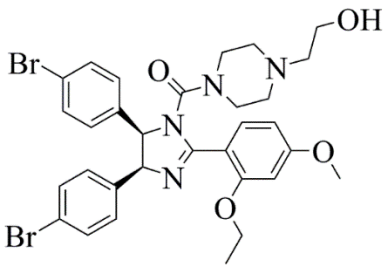

Nutlin-2

Figure 3.4: Chemical structure of nutlin-2 inhibitor of MDM2-p53 complex.

3.1.4.2.3 Cyclin-Dependent Kinase 2

Cyclin-dependent kinase 2 (CDK2) is a p53 target and is also involved in DNA-damage through cell-cycle arrest. This protein is likely to be activated during CIA by promoting cell cycle arrest and apoptosis. Inhibitors of CDK2 can decrease the damage within the HF caused by the chemotherapeutic agent, thus preventing apoptosis [1]. A natural inhibitor of CDK2, p21, has been associated with possible targets during CIA as it is expressed in the

keratinocytes, more specifically in the post-mitotic phase of the HF [4, 37]. Thus, inhibitors of CDK2 have been suggested to prevent CIA, however, a combination of therapy should be indicated in this case to not compromise the effectiveness of treatment as it could stop cell death [17, 37, 61]. (**Table 3.1**)

3.1.4.2.4 ABC Transporters

ABC transporters also known as ATP-binding cassette transporters use the energy released from ATP hydrolysis to remove a variety of substrates such as ions, amino acids, metabolites, lipids and drugs out of the cell. These transporters are involved in the removal of cytotoxic elements from the cell, therefore protecting the cell from the accumulation of anticancer agents, for instance. Haslam *et al.* have tested which chemotherapy induced agents are substrates of ABC family transporters [4]. They found that vindesine and vinorelbine, both vinca alkaloids drugs as VLB, are substrates of ABCB1 and ABCC1 transporters. VLB is well known to behave both as a substrate and inhibitor of subtype ABCB1, also known as P-glycoprotein (P-gp) or MDMR1 [4, 62].

ABC transporters might also be involved in protection of epithelial HF stem cells. ABC family transporters are located in the outer root sheath of the lower isthmus, which, specifically, subtype ABCC1 is more expressed in the HF than the others. ABCC1 seems to be highly expressed in the bulge and non-bulge HF at the outer root sheath of the HF for protection of the keratinocytes. Studies have suggested that by increasing the expression of ABC transporters in the epithelial hair follicle stem cell, the prevalence of CIA is reduced, thereby prevent damage in the HF [4]. (**Table 3.1**)

3.1.4.3 Hair Follicle Pathways

3.1.4.3.1 Notch Signaling

Notch are transmembrane proteins that are expressed throughout the HF, but especially in the proliferating matrix cells, hair bulb and outer root sheath. Notch has been strongly related to embryogenesis process as well as postnatal life of the HF. The expression of this protein and its ligands occur differently throughout the hair cycle [28]. A study performed in transgenic newborn mice has shown that overexpression of notch is involved in the development of abnormalities of HF and alopecia [29], thus demonstrating that notch expression is not required for early development of HF during embryogenesis. On the other hand, research have shown that knockdown mice of either notch or its ligands in postnatal mice leads to hair shortening and alopecia, hence suggesting the requirement of Notch signaling during HF development [28]. (**Table 3.1**)

Notch receptor contains two O-glycan in both serine residues 458 and 496; one O-flucose at Thr466; and one hexose at Ser435. In the EGF12 domain of notch receptor, residues Leu468, Asp469, Ile477 and Thr466-O-fucose interact with either Jagged or DLL, natural protein ligands of Notch. Residues Glu450 and Asp452 from the EGF11 also seem to be involved in the binding ligand-receptor. Among the glycosylated-residues, only Thr466-O-fucose directly interacts with the ligand whereas Ser435-O-glycan might indirectly aid in proteolytic cleavage of Notch, required for activation of the downstream signaling [63]. (**Figure 3.1**)

3.1.4.3.2 Bone Morphogenetic Protein and Noggin Signaling

Bone morphogenetic protein (BMP) is related with a variety of development signaling during embryonic process. BMP is secreted in many different types of cells such as bone, hair, skin and etc. The regulation of BMP occurs through inactivation by Noggin protein, an antagonist of BMP. This antagonism allows cell proliferation and growth in normal cell conditions. Thus, BMP by itself works as a negative controller of HF as its activation or inhibition of Noggin that can lead to minimization of HF and then alopecia. The only known BMP receptor in the HF is BMPRIA, which is expressed in the inner root sheath and hair shaft [11]. (**Figure 3.1** and **Table 3.1**)

BMP residues involved in Noggin binding are Trp52, Trp55, Phe75, Val87, Lys126, Tyr128, Met131, whereas noggin residues contacting BMP are Pro35, Asp39, Leu46, Glu48, Val186, Arg206, Ile218 and Cys232. Interestingly, noncovalent interactions with proline, leucine and isoleucine are the most important ones [64].

3.1.4.3.3 Sonic Hedgehog Signaling

Sonic Hedgehog (Shh) signaling is involved in embryonic and adult HF development and cycling. Xie *et al*. have demonstrated that feather proliferation is reduced, and that Shh transcription is downregulated during treatment with cyclophosphamide in chicken [26]. The authors have tested other chemotherapeutic drugs such as taxol and 5-fluoracil. According to Xie *et al*., taxol, an antimicrotubule just as VLB, seems to downregulate Shh expression in the chicken HF. Surprisingly, the same effects were demonstrated in murine HF, thus indicating that downregulation of Shh expression is also present in mammalian tissue as well [26]. (**Table 3.1**)

Both Shh and Wnt signaling work as crosstalk pathways, which activation of Wnt pathway can also regulate the Shh downstream signaling. [25]. The activation of Shh signaling is mediated by Shh ligand binding to PTCH1 that induces the release of Smoothened receptor (SMO) to stimulate cell responses. SMO protein also belongs to the Frizzled (FZD) classification of receptors. Thus, SMO activates the downstream signaling of Shh pathway by recruiting GLI and initiating cell responses within the HF. (**Figure 3.1**)

An extracellular domain (ECD) comprising a cysteine-rich domain (CRD), and ECD linker domain, a seven transmembrane helical domain (7TM) and a carboxy-terminal domain located intracellularly form the FZD structure of receptors. SMO protein also resemble the GCPRs due to their location at the cellular membrane, however, it only shares 10% of sequence identity with GCPRs [27].

Activation of hedgehog pathway is highly involved in cell proliferation and thus used as a cancer target, whereas inhibitors of SMO have significantly contributed to tumor suppression [65]. Despite the unknown identity of endogenous substrates that regulate SMO activity, a number of exogenous ligands have been developed. Among those, cyclopamine was the first inhibitor of Shh signaling discovered by directly modulating SMO through inhibition of its downstream signaling effect. In addition, the human crystal structures comprising the SMO-inhibitor complexes such as cyclopamine (4O9R) [66], LY2940680 (4JKV) [27], anta XV (4QIM) and SANT1 (4N4W) [65] are available. The exogenous agonist of SMO, SAG 1.5, have been also crystallized (4QIN) [65]. These designed compounds all bind to the narrow binding pocket of SMO which is characterized by the seven-transmembrane domain, ECD and ECLs of SMO [65].

In the SMO-cyclopamine complex (4O9R) [66], the structure of SMO is shown as a monomer whereas in the SMO-LY2940680 structure (4JKV) [27], SMO is represented as a dimer. The binding pocket of SMO receptor is narrow, long, and located at the ECD, extracellular loops 2 and 3 whereas helices I, II, V and VII interact with the antagonists. Residues Arg400, Lys395, Asn219, His470, Tyr394, Glu518, Asp473 are involved in the binding of antagonists cyclopamine, LY2940680, anta XV and SANT1, whereas residues Asp473 and Asn219 are mainly involved in binding with the agonist SAG1.5 of SMO [27, 65, 66]. Although both agonist and antagonist bind to the same binding pocket of SMO and share similar residues, their binding strength vary depending on the residue [27].

Cyclopamine is a natural steroidal alkaloid derived from *Veratrum californicum* gene of plants that was initially discovered as a teratogen chemical due to an abnormal eye formation in newborn lambs [67]. Cyclopamine was later related to embryonic and post-natal developmental phases as it inhibits Shh signaling by directly binding to the ECD of SMO. Residue Glu518 of SMO is involved in a H-bond with the inhibitor [66, 67]. As cyclopamine, anta XV is also a small molecule inhibitor of SMO with a higher MW than cyclopamine (439.6 g/mol compared to 411.6 g/mol). The agonist SAG1.5 has a MW of 564 g/mol due to two fluorine atoms attached at the benzothiophene group. (**Figure 3.5**)

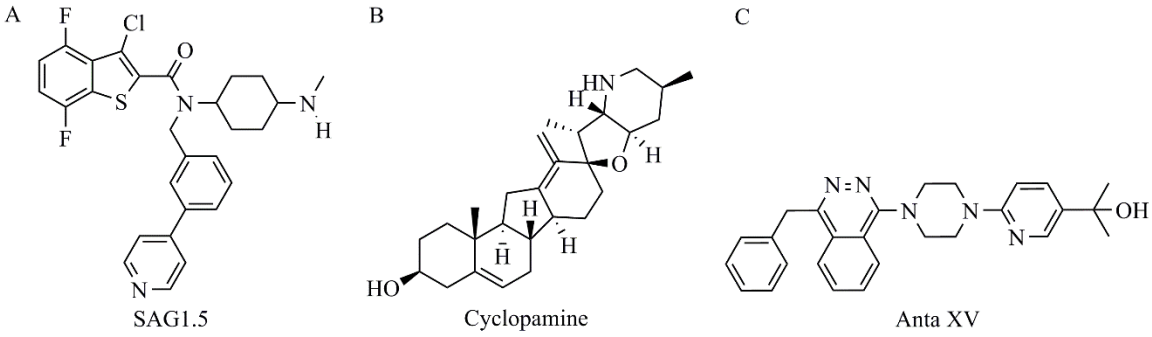

Figure 3.5: Chemical structures of SAG1.5, cyclopamine and anta XV.

3.1.4.3.4 Canonical Wingless-Related Integration Site and β-Catenin

Wingless-related integration site, also known as Wnt signaling, is divided into three pathways known as Canonical Wnt/β-catenin, Noncaninocal Wnt/β-catenin, and Wnt/Calcium. The canonical Wnt/β-catenin pathway is the one involved in HF proliferation and cell maintenance, which Wnt ligand is present in different phases of the HF cycle [7]. Wnt/β-catenin signaling induces cell response when Wnt binds to the Frizzled (FZD) receptor along with the co-receptor Low Density Lipoprotein Receptor Related (LRP) [68], thus forming a complex FZD-Wnt-LRP. The binding of Wnt to FZD and LRP causes phosphorylation of the cytoplasmic tail of LRP that sends signals to Dishevelled (Dsh) protein. This process inhibits the scaffold complex and leads to the accumulation of β-catenin. In the cytoplasm, the stabilized and non-phosphorylated form of β-catenin act as a transcriptional factor upon interaction of TCF/LEF with DNA-binding proteins. This causes initiation of a signaling cascade required for the HF development, including cell proliferation, migration and differentiation. This complex signaling is inhibited by a natural endogenous antagonist of Wnt, Dickkop (DKK) protein [69]. In a normal hair cycle,

Wnt/β-catenin signaling is active during anagen phase and it is required for HF maintenance throughout life [23, 68-70]. (**Figure 3.1**)

Wnt ligands are lipid-modified proteins that bind to the cysteine-rich domain (CRD) of FZD [68]. The CRD-FZD domain has been shown to be sufficient for signaling and binding of Wnt [69]. LRP5/6 has four β-propellers that are structures arranged toroidally followed by an epidermal-growth factor like, which the third and fourth domains (E3E4) are involved in binding [69]. There are currently 19 subtypes of Wnt, 10 FZD and 2 LRP in the mammalian tissue, hence different complexes can be formed. Although it is still not clear if all of them have biological relevance, the most known subtypes are Wnt3a, FZD8 and LRP6. The complete downstream mechanism by which Wnt pathway is activated/inhibited remains unknown, however, it is established that Wnt binds to both FZD and LRP for pathway activation and this interaction is prevented by DKK1 [69]. According to Bourhis *et al.*, the binding of DKK1 disrupts Wnt3a-LRP6 but not Wnt3a-FZD8 complexes, however this disruption is enough for prevention of the signaling. This also demonstrates the higher affinity of DKK1 for LRP6 than for FZD [69]. Moreover, it is suggested that one molecule of DKK1 can recognizes both E1E2 and E3E4 sites at LRP6 and inhibits a variety of Wnt ligands as they bind specifically to either E1E2 or E3E4, depending upon their subtype [69, 70].

This chapter focuses on the effects of VLB and its metabolites docked with protein receptors that are involved with alopecia induced by chemotherapy. Due to limited time, throughout the project program, this study covers only four receptors for molecular docking

with VLB and its metabolites, which are the mouse double minute 2 homolog (MDMD2), vitamin D receptor (VDR), androgen receptor (AR) and smoothened receptor (SMO).

3.2 Materials and Method

The crystal structures retrieved from the Protein Data Bank (PDB) were minimized with AMBER7 FF99 force field using SYBYL®-X 2.1.1 simulation package. Water molecules in the PDB files were removed, polar hydrogens were added and the side chains of residues were completed when they were unsolved in the crystal structures. All of the protein structures used in this study contain their ligand crystallized with the receptor, such as testosterone with AR (2AM9) [41], nutlin-2 with MDM2 (1RV1) [38], calcitriol with VDR (1DB1) [48], and anta XV with SMO (4QIM) [65]. For preparation of the ligands regarding VLB and its metabolites, please see the Materials and Method section of Chapter 2. The docking results with the lowest binding energy of each natural ligand or inhibitor were considered for further analysis of their binding profile.

AR: The binding site of the endogenous substrate of AR is surrounded by eleven α-helices and two β-sheets (UniProtKB P10275) [41]. The structure of AR is comprised of 266 amino acids which are divided into α1 (residues 671-681), a flexible linker (682-695), α2 (696-721), α3 (724-728), α4 (729-758), an antiparallel β-sheet (762-770), α5 (771-778), α6 (780-797), α7 (800-813), α8 (823-844), α9 (848-884), α10 (892-902) and α11 (902-908). A spherical region with a radius of 20 Å around the ligand testosterone was used as the binding site for molecular docking of VLB, its metabolites and the substrate into AR.

VDR: The PDB entry 1DB1 (UniProtKB P11473) [48] comprises the crystalized structure of the agonist and VDR, which is also used for molecular docking of the antagonist, TEI-9647, into the receptor. The VDR is formed by 14 α-helices and 3 β-sheets, defined as α1 (residues 125-143), α2 (149-153), α3 (216-224), α4 (226-247), α5 (250-254),

α6 (255-275), α7 (290-292), α8 (296-302), α9 (306-323), α10 (326-339), α11 (348-371), α12 (378-406), α13 (410-414) and α14 (415-423). A spherical region with a radius of 10 Å around the ligand was selected for the binding target of VLB, its metabolites, calcitriol and TEF-9647 into VDR.

MDM2: Four α-helices defined as α1 (residues 31-40), α2 (50-64), α3 (80-87), α4 (95-105) comprises receptor MDM2 (UniProtKB Q00987) [38]. A spherical region with a radius of 15 Å surrounding residue Gly58 was selected as the binding target site for the docking of VLB, its library and nutlin-2 into MDM2 receptor.

SMO: The binding site of SMO receptor is surrounded by the seven transmembrane domain, ECD and ECL 2 and 3. The crystal structure 4QIM (UniProtKB Q99835) contains 468 residues and is comprised of 20 α-helices [65]. Helices 10 and 11 formed by residues 396-404 and 405-1020, respectively, are mainly involved with the binding of antagonists and agonists of SMO. Therefore, a spherical region with a radius of 20 Å surrounding the anta XV was defined as the target site for the docking of antagonists, VLB and its metabolites.

3.3 Results and Discussion

3.3.1 Androgen Receptor

VLB, its metabolites and testosterone were docked into the binding pocket of androgen receptor as described in the Materials and Method section of Chapter 3. VLB and most of its metabolites did not obtain any docking solution in the AR. (**Table 3.2**)

3.3.1.1 Testosterone Binding to AR

Testosterone has a binding energy of -20.45 kJ/mol in the binding pocket of AR. Hydrophobic interactions are mainly seen with residues Met895, Gln711, Met745, Gly708 and Phe764. The ketone group at C3 shares its electrons to the guanidinium group of Arg752 within a distance of 1.9 Å, and the hydroxyl group makes two H-bonds with Asn705 and Thr877 within a distance of 3.0 Å and 2.1 Å, respectively. (**Figure 3.6B**)

3.3.1.2 Vinblastine and its Metabolites Binding to AR

The majority of metabolites of VLB, including the anticancer drug do not interact with AR. Metabolite 22 is the only one which has a binding affinity (-19.79 kJ/mol) near the binding energy of the natural substrate (-20.45 kJ/mol) for AR. Metabolite 22 interacts with two residues involved the binding pocket of testosterone, Arg752 and Gln711. The azacyclononane ring and the indole ring of metabolite 22 interact through hydrophobic interactions with residues Arg752 and Gln711, respectively. In addition, metabolite 22 makes H-bonds with the main chains of Gly683 and Val685, and with the side chain of Glu681. Hydrophobic interactions with residues Trp751 and His714 are also observed. This shows that metabolite 22 may be involved on the onset of alopecia through binding to AR. (**Table 3.2** and **Figure 3.6C**)

Table 3.2: Binding energies of VLB, its metabolites and testosterone docked into androgen receptor. The energy value of the metabolite with the lowest binding energy is shown in bold.

Androgen Receptor	$\Delta G_{binding}$ (kJ/mol)
Testosterone	-20.45
VLB	NB
MTB1	NB
MTB2	NB
MTB3	NB
MTB4	NB
MTB5	NB
MTB6	NB
MTB7	NB
MTB8	NB
MTB9	NB
MTB10	NB
MTB11	NB
MTB12	NB
MTB13	NB
MTB14	NB
MTB15	NB
MTB16	NB
MTB17	NB
MTB18	NB
MTB19	6.44
MTB20	6.79
MTB21	-1.12
MTB22	**-19.78**
MTB23	-12.78
MTB24	NB
MTB25	NB
MTB26	-8.00
MTB27	-5.40
MTB28	NB
MTB29	-1.08
MTB30	-3.35
MTB31	-6.12
MTB32	-3.78
MTB33	9.03

MTB34	-17.83
MTB35	-17.58

NB: non substrate

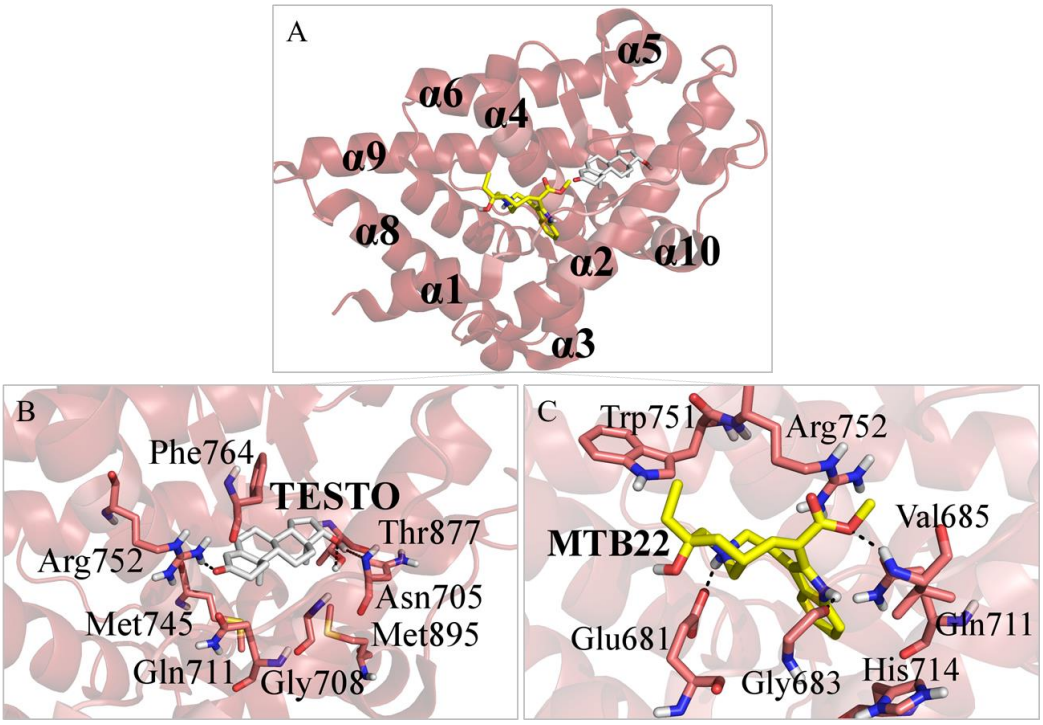

Figure 3.6: A) Pose view of testosterone and metabolites of VLB docked into the binding pocket of androgen receptor. Binding interactions of B) Testosterone, and C) Metabolite 22. Hydrogen bonds are shown in dashed lines.

3.3.2 Vitamin D Receptor

VLB, its metabolites, calcitriol and the antagonist TEI-9647 were docked into the binding pocket of vitamin D receptor as described in the Materials and Method section of Chapter 3. Due to the narrow size of the binding pocket of VDR, only metabolite 22, metabolite 23

and metabolite 34 could bind into the receptor, whereas the lowest binding energy was for metabolite 23 (-16.70 kJ/mol). (**Table 3.3**)

3.3.2.1 Calcitriol Binding to VDR

The binding energy calculated for calcitriol docked into the vitamin D receptor was -17.81 kJ/mol. Calcitriol makes an H-bond within the binding site of VDR with residue His305, which confers specificity and activation of the receptor. The 25-OH group acts as both hydrogen bond acceptor and donor with residues His305 and His397, within a distance of 1.9 Å and 1.7 Å, respectively. Moreover, the hydroxyl groups attached to the cyclohexane make H-bonds with Arg274, Ser237 and Ser278. Residues Val234, Val300, Trp286 and Ile268 participate in hydrophobic interactions with the agonist of VDR. (**Table 3.3** and **Figure 3.7B**)

3.3.2.2 TEI-9647 Binding to VDR

The inactivation of VDR is mediated by an interaction of the inhibitor with residue His397 that in turn stabilizes H12 by promoting a disulfide bond among residues Cys403 and Cys410 [49]. The antagonist of VDR, TEF-9647, has binding energy of -10.42 kJ/mol and binds to His397 within a distance of 2.0 Å. The docking results of both agonist and antagonist of VDR, demonstrate His397 interacts with calcitriol as an HBA group, while with TEI-9647 it interacts as HBD group. The hydroxyl group is placed close to residue Cys288, making an H-bond with the thiol side chain. Moreover, the antagonist also makes hydrophobic contacts with same residues involved with the agonist. (**Figure 3.7C**)

Table 3.3: Binding energies of VLB, its metabolites, calcitriol and TEI-9647 docked into vitamin D receptor. The energy value of the metabolite with the lowest binding energy is shown in bold.

Vitamin D Receptor	$\Delta G_{binding}$ (kJ/mol)
Calcitriol	-17.81
TEI-9647	-10.42
VLB	NB
MTB1	NB
MTB2	NB
MTB3	NB
MTB4	NB
MTB5	NB
MTB6	NB
MTB7	NB
MTB8	NB
MTB9	NB
MTB10	NB
MTB11	NB
MTB12	NB
MTB13	NB
MTB14	NB
MTB15	NB
MTB16	NB
MTB17	NB
MTB18	NB
MTB19	NB
MTB20	NB
MTB21	NB
MTB22	-12.06
MTB23	**-16.70**
MTB24	NB
MTB25	NB
MTB26	NB
MTB27	NB
MTB28	NB
MTB29	NB
MTB30	NB
MTB31	NB
MTB32	NB

MTB33	NB
MTB34	4.05
MTB35	NB

NB: non substrate

3.3.2.3 Vinblastine and its Metabolites Binding to VDR

The majority of the metabolites of VLB including VLB do not bind to VDR. Metabolite 23 has a binding affinity calculated as of -16.70 kJ/mol. It interacts with residues His397 and His305. The HBA group of hydroxyl moiety of metabolite 23 makes an H-bond with His397 within a distance of 1.9 Å, 0.1 Å closer than the antagonist and agonist of VDR (2.0 Å). On the other hand, the HBD group of hydroxyl makes an H-bond with His305 within a distance of 2.0 Å. The docking results show that both histidine residues bind to the antagonist and to metabolite 23 in a similar fashion, whereas position 397 act as HBD, and position 305 as a HBA group. In addition, hydrophobic interactions are seen with Val300, Ile268, Ile271, Ser237, Trp286 and Val234. Thus, due to similar binding profiles of metabolite 23 and the antagonist TEI-9647 with residue His397, it is suggested that metabolite 23 inhibits VDR may induce the onset of alopecia during chemotherapy with VLB. (**Figure 3.7D**)

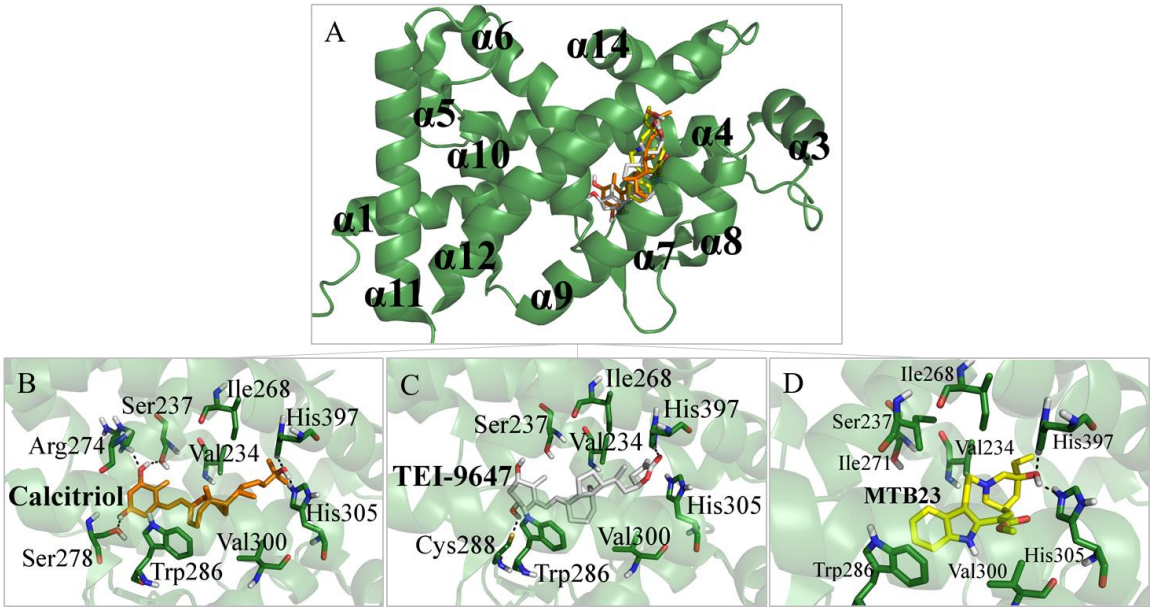

Figure 3.7: A) Overview of interactions into the binding pocket of vitamin D receptor. Binding interactions of B) Calcitriol, C) TEI-9647, and D) Metabolites 23. Hydrogen bonds are shown in dashed lines.

3.3.3 Murine Double Minute 2 Homolog Receptor

VLB, its metabolites and nutlin-2 were docked into MDM2 receptor as described in the Materials and Method section of Chapter 3. (**Table 3.4**)

3.3.3.1 Nutlin-2 Binding to MDM2

Nutlin-2 has a calculated binding energy of -10.66 kJ/mol in the binding site of MDM2, whereas it makes H-bonds with residues His96 and Val93. The hydroxyl group binds to the side chain of His96 (1.7 Å) and to the main chain of Val93 (2.1 Å), respectively. The protonated nitrogen also binds to residue Val93. The bromo-substituent groups are involved in hydrophobic interactions mainly with residues Gly58, Leu57 and Leu54 which

also bind to p53 transcription factor [38]. Isoleucine residues at positions 61 and 99 also interact with the ligand into MDM2 receptor. (**Table 3.4** and **Figure 3.8B**)

3.3.3.2 Vinblastine Binding to MDM2

Vinblastine has a binding energy of 1.02 kJ/mol for MDM2. Although it interacts with residues involved with the binding of Nutlin-2 (i.e. Leu54 and His96), its binding is energy consuming and less likely to take place. (**Figure 3.8C**)

3.3.3.2 Metabolites Binding to MDM2

Metabolite 35 has a calculated binding energy as of -18.71 kJ/mol when docked into the binding site of MDM2. Hydrophobic interactions are observed with Leu54, Leu57, Gly58, Ile61, Met62, Val93 and Ile99, which are seen in the binding of p53 [58] indicating that metabolite 35 interacts with the same residues as of p53. The main chain of Leu54 participates in an H-bond with the protonated nitrogen of metabolite 35 within a distance of 1.8 Å. The same type of interactions are observed with metabolite 34, with a binding energy of -17.59 kJ/mol and an H-bond with residue Leu54 within a distance of 1.7 Å. Therefore, it is expected that metabolite 35 contributes to the onset of alopecia through inhibition of the MDM2-p53 complex. (**Table 3.4** and **Figure 3.8D**)

All metabolites of VLB which interact with the binding site of MDM2 and have a binding energy lower than -10.66 kJ/mol (Nutlin-2) are potential alopecia inducers during chemotherapy with VLB. (**Table 3.4**)

Table 3.4: Binding energies of VLB, its metabolites and nutlin-2 docked into MDM2 receptor. The energy value of the metabolite with the lowest binding energy is shown in bold.

MDM2	$\Delta G_{binding}$ (kJ/mol)
Nutlin-2	-10.66
VLB	1.02
MTB1	-2.43
MTB2	3.43
MTB3	4.55
MTB4	-1.75
MTB5	0.57
MTB6	1.90
MTB7	3.76
MTB8	2.97
MTB9	-0.67
MTB10	3.75
MTB11	-1.48
MTB12	-1.63
MTB13	-10.35
MTB14	0.00
MTB15	-0.76
MTB16	-10.58
MTB17	-4.42
MTB18	-9.49
MTB19	-7.16
MTB20	0.56
MTB21	-9.70
MTB22	-13.85
MTB23	-11.83
MTB24	-9.50
MTB25	-9.70
MTB26	-10.42
MTB27	-8.57
MTB28	-1.95
MTB29	-7.18
MTB30	-11.10
MTB31	-11.37
MTB32	-6.09
MTB33	-11.72

MTB34	-17.59
MTB35	**-18.71**

NB: non substrate

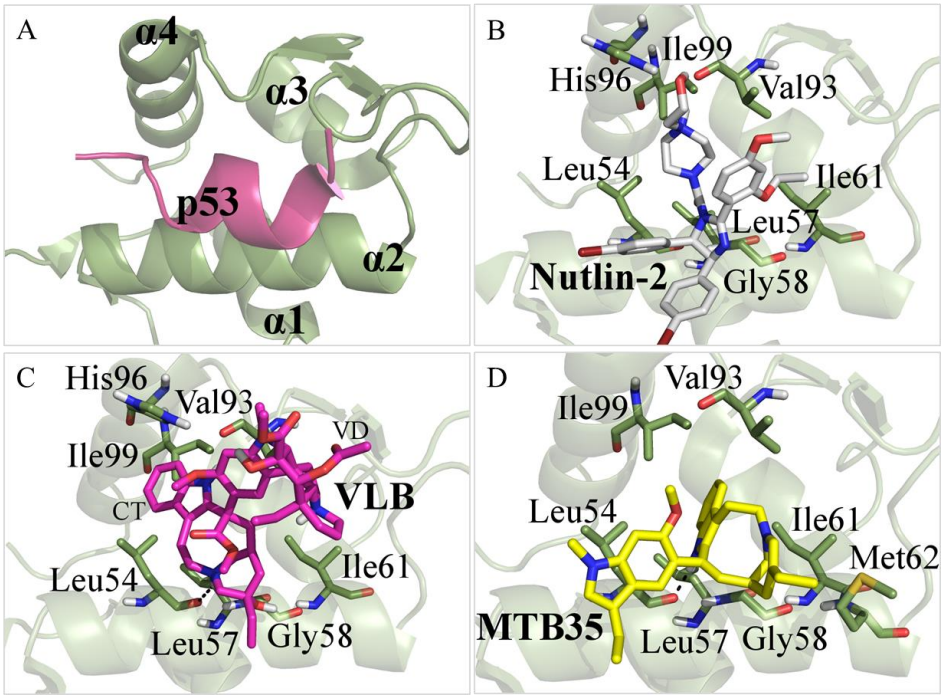

Figure 3.8: Interactions with MDM2 receptor. A) p53; B) Nutlin-2; C) Vinblastine, and D) Metabolite 35. Hydrogen bonds are shown in dashed lines.

3.3.4 Smoothened Receptor

VLB, its metabolites and the antagonist anta XV were docked into the binding site of SMO receptor as described in the Materials and Method section of Chapter 3. (**Table 3.5**)

3.3.4.1 Anta XV Binding to SMO

The binding energy of anta XV docked into SMO receptor was calculated to be -33.79 kJ/mol. The antagonist binds to Arg400, Asn219 and Lys395 through H-bonds and with His470, Leu522, Leu221, Ser387 and Asp384 through hydrophobic contacts. The propanol group act as a HBA group accepting the hydrogen deficient atom of the side chain of Lys395 (1.9 Å), the HBD group of Asn219 makes H-bond with the heteroatom of pyridine (2.0 Å), and both heteroatoms of benzylphthalazine interact with the guanidinium group of Arg400 (2.1 Å and 2.2 Å). (**Table 3.5**, **Figure 3.9A** and **3.9B**)

3.3.4.3 Vinblastine Binding to SMO

VLB has a binding energy for SMO receptor of 1.98 kJ/mol and it could interact with allosteric site between helices α2 and α5. Thus, it is suggested that the anticancer drug does not play a role in the function of the receptor. (**Figure 3.9C**)

3.3.4.4 Metabolites Binding to SMO

Metabolite 22 has a binding energy of -16.63 kJ/mol against SMO receptor. Although metabolite 22 is located next to α11, which is the main helix involved in the binding of SMO ligands, it interacts with only one residue that also participates in the interactions with anta XV (Lys395) [65]. (**Table 3.5** and **Figure 3.9A**)

Table 3.5: Binding energies of VLB, its metabolites and anta XV docked into SMO receptor. The energy value of the metabolite with the lowest binding energy is shown in bold.

SMO-Shh	$\Delta G_{binding}$ (kJ/mol)
Anta XV	-33.79
VLB	1.98
MTB1	-1.55
MTB2	-0.56
MTB3	0.74
MTB4	-1.37
MTB5	-3.82
MTB6	1.50
MTB7	1.26
MTB8	4.69
MTB9	-1.23
MTB10	-7.04
MTB11	1.94
MTB12	-1.54
MTB13	-3.75
MTB14	-2.29
MTB15	-1.44
MTB16	-1.34
MTB17	5.39
MTB18	-8.43
MTB19	-7.87
MTB20	-4.37
MTB21	-6.76
MTB22	**-16.63**
MTB23	-10.62
MTB24	-5.91
MTB25	-6.95
MTB26	-5.60
MTB27	-6.97
MTB28	-3.71
MTB29	-11.83
MTB30	-8.86
MTB31	-8.45
MTB32	-5.68
MTB33	-5.01

MTB34	-15.58
MTB35	-14.89

NB: non substrate

Metabolite 22 makes H-bonds with residues Glu481, Glu208 and Asn396, and hydrophobic interactions with Lys395 and Tyr397. However, it has ~16 kJ/mol higher binding energy, thus it cannot compete with anta XV. (**Table 3.5** and **Figure 3.10C**)

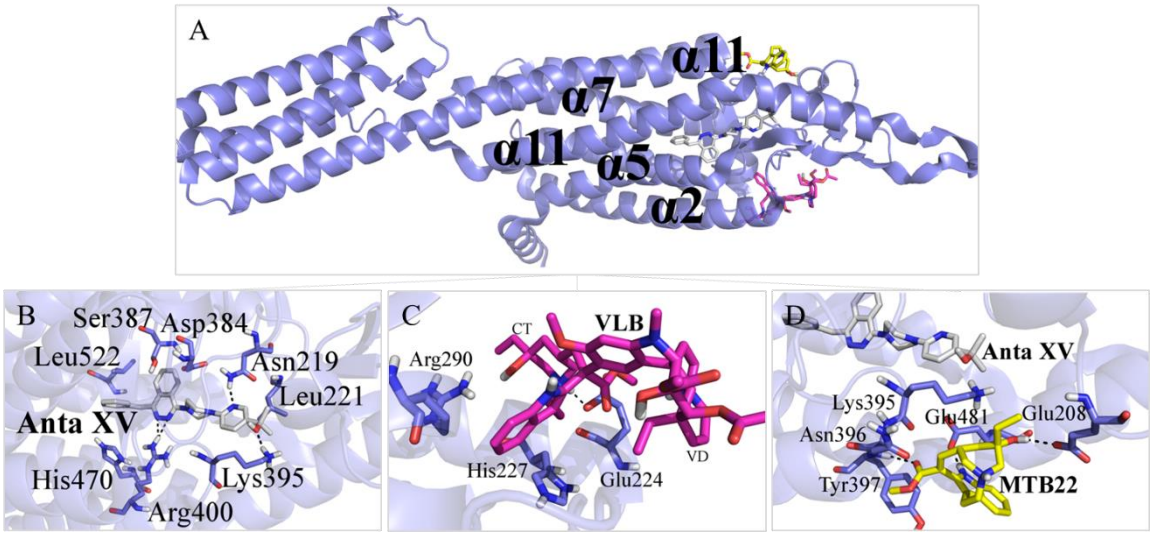

Figure 3.9: A) Overview of interactions with SMO receptor. B) Anta XV; C) Vinblastine, and D) Metabolite 22. Hydrogen bonds are shown in dashed lines.

3.4 Conclusion

A variety of complex signaling pathways are involved in inducing anagen to catagen transition in the hair follicle, promoting apoptosis and eventually hair loss during CIA [1]. In this research, four receptors were evaluated possible off-targets for binding of VLB and its metabolites in connection with alopecia adverse reaction during chemotherapy with VLB. The receptors chosen cover the known pathways of CIA, such as hormones related that includes androgen and vitamin D receptors, cellular control pathways that include MDM2 receptor, and the hair follicle cycle signaling which covers Shh-SMO pathway. Therefore, this study provides an overview of the molecular signaling involved in CIA, and the VLB effect on the likelihood of its metabolites to induce alopecia through the binding to these receptors. (**Table 3.1**)

In the VDR, metabolite 23 binds to residues His397 and His305 in a similar way to the exogenous antagonist TEI-9647, thus it could inhibit the receptor during chemotherapy. The binding energy of metabolite 23 is stronger than of TEI-9647 for the binding site of VDR (-16.70 kJ/mol vs. -10.42 kJ/mol). Although metabolite 23 has a higher binding energy than the endogenous substrate (-16.70 kJ/mol vs. -17.81 kJ/mol), it binds to the receptor and could inhibit VDR.

Studies have shown an association of low levels of calcitriol and the probability of developing cancer due to the anti-proliferative and antioxidants effects of vitamin D analogs [71, 72]. Kitchen *et al.* have analyzed the levels of calcitriol in 241 patients under 6 months of chemotherapy and found that 200 of those have abnormal levels of vitamin D (<75 nmol/L) during cancer treatment, thus suggesting that cancer patients have low levels

of vitamin D (<75 nmol/L) during chemotherapy [73]. However, it is not clear whether cancer or chemotherapy causes a reduction on the levels of calcitriol, even though both will eventually lead to low levels of vitamin D. Therefore, due to the binding affinity of metabolite 23 and its antagonism behavior in the VDR as well as the associated low levels of vitamin D during chemotherapy and/or cancer, metabolite 23 could contribute to the onset of alopecia through inhibition of VDR. (**Table 3.3**)

In the MDM2 receptor, metabolite 35 has a binding affinity for the binding pocket of p53 into MDM2 and similar binding profile to exogenous inhibitor nutlin-2. Metabolites of VLB which occupy the same site as of p53 and nutlin-2 in the binding site of MDM2, interact with known residues involving p53, such as Gly58, Leu57 and Leu54 [38]. Therefore, the metabolites of VLB may inhibit MDM2 receptor inducing alopecia during chemotherapy with VLB. (**Table 3.4**)

Although the metabolites of VLB do not display significant binding energies for the binding site of AR, metabolite 22 interacts with the same residues involved with the natural substrate (Arg752 and Gln711). For instance, metabolite 22 interacts with Arg752 and Gln711, known residues that participate in the activation of the receptor mediated by either testosterone or DHT [41]. As seen with vitamin D, the levels of testosterone also seem to be lowered during chemotherapy due to the release of cytokines that in turn promotes hypogonadism, or low levels of testosterone [74]. Thus, due to the possible low levels of testosterone induced by chemotherapy and similar binding profile as of testosterone, metabolite 22 may induce the onset of alopecia through activation of AR. (**Table 3.2**)

The molecular docking of the exogenous antagonist of SMO, anta XV, has demonstrated that the ligand makes H-bonds with Lys395, Arg400 and Asn219 which are residues involved in the inhibition of SMO receptor [65]. Metabolite 22 shares one residue (Lys395) with the binding network of the antagonist. Its binding affinity is not significant as for anta XV (-16.63 kJ/mol vs. -33.79 kJ/mol). However, anta XV is not a natural inhibitor of SMO, and thus metabolite 22 in any respect would compete with the exogenous antagonist for the binding of SMO. Instead, it is suggested that metabolite 22 may block the passage of unknown natural ligands of SMO due to binding to Lys395, thus impairing the normal function of SMO receptor and the downstream Shh signaling within the hair follicle. (**Table 3.5**)

Therefore, this study has demonstrated the effects of VLB and its metabolites on alopecia associated receptors. The metabolites of VLB may induce alopecia through different mechanisms that lead to HF apoptosis during chemotherapy with VLB, such as inhibition of receptors MDM2, SMO and VDR, and activation of AR.

3.5 Bibliography

1. Dunnill, C.J., et al., *A Clinical and Biological Guide for Understanding Chemotherapy-Induced Alopecia and Its Prevention.* Oncologist, 2018. **23**(1): p. 84-96.
2. Patel, M., S. Harrison, and R. Sinclair, *Drugs and hair loss.* Dermatol Clin, 2013. **31**(1): p. 67-73.
3. Chon, S.Y., et al., *Chemotherapy-induced alopecia.* J Am Acad Dermatol, 2012. **67**(1): p. e37-47.
4. Paus, R., et al., *Pathobiology of chemotherapy-induced hair loss.* Lancet Oncol, 2013. **14**(2): p. e50-9.
5. Rubio-Gonzalez, B., et al., *Pathogenesis and treatment options for chemotherapy-induced alopecia: a systematic review.* Int J Dermatol, 2018.
6. Trueb, R.M., *Chemotherapy-induced alopecia.* Curr Opin Support Palliat Care, 2010. **4**(4): p. 281-4.
7. Cotsarelis, G. and S.E. Millar, *Towards a molecular understanding of hair loss and its treatment.* Trends Mol Med, 2001. **7**(7): p. 293-301.
8. Crounse, R.G. and E.J. Van Scott, *Changes in scalp hair roots as a measure of toxicity from cancer chemotherapeutic drugs.* J Invest Dermatol, 1960. **35**: p. 83-90.
9. West, H.J., *Chemotherapy-Induced Hair Loss (Alopecia).* JAMA Oncol, 2017.
10. Hershman, D.L., *Scalp Cooling to Prevent Chemotherapy-Induced Alopecia: The Time Has Come.* JAMA, 2017. **317**(6): p. 587-588.

11. Rishikaysh, P., et al., *Signaling involved in hair follicle morphogenesis and development.* Int J Mol Sci, 2014. **15**(1): p. 1647-70.

12. Plikus, M.V., *New activators and inhibitors in the hair cycle clock: targeting stem cells' state of competence*. J Invest Dermatol, 2012. **132**(5): p. 1321-4.

13. Wang, J., Z. Lu, and J.L. Au, *Protection against chemotherapy-induced alopecia.* Pharm Res, 2006. **23**(11): p. 2505-14.

14. Paus, R., et al., *Chemotherapy-induced alopecia in mice. Induction by cyclophosphamide, inhibition by cyclosporine A, and modulation by dexamethasone.* Am J Pathol, 1994. **144**(4): p. 719-34.

15. Flynn, M., K.A. Heale, and L. Alisaraie, *Mechanism of Off-Target Interactions and Toxicity of Tamoxifen and Its Metabolites.* Chem Res Toxicol, 2017. **30**(7): p. 1492-1507.

16. Hussein, A.M., et al., *Protection from chemotherapy-induced alopecia in a rat model.* Science, 1990. **249**(4976): p. 1564-6.

17. Botchkarev, V.A., *Molecular mechanisms of chemotherapy-induced hair loss.* J Investig Dermatol Symp Proc, 2003. **8**(1): p. 72-5.

18. Santos, Z., P. Avci, and M.R. Hamblin, *Drug discovery for alopecia: gone today, hair tomorrow.* Expert Opin Drug Discov, 2015. **10**(3): p. 269-92.

19. Botchkarev, V.A., et al., *p53 is essential for chemotherapy-induced hair loss.* Cancer Res, 2000. **60**(18): p. 5002-6.

20. Lindner, G., et al., *Analysis of apoptosis during hair follicle regression (catagen).* Am J Pathol, 1997. **151**(6): p. 1601-17.

21. Sharov, A.A., et al., *Fas and c-kit are involved in the control of hair follicle melanocyte apoptosis and migration in chemotherapy-induced hair loss.* J Invest Dermatol, 2003. **120**(1): p. 27-35.

22. Skrok, A., et al., *The effect of parathyroid hormones on hair follicle physiology: implications for treatment of chemotherapy-induced alopecia.* Skin Pharmacol Physiol, 2015. **28**(4): p. 213-25.

23. Myung, P.S., et al., *Epithelial Wnt ligand secretion is required for adult hair follicle growth and regeneration.* J Invest Dermatol, 2013. **133**(1): p. 31-41.

24. Kwack, M.H., et al., *Dickkopf 1 promotes regression of hair follicles.* J Invest Dermatol, 2012. **132**(6): p. 1554-60.

25. Dessinioti, C., C. Antoniou, and A.J. Stratigos, *From basal cell carcinoma morphogenesis to the alopecia induced by hedgehog inhibitors: connecting the dots.* Br J Dermatol, 2017. **177**(6): p. 1485-1494.

26. Xie, G., et al., *Testing chemotherapeutic agents in the feather follicle identifies a selective blockade of cell proliferation and a key role for sonic hedgehog signaling in chemotherapy-induced tissue damage.* J Invest Dermatol, 2015. **135**(3): p. 690-700.

27. Wang, C., et al., *Structure of the human smoothened receptor bound to an antitumour agent.* Nature, 2013. **497**(7449): p. 338-43.

28. Aubin-Houzelstein, G., *Notch signaling and the developing hair follicle.* Adv Exp Med Biol, 2012. **727**: p. 142-60.

29. Uyttendaele, H., et al., *Activation of Notch1 in the hair follicle leads to cell-fate switch and Mohawk alopecia.* Differentiation, 2004. **72**(8): p. 396-409.

30. Gensure, R.C., *Parathyroid hormone-related peptide and the hair cycle - is it the agonists or the antagonists that cause hair growth?* Exp Dermatol, 2014. **23**(12): p. 865-7.

31. Saini, V., et al., *Absence of vitamin D receptor (VDR)-mediated PPARgamma suppression causes alopecia in VDR-null mice.* FASEB J, 2017. **31**(3): p. 1059-1066.

32. He, X., et al., *Fibroblast growth factor 5-short (FGF5s) inhibits the activity of FGF5 in primary and secondary hair follicle dermal papilla cells of cashmere goats.* Gene, 2016. **575**(2 Pt 2): p. 393-398.

33. Braun, S., et al., *Keratinocyte growth factor protects epidermis and hair follicles from cell death induced by UV irradiation, chemotherapeutic or cytotoxic agents.* J Cell Sci, 2006. **119**(Pt 23): p. 4841-9.

34. Danilenko, D.M., et al., *Keratinocyte growth factor is an important endogenous mediator of hair follicle growth, development, and differentiation. Normalization of the nu/nu follicular differentiation defect and amelioration of chemotherapy-induced alopecia.* Am J Pathol, 1995. **147**(1): p. 145-54.

35. Kretzschmar, K., et al., *The Androgen Receptor Antagonizes Wnt/beta-Catenin Signaling in Epidermal Stem Cells.* J Invest Dermatol, 2015. **135**(11): p. 2753-2763.

36. Bichsel, K.J., et al., *Role for the epidermal growth factor receptor in chemotherapy-induced alopecia.* PLoS One, 2013. **8**(7): p. e69368.

37. Sharov, A.A., et al., *Fas signaling is involved in the control of hair follicle response to chemotherapy.* Cancer Res, 2004. **64**(17): p. 6266-70.

38. Vassilev, L.T., et al., *In vivo activation of the p53 pathway by small-molecule antagonists of MDM2.* Science, 2004. **303**(5659): p. 844-8.

39. Jeffrey, P.D., et al., *Mechanism of CDK activation revealed by the structure of a cyclinA-CDK2 complex.* Nature, 1995. **376**(6538): p. 313-20.

40. Nelson, A.M. and L.A. Garza, *Bad Hair Day: Testosterone and Wnts.* J Invest Dermatol, 2015. **135**(11): p. 2567-2569.

41. Pereira de Jesus-Tran, K., et al., *Comparison of crystal structures of human androgen receptor ligand-binding domain complexed with various agonists reveals molecular determinants responsible for binding affinity.* Protein Sci, 2006. **15**(5): p. 987-99.

42. Joo, H.W., et al., *15-deoxy prostaglandin J2, the nonenzymatic metabolite of prostaglandin D2, induces apoptosis in keratinocytes of human hair follicles: a possible explanation for prostaglandin D2-mediated inhibition of hair growth.* Naunyn Schmiedebergs Arch Pharmacol, 2016. **389**(7): p. 809-13.

43. Garza, L.A., et al., *Prostaglandin D2 inhibits hair growth and is elevated in bald scalp of men with androgenetic alopecia.* Sci Transl Med, 2012. **4**(126): p. 126ra34.

44. Wang, D. and R.N. Dubois, *Prostaglandins and cancer.* Gut, 2006. **55**(1): p. 115-22.

45. Pioszak, A.A. and H.E. Xu, *Molecular recognition of parathyroid hormone by its G protein-coupled receptor.* Proc Natl Acad Sci U S A, 2008. **105**(13): p. 5034-9.

46. Shimizu, N., et al., *Novel parathyroid hormone (PTH) antagonists that bind to the juxtamembrane portion of the PTH/PTH-related protein receptor.* J Biol Chem, 2005. **280**(3): p. 1797-807.

47. Amor, K.T., R.M. Rashid, and P. Mirmirani, *Does D matter? The role of vitamin D in hair disorders and hair follicle cycling.* Dermatol Online J, 2010. **16**(2): p. 3.

48. Rochel, N., et al., *The crystal structure of the nuclear receptor for vitamin D bound to its natural ligand.* Mol Cell, 2000. **5**(1): p. 173-9.

49. Kakuda, S., et al., *Structural basis of the histidine-mediated vitamin D receptor agonistic and antagonistic mechanisms of (23S)-25-dehydro-1alpha-hydroxyvitamin D3-26,23-lactone.* Acta Crystallogr D Biol Crystallogr, 2010. **66**(Pt 8): p. 918-26.

50. Beenken, A. and M. Mohammadi, *The FGF family: biology, pathophysiology and therapy.* Nat Rev Drug Discov, 2009. **8**(3): p. 235-53.

51. Ornitz, D.M. and N. Itoh, *The Fibroblast Growth Factor signaling pathway.* Wiley Interdiscip Rev Dev Biol, 2015. **4**(3): p. 215-66.

52. Mohammadi, M., et al., *Crystal structure of an angiogenesis inhibitor bound to the FGF receptor tyrosine kinase domain.* EMBO J, 1998. **17**(20): p. 5896-904.

53. Hebert, J.M., et al., *FGF5 as a regulator of the hair growth cycle: evidence from targeted and spontaneous mutations.* Cell, 1994. **78**(6): p. 1017-25.

54. X.L. He, C.Y., Y.L. Chen, *Isolation, characterization, and expression analysis of FGF5 isoforms in cashmere goat.* Small Ruminant Research, 2014. **116** p. 111–117.

55. Liu, W., et al., *Crystal Structure of the Complex of Human FasL and Its Decoy Receptor DcR3.* Structure, 2016. **24**(11): p. 2016-2023.

56. Schneider, P., et al., *Characterization of Fas (Apo-1, CD95)-Fas ligand interaction.* J Biol Chem, 1997. **272**(30): p. 18827-33.

57. Kussie, P.H., et al., *Structure of the MDM2 oncoprotein bound to the p53 tumor suppressor transactivation domain.* Science, 1996. **274**(5289): p. 948-53.

58. Shangary, S. and S. Wang, *Targeting the MDM2-p53 interaction for cancer therapy.* Clin Cancer Res, 2008. **14**(17): p. 5318-24.

59. Khoury, K. and A. Domling, *P53 mdm2 inhibitors.* Curr Pharm Des, 2012. **18**(30): p. 4668-78.

60. Zhao Y., B.D.a.W.S., *Small Molecule Inhibitors of MDM2-p53 and MDMX-p53 Interactions as New Cancer Therapeutics.* BioDiscovery, 2013. **8**(4).

61. Trueb, R.M., *Chemotherapy-induced hair loss.* Skin Therapy Lett, 2010. **15**(7): p. 5-7.

62. Long, Q.Z., et al., *Interaction of CCN1 with alphavbeta3 integrin induces P-glycoprotein and confers vinblastine resistance in renal cell carcinoma cells.* Anticancer Drugs, 2013. **24**(8): p. 810-7.

63. Luca, V.C., et al., *Structural biology. Structural basis for Notch1 engagement of Delta-like 4.* Science, 2015. **347**(6224): p. 847-53.

64. Groppe, J., et al., *Structural basis of BMP signalling inhibition by the cystine knot protein Noggin.* Nature, 2002. **420**(6916): p. 636-42.

65. Wang, C., et al., *Structural basis for Smoothened receptor modulation and chemoresistance to anticancer drugs.* Nat Commun, 2014. **5**: p. 4355.

66. Weierstall, U., et al., *Lipidic cubic phase injector facilitates membrane protein serial femtosecond crystallography.* Nat Commun, 2014. **5**: p. 3309.

67. Chen, J.K., *I only have eye for ewe: the discovery of cyclopamine and development of Hedgehog pathway-targeting drugs.* Nat Prod Rep, 2016. **33**(5): p. 595-601.

68. Janda, C.Y., et al., *Structural basis of Wnt recognition by Frizzled.* Science, 2012. **337**(6090): p. 59-64.

69. Bourhis, E., et al., *Reconstitution of a frizzled8.Wnt3a.LRP6 signaling complex reveals multiple Wnt and Dkk1 binding sites on LRP6.* J Biol Chem, 2010. **285**(12): p. 9172-9.

70. Ahn, V.E., et al., *Structural basis of Wnt signaling inhibition by Dickkopf binding to LRP5/6.* Dev Cell, 2011. **21**(5): p. 862-73.

71. Steck, S.E., et al., *Association between Plasma 25-Hydroxyvitamin D, Ancestry and Aggressive Prostate Cancer among African Americans and European Americans in PCaP.* PLoS One, 2015. **10**(4): p. e0125151.

72. Deeb, K.K., D.L. Trump, and C.S. Johnson, *Vitamin D signalling pathways in cancer: potential for anticancer therapeutics.* Nat Rev Cancer, 2007. **7**(9): p. 684-700.

73. Kitchen, D., et al., *The relationship between vitamin D and chemotherapy-induced toxicity - a pilot study.* Br J Cancer, 2012. **107**(1): p. 158-60.

74. Burney, B.O. and J.M. Garcia, *Hypogonadism in male cancer patients.* J Cachexia Sarcopenia Muscle, 2012. **3**(3): p. 149-55.

CHAPTER 4 Vinblastine and its Metabolites Binding to Tubulin

4.1 Introduction

Microtubules (MTs) are complex structures that constitute part of the cytoskeleton. They are structurally formed by 13-16 protofilaments of tubulin which are aligned side-by-side with a head-to-tail lay out forming hollow cylindrical microtubules. Highly dynamic in nature, MTs denote the mitotic spindle of eukaryotic cells and are strongly involved in cellular proliferation [1].

The cellular division promoted by the MTs have made these structures an attractive target for anticancer drug design, more specifically by targeting the tubulin heterodimer. The structure of tubulin is comprised of two distinct subunits of proteins known as α- and β-tubulin that forms the heterodimer of tubulin. Each of these proteins have approximately ~50 kDa weight and have a high sequence similarity and identity [2, 3].

The α- and β-subunit of tubulin are comprised of 451 and 445 residues, respectively. These dimers can adopt different conformations depending on their GTP/GDP-bound state. The heterodimer αβ-tubulin polymerizes in the presence of GTP in the microtubule ends, a process known as the growing phase. On the contrary, the presence of GDP can induce depolymerization of the microtubules, known as the shrinking phase. These two states are also recognized as assembly and disassembly of the MTs, respectively [2, 3].

VLB targets the MTs by inhibiting the polymerization of the protofilaments impairing the mitotic spindle of cells that would divide [4]. Our lab has previously

demonstrated the binding interactions of VLB with the αβ-tubulin heterodimer by molecular dynamics [1]. In addition, our research group has investigated how carbon nanotubes function as a drug delivery option for VLB in order to enhance target specificity and decrease ADRs [5]. This chapter looks into whether the metabolites of VLB can also display a similar mode of action to that of VLB and elucidate the possibility of chemical modifications of VLB structure to reduce production of several metabolites, while maintaining its anti-mitotic function, with minimum side effects.

4.2 Materials and Method

The preparation of the ligand library consisting of VLB and its metabolites used for their docking into the vinca site of tubulin is described in the Materials and Method section of Chapter 2. The crystalized structure of tubulin was retrieved from Protein Data Bank with entry code of 4EB6 [6]. Water molecules were removed, side chains with missing residues were completed and atom charges were set as appropriate. Protonation states were adjusted prior to energy minimization with AMBER7 FF99 force field. The crystal structure used in this study (4EB6) is originated from *Ovis aries* species (sheep). However the amino acids sequence is more than 90% similar to the human sequence. The residues known to be involved in the binding of VLB share 100% sequence identity with the *Homo sapiens* [4, 6].

The α-subunit is folded to 18 α-helices considering in α1 (residues 10-21), α2 (22-25), α3 (48-51), α4 (72-81), α5 (82-85), α6 (102-108), α7 (109-127), α8 (148-162), α9 (182-195), α10 (206-211), α11 (223-239), α12 (239-244), α13 (297-301), α14 (324-337), α15 (381-386), α16 (387-401), α17 (404-411) and α18 (415-435). The β-subunit is also folded to 18 α-helices which are comprised of α1 (residues 10-29), α2 (73-77), α3 (88-90), α4 (102-108), α5 (108-128), α6 (147-161), α7 (182-198), α8 (206-211), α9 (224-239), α10 (251-260), α11 (287-295), α12 (296-301), α13 (306-310), α14 (324-339), α15 (340-343), α16 (384-400), α17 (405-410) and α18 (415-437). The structure of tubulin crystalized with VLB [6] shows that the drug binds to the interface of β- and α-tubulin. Thus, a spherical region with a radius of 10 Å surrounding the reference ligand was selected as the target site for docking VLB and its metabolites.

4.3 Results and Discussion

4.3.1 Vinblastine and Metabolites Binding to Tubulin

Vinblastine and its metabolites were docked into the vinca site of tubulin as described in the Materials and Method section of Chapter 4 and Chapter 2. (**Table 4.1**)

4.3.1.1 Vinblastine Binding to Tubulin

The virtual screening of the ligand library docked into tubulin vinca site results in a binding energy of -11.23 kJ/mol for VLB. The conformation adopted by VLB at the vinca site of tubulin shows that the catharantine portion plays a major role in the binding interactions. VLB makes H-bonds with residues Asn329 and Lys336 of α-tubulin along with residues Lys176 and Val177 of β-tubulin. All of the residues located at β-tubulin interacting with VLB are in agreement with previous research [1, 7, 8]. The catharantine portion of VLB which is known to play a major role in the interactions with tubulin [1, 7-9], is also in agreement with the findings for the best binding energy of VLB into the vinca site of tubulin. (**Figure 4.1** and **Table 4.2**)

More specifically, the protonated N16′ interacts with the carbonyl group of the main chain of Lys176 within a distance of 2.3 Å; the hydroxyl group at C4′ interacts with the main chain of Val177 within a distance of 1.9 Å; the carbonyl of ester at C18′ interacts with the amide group of Asn329 (2.1 Å), and the carbonyl group at C3 interacts with Lys336 within a distance of 2.3 Å. (**Figures 4.1**, **Figure 4.2B** and **Table 4.3**)

Table 4.1: Binding energy of VLB and its metabolites docked into the vinca site of tubulin. The energy value of the metabolite with the lowest binding energy is shown in bold.

Drug & Metabolites	$\Delta G_{Binding}$ (kJ/mol)
VLB	-11.23
MTB1	-10.05
MTB2	-9.32
MTB3	-10.99
MTB4	-0.45
MTB5	-9.78
MTB6	-3.33
MTB7	-6.43
MTB8	-12.18
MTB9	-1.87
MTB10	-13.39
MTB11	-14.24
MTB12	-9.84
MTB13	-17.94
MTB14	-9.17
MTB15	-6.92
MTB16	-12.93
MTB17	-0.43
MTB18	-16.32
MTB19	**-21.90**
MTB20	-5.43
MTB21	-15.30
MTB22	-20.12
MTB23	-18.60
MTB24	-13.88
MTB25	-16.68
MTB26	-10.57
MTB27	-11.88
MTB28	-5.27
MTB29	-16.39
MTB30	-16.20
MTB31	-17.13
MTB32	-15.15
MTB33	-12.34
MTB34	-18.58
MTB35	-16.68

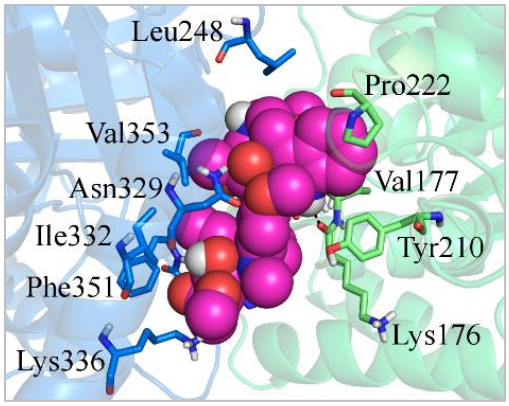

Figure 4.1: Binding interactions of VLB docked into the vinca site of tubulin.

Table 4.2: Residues involved in the binding of VLB into the tubulin heterodimer. Residues shown underlined bind through H-bonds with the catahrantine portion and in italic with the vindoline portion of VLB.

Subunit	Hydrogen Bonds	Hydrophobic Interactions
α-tubulin	Asn329, *Lys336*	Leu248, Ile332 Thr349, Gly350, Phe351, Val353
β-tubulin	Lys176, Val177	Ser178, Asp179, Tyr210, Pro222

4.3.1.2 Metabolites Binding to Tubulin

VLB and its metabolites were docked into the vinca site of tubulin. Most of the VLB metabolites bind to the heterodimer of tubulin and their binding energy vary from -21.90 kJ/mol (metabolite 19) to -0.45 kJ/mol (metabolite 4). (**Table 4.2**)

Metabolite 19 has the lowest binding energy among the metabolites, calculated as of -21.90 kJ/mol, compared to highest binding energy -0.43 kJ/mol of metabolite 17. That could be due to the fact that the three aromatic rings of vindoline portion of VLB are opened after metabolism and thus gives metabolite 19 more flexibility to find a conformation that

fits deep in the binding pocket of tubulin. Although metabolite 19 makes an H-bond with Asn329 (α-tubulin) similar to VLB [1], with a shorter distance (1.6 Å vs. 2.1 Å), and with a stronger binding energy than VLB (-21.90 kJ/mol vs. -11.23 kJ/mol), the metabolite does not bind to all of the residues interacting with VLB. However, metabolite 19 makes H-bonds with residues from β-tubulin that are also involved in binding interactions with VLB such as Asp179 and Pro222. Moreover, hydrophobic interactions are observed with Ser178, Val177, Tyr210 (β-tubulin) and Leu248 (α-tubulin), while all of them also interact with VLB. Although metabolite 19 has a high binding energy for the vinca site of tubulin and share a few similar residues involved in the VLB binding, it is not likely that it gives the same conformational changes on the tubulin structure as its parent drug. Different from VLB, metabolite 19 interacts with more residues of β-tubulin than of α-tubulin. Thus the structure of tubulin is likely to adopt other induced-fit conformation upon binding of metabolite 19. More research is required to evaluate whether metabolite 19 would induce the same conformation state of tubulin as VLB to impose depolymerization effect. (**Figure 4.2D**)

Metabolites that have adopted similar conformation to that of VLB in the vinca site of tubulin are metabolite 8, metabolite 10 and metabolite 11. These compounds have additional moieties in their structure that enhances their binding affinity for tubulin. Metabolite 11 has undergone an N-oxidation reaction at N6′ during metabolism of VLB. Metabolite 10 is hydroxylated at position C20 of VD and metabolite 8 has gone through aromatic hydroxylation at C13′ of CT. (**Figure 1.3** – **M10** and **M11**)

Besides adopting similar conformation of VLB at the tubulin heterodimer, metabolite 8, metabolite 10 and metabolite 11 have stronger binding energy (-12.18 kJ/mol, -13.39 kJ/mol and -14.24 kJ/mol, respectively) than VLB (-11.23 kJ/mol). As expected, these metabolites bind to the same residues that interact with the parent drug through H-bonds (Lys176, Val177, Asn329 and Lys336). However, the strength of these interactions and high binding energy are due to the close proximity of atoms involved in H-bonds. (**Table 4.3**)

Table 4.3: Distances among heteroatoms of the vinca site of tubulin and heteroatoms of VLB, metabolites 8, 10 and 11 involved in hydrogen bonds.

Subunit	H-bonds Interactions	Distance among HBD and HBA atoms (Å)			
		VLB	MTB8	MTB10	MTB11
CT	N16′ + Lys176	2.3	2.2	2.4	2.3
	OH + Val177	1.9	2.0	2.0	1.7
VD	Ester C4 + Asn329	2.1	2.0	2.1	1.9
	Ester C3 + Lys336	2.3	2.4	2.6	2.5
$\Delta G_{Binding}$ (kJ/mol)		-11.23	-12.18	-13.39	-14.24

As compared to VLB, metabolite 10 has one extra H-bond with Asp179. The hydroxyl group added at C5 of VD (attached to C20) shares its electron deficient to the side chain of Asp179 of β-tubulin within a distance of 2.2 Å. Although the distance among the heteroatoms involving residues Lys336, Asn329, Val177 and Lys176 and metabolite 10 are longer than those of VLB, an extra H-bond among the hydroxyl group at C5 of metabolite 10 with Asp179 strengthens the interaction of the metabolite with tubulin. Thus, metabolite 10 is a stronger binder than VLB (-13.39 kJ/mol vs. -11.23 kJ/mol) which display same binding profile as VLB. (**Figure 4.2C** and **Table 4.3**)

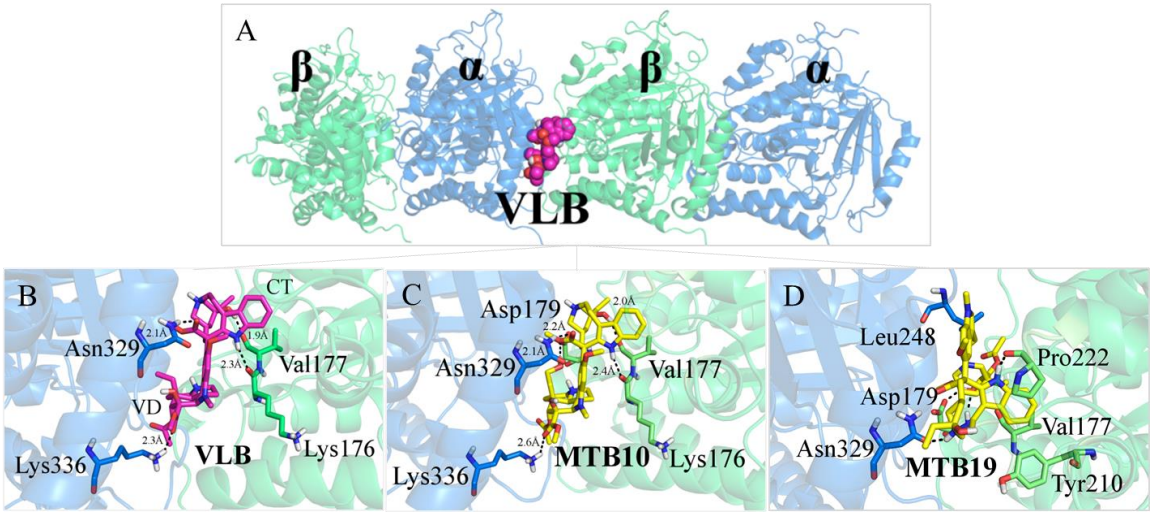

Figure 4.2: A) Structure of α- and β-tubulin coupled with docked VLB, colored in blue and green, respectively. Binding interactions of B) VLB, C) Metabolite 10, and D) Metabolite 19. Hydrogen bonds are shown in dashed lines.

4.4 Conclusion

VLB binds to its target tubulin with a binding energy of -11.23 kJ/mol, and interacts with Lys176, Val177, Asn329 and Lys336 that belong to the vinca site [1]. Molecular docking simulation of metabolites of VLB into the vinca site of tubulin demonstrates that the majority of the metabolites have a better binding energy than their parent drug. (**Table 4.2**)

Metabolite 19 has the lowest binding energy among the metabolites of VLB calculated to be -21.90 kJ/mol. Despite the fact that metabolite 19 interacts with Asn329 (α-tubulin) similar to VLB, it adapts nearly similar conformation to VLB in the vinca site of tubulin. It interacts to more residues of β-tubulin than of α-tubulin, whereas the opposite is observed for VLB [5]. Hence it is possible that tubulin adapts other induced-fit conformation upon binding of metabolite 19. Thus, more research is required to evaluate whether metabolite 19 induces the same anti-mitotic effects of VLB.

Metabolite 8, metabolite 10 and metabolite 11 have stronger binding energies than of VLB (-12.18 kJ/mol, -13.39 kJ/mol and -14.24 kJ/mol vs. -11.23 kJ/mol, respectively). They adapt similar conformation to VLB in the vinca site of tubulin and interact with the same residues as their parent drug (Lys176, Val177, Asn329 and Lys336) with similar or shorter distances in H-bonds than of VLB. This indicates their probability in causing the same “induced-fit” to tubulin and resulting in destabilization of the microtubules similar to binding of VLB. (**Table 4.2** and **Table 4.3**)

Metabolite 8 and metabolite 11 have similar ADMET profiles with VLB hence are potential analogs candidates to be taken into account for structural modifications of VLB.

Metabolite 10 has better PK parameters and possibly more tolerable than those of VLB, and thus it could provide a less unpleasant cancer therapy.

Metabolite 10 is a unique compound due to the fact that it has the same mechanism of action as of VLB in the tubulin as well as a more acceptable PK profile than the anticancer drug. This is mainly due to the fact that metabolite has a better gastric and intestinal solubility, and is less bound to plasma proteins than VLB. Metabolite 10 has a gastric solubility (FaSSGF) (4.65 mg/mL vs. 4.61 mg/mL), intestinal solubility (FeSSIF) (2.95×10^{-2} mg/mL vs. 3.12×10^{-2} mg/mL) and log P (2.99 vs. 3.95) similar to VLB, which are all essential drug features for desired drug bioavailability. Moreover, metabolite 10 is less bound to plasma proteins than VLB (81.2% vs. 89.2%), thus more available throughout the body than VLB. (**Tables 2.7** and **2.8**)

Furthermore, metabolite 10, also known as 20-Hydroxy-VLB, is not an inhibitor of CYP2D6 and CYP3A4 as VLB is, and thus tends to cause less drug-drug interactions and adverse drug reactions than its parent drug. The *in silico* results show that metabolite 10 does not undergo glucoronidation, hence it has a similar phase II metabolism similar to VLB. (**Tables 2.9** and **2.10**)

The hydroxyl group added upon metabolism of VLB producing metabolite 10 suggests that this compound can also be a candidate for modifications of VLB to overcome P-gp-mediated multidrug resistance that is often observed with vinca alkaloids [10]. This is due to the fact that the addition of hydrophobic groups on drug molecules can potentially decrease their binding affinity for P-gp and likelihood of being removed out of the cell [11], thus enhancing drug efficacy.

Studies have been investigated possible analogues of VLB that display stronger target selectivity hence higher cytotoxicity. Chemical modifications on the catharantine portion of VLB (CT) at the C20′ ethyl substituent, such as the addition of hydrophobic groups, have shown significant increased potency towards destabilization of tubulin [9]. In a lesser extent, the vindoline portion of VLB (VD) at the C5 ethyl substituent, an important chemical group for biological activity of VLB, has also been chemically modified [12]. Va *et al.* have analyzed different compounds and their cytotoxic potency against cancer cell lines (i.e. colon cancer HCT116) by mainly modifying the C5 ethyl moiety. However, the chemical bond among C6 and C7 of VD was also modified to either a double or single bond. (**Figure 1.1**)

In a C6-C7 single bond version, the addition of CH_2OH group at C5 position (referring C19 of VD) has reduced the biological activity by 10-fold (compound 56) [12]. In the present work, the C6-C7 bond of VLB is double, however, Va *et al.* have not synthesized any hydrophobic moiety added on C5 ethyl in a C6-C7 double bond version that could mimic the same effects of the hydroxyl group of metabolite 10 into tubulin [12]. In addition, the hydroxyl moiety of metabolite 10 is bound to C20 of VD, and not to C19 as the authors have investigated. This is, the chemical group $(CH_2)_2OH$ of metabolite 10 is located at a different position from CH_2OH added on C5 ethyl of compound 59 [12].

Despite the fact that Va *et al.* have investigated possible chemical moieties added on C5 ethyl of VD that are not aligned with the hydroxyl group of metabolite 10, it can still display cytotoxic properties as its stereochemistry differs from compound 56. This indeed can facilitate the extra H-bond of metabolite 10 among its hydroxyl group at C20 and

Asp179, which strengthens its binding affinity for tubulin (-13.39 kJ/mol vs. -11.23 kJ/mol of VLB). This indicates the possibility of metabolite 10 to be a potential VLB analog that upon binding destabilizes microtubules. Therefore, this study provides insights into modifications of the chemical structure of VLB in order to make it more target-specific and less toxic to cancer patients suggesting that metabolite 10 can be a potential analog of VLB.

4.5 Bibliography

1. Li, Z. and L. Alisaraie, *Microtubules dual chemo and thermo-responsive depolymerization.* Proteins, 2015. **83**(5): p. 970-81.
2. Brouhard, G.J. and L.M. Rice, *The contribution of alphabeta-tubulin curvature to microtubule dynamics.* J Cell Biol, 2014. **207**(3): p. 323-34.
3. Stanton, R.A., et al., *Drugs that target dynamic microtubules: a new molecular perspective.* Med Res Rev, 2011. **31**(3): p. 443-81.
4. Gigant, B., et al., *Structural basis for the regulation of tubulin by vinblastine.* Nature, 2005. **435**(7041): p. 519-22.
5. Li, Z.T., T.; Alisaraie, L., *Molecular dynamics studies for optimization of noncovalent loading of vinblastine on single-walled carbon nanotube.* The Journal of Physical Chemistry, 2016. **120**: p. 4061−4070.
6. Ranaivoson, F.M., et al., *Structural plasticity of tubulin assembly probed by vinca-domain ligands.* Acta Crystallogr D Biol Crystallogr, 2012. **68**(Pt 8): p. 927-34.
7. Rashid, A., et al., *Thalidomide (5HPP-33) suppresses microtubule dynamics and depolymerizes the microtubule network by binding at the vinblastine binding site on tubulin.* Biochemistry, 2015. **54**(12): p. 2149-59.
8. Chi, S., et al., *Theoretical insight into the structural mechanism for the binding of vinblastine with tubulin.* J Biomol Struct Dyn, 2015. **33**(10): p. 2234-54.

9. Allemann, O., et al., *Key analogs of a uniquely potent synthetic vinblastine that contain modifications of the C20' ethyl substituent.* Bioorg Med Chem Lett, 2017. **27**(14): p. 3055-3059.

10. Szakacs G., P.J.K., Ludwig J. A., Booth-Genthe C., Gottesman M., *Targeting multidrug resistance in cancer*. Nature Reviews Drug Discovery, 2006. **5**(3): p. 219-234.

11. Lambidis T. J., K.D., POdona T., Israel M., Safa A. R., Lothstein L., Savaraj N., Tapiero H., Priebe W., *Circumvention of P-gp MDR as a Function of Anthracycline Lipophilicity and Charge.* Biochemistry, 1997. **36**(9): p. 2679-2685.

12. Va P., C.E.L., Robertson E. M., Boger D. L., *Total Synthesis and Evaluation of a Key Series of C5-Substituted Vinblastine Derivatives.* Journal of the American Chemical Society, 2010. **132**(24): p. 8489-8495.

CHAPTER 5 Summary

VLB is extensively metabolized into thirty-five known metabolites which up to date, their off-targets events and effects on nausea and alopecia associated receptors have not yet been fully determined. This *in silico* research project provides in-depth and novel findings on binding mechanisms and main interactions of VLB and its metabolites into the binding sites of dopaminergic D_2, histaminic H_1 and H_3, and muscarinic M_1, M_4 and M_5 receptors involved in nausea, as well as with receptors MDM2, VDR, AR and SMO involved in induced-alopecia. In addition, it demonstrates a detailed understanding of the *in silico* predicted pharmacokinetics properties of VLB and its metabolites along with their possible involvement with adverse drug reactions. Finally, the cytotoxic activity of metabolites of VLB is also elucidated by means of molecular docking, giving insights into potential analogs to be studied for VLB modifications to obtain drugs with a desired target selectivity for the vinca site of tubulin.

In the inducing nausea receptors, VLB only has a better binding energy than the natural substrate ACh docked into M_5R (-9.28 kJ/mol vs. -4.51 kJ/mol). The *in silico* results indicate that VLB does not trigger hair loss due to its low or no affinity for alopecia associated receptors used in this study. Thus, VLB is not expected to be involved in the onset of alopecia through MDM2, AR, VDR and SMO signaling pathways. However, it may have an effect on other alopecia associated receptors not included in this study, and raising the attention for further investigation of induced-alopecia by VLB. Although VLB

does not affect any of the alopecia receptors studied in this project, it has a significant role on nausea symptoms due to its binding affinity particularly for the muscarinic M_5 receptor.

Interestingly, I found that the majority of metabolites of VLB interact with nausea and alopecia associated receptors included in this study with significant binding affinities, thus capable of inducing such ADRs. They often bind to the same residues involved in the binding of substrates activators (ACh, dopamine, histamine, testosterone, calcitriol) or exogenous inhibitors (nutlin-2, TEI-4696, anta XV) of these receptors.

In particular, the metabolites of VLB display a significant role in the activation of the muscarinic receptors M_1, M_4 and M_5 involved in nausea. Although D_2, H_1 and H_3 receptors of nausea pathway are also affected by a few metabolites of VLB, these are not the major off-targets proteins of VLB metabolites in causing nausea.

In addition, the majority of VLB metabolites have binding affinities for MDM2 receptor, which its inhibition by the metabolites can lead to the activation of p53 and consequently to hair follicle apoptosis. A few metabolites also have binding affinities for VDR and SMO, thus may induce alopecia through different signaling pathways. Therefore, metabolites of VLB contribute to nausea and alopecia symptoms during treatment with VLB.

Moreover, the *in silico* molecular docking along with the *in silico* predicted pharmacokinetics properties of VLB and its metabolites have revealed that metabolite 10 is a potential candidate for redesign of VLB. This is because it adapts similar conformation to VLB in the vinca site of tubulin and has a stronger binding energy than its parent drug

(-13.39 kJ/mol vs. -11.23 kJ/mol). Moreover, the ADMET parameters calculated for metabolite 10 resemble those of VLB (i.e. gastric/intestinal solubility, log P, Vd, % unbound to plasma proteins, likelihood of being a substrate of CYP2D6/CYP3A4, phase II metabolism). Metabolite 10 also has a more tolerable pharmacokinetics profile than VLB which can be better accepted by patients undergoing chemotherapy.

Therefore, through the use of molecular docking techniques and *in silico* ADMET predicted data, the novel findings of this study provide a better understanding of the metabolites of VLB and their binding profiles with respect to nausea (H_1, H_3, D_2, M_1, M_4 and M_5) and alopecia (MDM2, VDR, AR, SMO) associated receptors. My study has explored how nausea and alopecia are often experienced during chemotherapy with VLB due to the off-target binding of VLB metabolites. In addition, this research have predicted the interactions of metabolites of VLB in the vinca site of tubulin, suggesting new possible modifications on the chemical structure of VLB for more target selectivity. This calls for designing simpler and target specific drugs that meet the desired drug effectiveness.